A STUDY OF INELASTIC DECAY AMPLITUDES IN ^{49}V

by

BIING-HUI CHOU

A thesis submitted to the Graduate Faculty of
North Carolina State University
in partial fulfillment of the
requirements for the Degree of
Doctor of Philosophy

DEPARTMENT OF PHYSICS

RALEIGH

1 9 8 0

APPROVED BY:

_____ _____

_____ _____

Chairman of Advisory Committee

ABSTRACT

BIING-HUI CHOU, A Study of Inelastic Decay Amplitudes in ^{49}V. (Under the direction of Gary E. Mitchell).

Inelastic decay amplitudes from d-wave resonances in ^{49}V were obtained for 80 resonances in the proton energy range 2.2 to 3.1 MeV. With the 3 MV Van de Graaff accelerator and high resolution system at the Triangle Universities Nuclear Laboratory, an overall resolution of 350 eV was obtained. The experiment consisted of measurements of the angular distributions of the inelastically scattered protons and the subsequent de-excitation gamma rays.

Forty five resonances were assigned $J^{\pi}=5/2^{+}$, while thirty five resonances were assigned $3/2^{+}$. The magnitudes of three inelastic decay amplitudes and the relative signs between these three amplitudes were determined. Large amplitude correlations were observed; the data are in striking disagreement with the extreme statistical model. The present results provide the first explicit test of the multivariate reduced width amplitude distribution of Krieger and Porter; the agreement is excellent. The physical origin of these channel correlations has not yet been explained.

BIOGRAPHY

Biing-Hui Chou

Personal:	Born September 14, 1952, Taipei, Taiwan, R.O.C.
Education:	B.S. in Physics, National Central University, Chung-Li, Taiwan, R.O.C., 1975
Positions:	Teaching Assistant, N.C.S.U., 1975 to 1977
	Research Assistant, N.C.S.U., 1977 to present
Membership:	Sigma Pi Sigma
	American Physical Society

ACKNOWLEDGEMENT

I would like to express my appreciation to my advisor, Dr. G. E. Mitchell for his guidance and support and for his time and understanding during all phases of this research project. Sincere appreciation is also extended to Dr. E. G. Bilpuch for his advice and support during the course of this experiment. The support of other members of my committee, Drs. D. R. Tilley, A. W. Jenkins, Dr. J. W. Bishir, and Dr. J. Luh is greatly appreciated.

I owe special thanks to C. R. Westerfeldt and Dr. K. B. Sales for their invaluable assistance and unfailing support in all phases of this experiment. I am also grateful to W. A. Watson and Dr. J. R. Chandler for many helpful discussions and suggestions. The assistance of K. M. Whatley, J. F. Shriner, R. O. Nelson, and B. H. Duberdorff in taking portions of these data is appreciated.

The assistance of Mr. S. E. Edwards, Mr. R. Rummel, and Mr. A. W. Lovette in maintaining the equipment used in this experiment is appreciated. Also, I would like to thank Mrs. Joseph Bailey for her careful preparation of the figures in this dissertation.

I owe a warm thanks to my parents and family for their constant support and encouragement throughout my life.

This work was supported in part by the United States

Department of Energy. Some of the data analysis was performed at the Triangle Universities Computer Center, which is supported in part by the National Science Foundation.

TABLE OF CONTENTS

Page

LIST OF FIGURES vii

LIST OF TABLES. x

1. INTRODUCTION 1

2. ANGULAR CORRELATIONS 5

A. Theoretical Background 5

2.A.1. Mixture States, Density Matrix, and Efficiency Matrix. 6
2.A.2. Statistical Tensors, Efficiency Tensors, and the Tensor of a Vector Sum Formula . 8
2.A.3. The General Angular Correlation Functions. 10
2.A.4. Matrix Elements, Phase Shift, and Mixing Ratios. 15
2.A.5. The Coupling Scheme and D-Wave Angular Correlation Expressions. 23
2.A.6. Transformation Equations 33
2.A.7. Properties of $5/2^+$ Compound States . . . 35

B. Data Analysis 51

2.B.1. Spin Assignment for the D-Wave Compound State 52
2.B.2. Mixing Ratios. 53
2.B.3. χ^2 Search. 56
2.B.4. The $1'=2$ Admixture ϵ_m^2 for Matrix Elements 94
2.B.5. Properties of Mixing Ratios Related to Line $a_{2\beta}=-a_{4\beta}$ and the Sign of a_{2P} . . . 95

3. EXPERIMENTAL EQUIPMENT AND PROCEDURE. 99

3.1 3 MV Van de Graaff System. 99
3.2 Scattering Chambers. 106

page

3.3 Targets. 116
3.4 Electronics. 117
3.5 Procedure. 121

4. DATA AND PRELIMINARY ANALYSIS 123

4.1 Proton Elastic Scattering Experiment 123
4.2 Preliminary Analysis 123
4.3 Total Inelastic Width and Channel Reduced Widths 135

5. STATISTICAL PROPERTIES. 156

A. INTRODUCTION 156

5.A.1 Canonical Groups. 156
5.A.2 The Random Matrix Hypothesis and the Joint Probability for the Hamiltonian Matrix Elements 159
5.A.3 Spacing Distributions 162
5.A.4 The Reduced Width Distribution. 166
5.A.5 The Covariance Matrix and the Channel Width Correlation Coefficient . 171
5.A.6 The Probability Distribution for Mixing Ratios 174

B. DATA ANALYSIS. 189

5.B.1 Non-Statistical Effects 189
5.B.2 Proton Strength Functions and the Statistical Fluctuations of Reduced Widths 197
5.B.3 Linear Correlation Coefficients 206

6. SUMMARY 212

7. BIBLIOGRAPHY. 214

LIST OF FIGURES

Page

2.1 Energy Level Scheme and Angular Momentum Coupling Scheme for the Reaction $^{48}Ti(p,p'\gamma)^{48}Ti$. 25

2.2 The Physical Region of Legendre Polynomial Coefficients a_2, a_4 in the Angular Momentum Representation 38

2.3 The Physical Region of Legendre Polynomial Coefficients a_2, a_4 in the Channel Spin Representation 42

2.4 The Experimental Legendre Polynomial Coefficients for Forty Five 5/2+ Resonances 45

2.5 χ^2 Plot for a 5/2+ Resonance (No. 102) in the Angular Momentum Representation. 58

2.6 χ^2 Plot for a 5/2+ Resonance (No. 106) in the Channel Spin Representation. 60

2.7 χ^2 Plot for a 3/2+ Resonance (No. 29) in the Angular Momentum Representation. 62

2.8 χ^2 Plot for a 3/2+ Resonance (No. 67) in the Channel Spin Representation. 64

3.1 Floor Plan of the 3 MV Van de Graaff Accelerator Laboratory 101

3.2 The Block Diagram of the Present Electrostatic Analyzer-Homogenizer Circuitry 104

3.3 Top View of the Charged Particle Scattering Chamber and Collimator Assembly. 108

3.4 Typical Spectrum for Protons on ^{48}Ti at $E_p = 2.9196$ MeV 110

3.5 Gamma-Ray Detection Chamber and Collimator Assembly. 112

3.6 Gamma-Ray Spectrum for $^{48}Ti(p,p'\gamma)^{48}Ti$ at $E_p = 2.7725$ MeV. 115

3.7 Block Diagram of the Proton and Gamma-Ray Detection Electronics. 119

Page

4.1 Differential Cross Section of Proton Elastic and Inelastic Scattering on ^{48}Ti at 160° 125

4.2 Plot of $\emptyset_{5l}$ versus $\emptyset_{3l}$ for 5/2+ Resonances in the Angular Momentum Pepresentation 132

4.3 Plot of $\emptyset_{5l}$ versus $\emptyset_{3l}$ for 5/2+ Resonances in the Channel Spin Representation 134

4.4 Plot of $\emptyset_{5l}$ versus $\emptyset_{3l}$ for 3/2+ Resonances in the Angular Momentum Representation 137

4.5 Plot of $\emptyset_{5l}$ versus $\emptyset_{3l}$ for 3/2+ Resonances in the Channel Spin Representation 139

4.6 Elastic and Three Inelastic Channel Widths and Sum of Peduced Widths versus Energy. 149

4.7 Total Inelastic and Three Inelastic Channel Widths and Sum of Reduced Widths versus Energy . 151

4.8 Product of Channel Reduced Width Amplitudes and Sum of the Product versus Energy in the Angular Momentum Representation. 153

4.9 Product of Channel Reduced Width Amplitudes and Sum of the Product versus Energy in the Channel Spin Representation. 155

5.1 Hamiltonian Matrix Diagonalized into Blocks with Specific Spin and Parity. 161

5.2 (a) Geometric Relation between Amplitude Reduced Width and Mixing Ratio Parameters for Two Channels.
(b) Geometric Relation between Peduced Width Amplitudes ($\gamma_1, \gamma_2, \gamma_3$) and Mixing Ratio Parameters ($\emptyset_1, \emptyset_2$) for Three Channels.
(c) Geometric Relation between Three Channel Peduced Amplitudes ($\gamma_1, \gamma_2, \gamma_3$) and the Spherical Coordinates ($r, \theta, \emptyset$). 176

Page

5.3 Distribution of Ø for Inelastic Decay from 5/2+ Resonances in ^{49}V in the Angular Momentum Representation 186

5.4 Distribution of Ø for Inelastic Decay from 5/2+ Resonances in ^{49}V in the Channel Spin Representation 188

5.5 The Normalized Distribution of Ø for Inelastic Decay from 5/2+ Resonances in ^{49}V in the Angular Momentum Representation. 191

5.6 The Normalized Distribution of Ø for Inelastic Decay from 5/2+ Resonances in ^{49}V in the Channel Spin Representation. 193

5.7 Distribution of the Z Statistic for 100,000 Cases. 196

5.8 The Distribution of Elastic and Total Inelastic Partial Reduced Widths 201

5.9 The Distribution of Inelastic Reduced Widths in Channels <j,0,1>, <j,2,3>, and <j,2,5> 203

5.10 The Distribution of Inelastic Reduced Widths in Channels <s,0,5>, <s,2,3>, and <s,2,5> 205

LIST OF TABLES

		Page
2.1	Values of Resonance Phase and Penetrability Ratio.	19
2.2	Legendre Polynomial Coefficients for l=2 Resonances in ^{49}V.	67
2.3	Values of Mixing Ratios, ϵ_r^2, ϵ_m^2, and χ^2 for $5/2^+$ Resonances in ^{49}V (j-spin).	74
2.4	Values of Mixing Ratios, ϵ_r^2, ϵ_m^2, and χ^2 for $5/2^+$ Resonances in ^{49}V (s-spin).	78
2.5	Values of Mixing Ratios, ϵ_r^2, ϵ_m^2, and χ^2 for $3/2^+$ Resonances in ^{49}V (j-spin).	82
2.6	Values of Mixing Ratios, ϵ_r^2, ϵ_m^2, and χ^2 for $3/2^+$ Resonances in ^{49}V (s-spin).	88
4.1	Resonance Parameters for D-Wave Resonances in ^{49}V.	127
4.2	Channel Reduced Widths and Amplitude Products (j-spin).	142
4.3	Channel Reduced Widths and Amplitude Products (s-spin).	145
5.1	D-Wave Strength Function of Compound Nucleus ^{49}V.	198
5.2	Linear Correlation Coefficients between Channels (j-spin).	208
5.3	Linear Correlation Coefficients between Channels (s-spin).	209
5.4	Values of $\overline{\gamma_1^2\gamma_2^2} - \overline{\gamma_1^2}\,\overline{\gamma_2^2}$ and $2(\overline{\gamma_1\gamma_2})^2$	211

Introduction

For the past decade at the Triangle Universities Nuclear Laboratory, compound nuclei formed by the addition of an incident proton to even-even nuclei have been studied with the 3 MV Van de Graaff accelerator and its associated high resolution system. These experiments yielded the resonance energies, angular momentum and parity values, and partial widths of the highly excited compound nuclear states. With this resonance information, both non-statistical and statistical properties of the compound nucleus have been studied.

Recently, a new technique for measuring the magnitude and relative sign of inelastic decay amplitudes for isolated resonances has been developed and successfully applied to a two-channel case. The present work is an extension of this technique to a three-channel case. The absence of isobaric analog states in the energy region examined makes this experiment suitable for study of statistical behavior.

In this technique angular distributions of both the inelastically scattered protons and of the subsequent gamma-ray decay are measured. The spin j ($j=l\pm1/2$) of the compound state can be uniquely determined from the angular distributions. For example, in terms of an expansion in

$\cos^2\theta$, both angular distributions $W_{p'}(\theta_i)$ and $W_\gamma(\theta_i)$ for p-wave compound states are isotropic for $1/2^-$ states and straight lines (with at least one distribution non-isotropic) for $3/2^-$ states. For d-wave compound states, both $W_{p'}(\theta_i)$ and $W_\gamma(\theta_i)$ are straight lines for $3/2^+$ states, and parabolas or straight lines for $5/2^+$ states (the probability for both distributions to be straight lines is extremely small). In the present experiment, l=2 resonances in ^{49}V were selected for study. Previous measurements had established the existence of more than one hundred l=2 resonances, with no analog observed or expected. All of these resonances were examined, and detailed information obtained on 80 resonances, 45 of which were assigned $J = 5/2^+$ and 35 were assigned $3/2^+$.

The angular distribution functions $W_{p'}(\theta_i)$ and $W_\gamma(\theta_i)$ for $5/2^+$ states are derived in the form $W(\theta) \sim 1 + a_2 P_2(\cos\theta) + a_4 P_4(\cos\theta)$, where a_2 and a_4 are functions of the decay amplitudes. The distributions are conveniently expressed as functions of ratios of amplitudes, or mixing ratios. From the Legendre polynomial fit to the angular distributions, four equations are obtained which are quadratic functions of these mixing ratios. This is sufficient information to determine a unique solution for these (two) mixing ratios. From the two known mixing ratios and the total inelastic width, the three inelastic channel reduced widths can be

determined. Various statistical properties of the width distribution can then be tested.

For $3/2^+$ states, $W(\theta)$ has the form $W(\theta) \sim 1+a_2 P_2(\cos\theta)$. Due to the absence of the a_4 term, there are two acceptable solutions. There is not sufficient information to remove this ambiguity. Therefore, for the $3/2^+$ states the two solutions are merely listed without any further analysis.

The sign of the mixing ratio represents the relative sign between two channel reduced width amplitudes. This relative sign determination enables one to test both the random phase hypothesis and the relation of correlation coefficients between reduced widths and reduced width amplitudes. The random phase hypothesis predicts a random distribution of mixing ratios in sign and magnitude. For measured 45 $5/2^+$ resonances in ^{49}V a strong non-random phenomenon exists, contradicting the random phase hypothesis. Lane(1971) predicted that the reduced width correlation coefficient should be approximately equal to the square of the reduced width amplitude correlation coefficient. The experimental results disagree with this prediction.

Following the random matrix hypothesis, Krieger and Porter (1963) derived the probability density function (p.d.f.) for reduced width amplitudes by making independence and invariance assumptions. Starting from

this reduced width amplitude p.d.f., the marginal p.d.f. of mixing ratios was explicitly obtained for the first time in the present work. The experimental results agree very well with this distribution.

A brief introduction to the theory of angular distributions is presented in chapter two. Explicit expressions are derived for the angular distributions for the decay of $3/2^+$ and $5/2^+$ resonances. The procedure for extracting the mixing ratios from the measured angular distributions is described. The experimental equipment and procedure are outlined in chapter three, while in chapter four, the data, preliminary analysis, and results are presented. In chapter five, the statistical fluctuations of compound states are discussed, and the marginal probability density functions of reduced width amplitudes for two and three channels are derived. The results are summarized in chapter 6.

Chapter 2

Angular Correlations

A. Theoretical Background

Angular correlation measurements on radiation emitted or absorbed in a nuclear reaction have provided a powerful method for determining spins and parities of excited compound states. In the process of deriving a complete angular correlation formula, the extensive summations over magnetic quantum numbers result in lengthy and tedious calculations. In order to overcome this difficulty, certain alternate mathematical procedures have been developed independently by Fano (1952) and by Coester and Jauch (1953). An explicit derivation of angular correlations for inelastically scattered protons and subsequent gamma-ray decay has been given by Dittrich(1976). The main mathematical concepts will be briefly outlined in sec. 1 through sec. 4. In later sections, applications of these results to our particular reaction are presented.

2.A.1. Mixture States, Density Matrix and Efficiency Matrix

If the information about the dynamical states of a quantum system is not completely available, certain predictions about the behavior of the system can still be made with statistical methods. Assuming that the system has probabilities $p_1, p_2 \cdots p_m \cdots$ of being in the dynamical states (represented by the ket vectors $|1\rangle, |2\rangle \cdots |m\rangle \cdots$, respectively), then the system is no longer represented by a unique vector (pure state), but by a statistical mixture of vectors, the so-called mixture state. The expectation value (a physical measurement) of an operator Ω over a pure state $|\alpha\rangle$ is

$$\begin{aligned}\langle\Omega\rangle &= \langle\alpha|\Omega|\alpha\rangle = \langle\alpha|i\rangle\langle i|\Omega|j\rangle\langle j|\alpha\rangle \\ &= \langle i|\Omega|j\rangle\langle j|\alpha\rangle\langle\alpha|i\rangle \\ &= \langle i|\Omega|j\rangle\langle j|P_\alpha|i\rangle \\ &= \langle i|\Omega P_\alpha|i\rangle \\ &= \mathrm{Tr}(\Omega P_\alpha) \qquad (2.1)\end{aligned}$$

where $|i\rangle$, $|j\rangle$ are unit vectors, and the projection operator $P_\alpha = |\alpha\rangle\langle\alpha|$ is also called the density operator. The expectation value of any operator in a certain state is therefore equivalent to the trace of the product of this operator and the density matrix corresponding to that

state. Similarly, the density operator for a mixture state is defined as

$$\rho = \sum_{\alpha} p_{\alpha} P_{\alpha} = \sum_{\alpha} |\alpha\rangle p_{\alpha} \langle\alpha| \tag{2.2}$$

where p_{α} are the above mentioned probabilities of the system being in the corresponding states. Hence, the average expectation value of Ω over this mixture state is

$$\langle\Omega\rangle = \sum_{\alpha} p_{\alpha} \langle\alpha|\Omega|\alpha\rangle = \mathrm{Tr}(\Omega\rho) \tag{2.3}$$

In actual experiments, the finite size of the counter attenuates the correlation. This effect is accounted for by an efficiency matrix ϵ, a matrix whose eigenvalues specify the detection probability of the outgoing radiation. The efficiency matrix is a function of the geometric arrangement (positions and sizes) of the counters.

According to Eqn. 2.1, we choose the operator Ω as the efficiency matrix ϵ such that if a measurement W is made on a system (represented by mixture states) having density matrix ρ, then W is equal to the expectation value of the efficiency operator , i. e.,

$$W = \langle\epsilon\rangle = \mathrm{Tr}(\epsilon\rho) \tag{2.4}$$

W represents the probability that an event will be recorded in a detector, and in a nuclear scattering

reaction W is a function of the relative angle between the incident beam and the position of the detector.

2.1.2. Statistical Tensors, Efficiency Tensors, and the Tensor of a Vector Sum Formula

Under coordinate system rotations, tensors have definite and simple transformation properties. For practical convenience, a transformation relation between matrices and tensors is defined. If a density matrix is constructed by eigenfunctions $|B_1\beta_1\rangle$, $|B_2\beta_2\rangle$ of angular momenta B_1, B_2, then its associated irreducible tensor $\rho_{kn}(B_1 B_2)$ is defined as

$$\rho_{kn}(B_1 B_2) = \sum_{\beta_1\beta_2} (-1)^{B_1 - \beta_2} (B_1\beta_1 B_2 - \beta_2 | kn) \langle B_1 \beta_1 | \rho | B_2 \beta_2 \rangle \qquad (2.5)$$

Each term has 2k+1 parameters, labelled by n=-k,-k+1...,k, where $\vec{k}=\vec{B}_1 - \vec{B}_2$. Notice that the unobserved magnetic quantum number is eliminated in the tensor notation. In a similar manner, an efficiency tensor is defined as

$$\epsilon_{kn}(B_1 B_2) = \sum_{\beta_1\beta_2} (-1)^{B_2 - \beta_2} (B_1\beta_1 B_2 - \beta_2 | kn) \langle B_1 \beta_1 | \epsilon | B_2 \beta_2 \rangle \qquad (2.6)$$

Replacing matrices in Eqn. 2.3 by the corresponding

tensors, W is found to be

$$W=\mathrm{Tr}(\epsilon\rho)=\sum_{B_1\beta_1B_2\beta_2}\langle B_1\,\beta_1|\rho|B_2\,\beta_2\rangle\langle B_2\,\beta_2|\epsilon|B_1\,\beta_1\rangle^*$$

$$=\sum_{B_1\beta_1B_2\beta_2}\rho_{kn}(B_1\,B_2)\,\epsilon^*_{kn}(B_1\,B_2) \qquad (2.7)$$

Nuclear reactions consist of a succession of transitions, with each transition involving an initial and final state. In forming the total angular momentum of this system, a series of vector sums of two component angular momenta is repeatedly involved. One of the key points in developing the correlation theory is to express vector sums in terms of tensors. With the convenient symmetry properties of tensors, the evaluation of the trace is greatly simplified. This is done by the theorem called "Tensor of a Vector Sum".

Consider $\vec{B}$ as the sum of two angular momenta $\vec{C}$ and $\vec{j}'$; then the statistical tensor notation for $\vec{B}=\vec{C}+\vec{j}'$ can be stated as:

$$\rho_{k_Bn_B}(B_1\,B_2)=\sum_{k_cn_ck_{j'}n_{j'}}(k_c\,n_c\,k_{j'},n_{j'}\,|\,k_B\,n_B)\,\hat{k}_c\,\hat{k}_{j'}\,\hat{B}_1\,\hat{B}_2$$

$$\cdot\begin{Bmatrix} C_1 & j'_1 & B_1\\ C_2 & j'_2 & B_2\\ k_c & k_{j'} & k_B\end{Bmatrix}\cdot\rho_{k_cn_c}(C_1,C_2)\,\rho_{k_{j'}n_{j'}}(j'_1\,j'_2) \qquad (2.8)$$

where $\rho_{k_cn_c}(C_1,C_2)$, $\rho_{k_{j'}n_{j'}}(j'_1j'_2)$ are the statistical tensors of the respective angular momenta. The circumflex over

quantum number k means $\hat{k}=(2k+1)^{1/2}$, and the quantity in the bracket [] is the Wigner 9-j coefficient.

2.A.3 The General Angular Correlation Functions

Three angular momenta are involved in the transition of a nuclear reaction where particle absorption or emission occurs; the spins of the target and the particle, and the orbital angular momentum of the incident particle. There are two conventional ways of combining these momenta, the so-called channel spin representation (s-spin) and the angular momentum representation (j-spin). The general correlation functions for the inelastically scattered proton and the subsequent gamma-ray decay are given in both representations. As an example, the angular distribution for the proton decay in the channel spin representation is discussed; the other results are simply quoted.

The tensor form for the angular correlation equation W is evaluated by proceeding back through the successive transitions until the initial state is reached. For instance, in proton inelastic scattering a reaction scheme

in the channel spin representation is given as

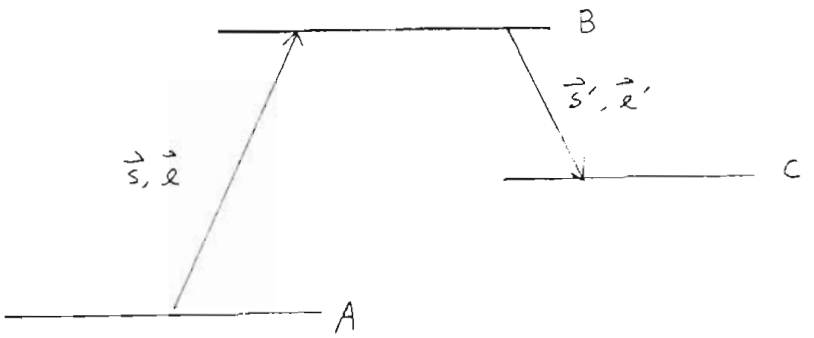

We start by examining the decomposition of state $\vec{B}$ into angular momentum $\vec{s}'$ and $\vec{l}'$.

The probability for a transition from one state to another in a time interval δt is proportional to $|R|^2\delta t$, where R is the reaction matrix and is related to the scattering matrix (Heisenberg (1943)) S by the relation $S=R+1$. The statistical tensor $\rho_{kn}(B_1 B_2)$ in Eqn. 2.7 describes the end products of this nuclear reaction. If the statistical tensor that describes the initial state is denoted as $\rho_{k_B n_B}(B_1 B_2)$, then the relation for the statistical tensor before and after a reaction is given by:

$$\rho_{kn}(B_1 B_2) = \rho_{kn}(B_1 s_1' l_1', B_2 s_2' l_2')$$
$$= \langle B_1 s_1' l_1' | R | B_1 \rangle \rho_{k_B n_B}(B_1 B_2) \langle B_2 s_2' l_2' | R | B_2 \rangle^* \qquad (2.9)$$

The statistical tensor $\rho_{k_B n_B}(B_1 B_2)$ in the above equation is then decomposed into the statistical tensors

$\rho_{k_s n_s}(s_1 s_2)$ and $\rho_{k_\ell n_\ell}(l_1 l_2)$ associated with the initial state by using the tensor-of-a-vector-sum formula. The efficiency tensor $\epsilon_{kn}(B_1 B_2)$ in Eqn. 2.7 is also decomposed into $\epsilon_{k_{s'} n_{s'}}(s_1' s_2')$ and $\epsilon_{k_{\ell'} n_{\ell'}}(l_1' l_2')$ (associated with the outgoing radiation) by using the tensor-of-a-vector-sum-formula. Hence, the angular correlation equation W is found to be:

$$W(\theta_{p'}) = \bar{\sum}(k_s\, n_s\, k_\ell\, n_\ell \mid k_B\, n_B)(k_{s'}\, n_{s'}\, k_{\ell'}\, n_{\ell'} \mid k_B\, n_B)\,\hat{k}_{s'}\,\hat{k}_s\,\hat{k}_{\ell'}\,\hat{k}_\ell\,(\hat{B}_1 \hat{B}_2)^2$$

$$\cdot \begin{Bmatrix} s_1 & l_1 & B_1 \\ s_2 & l_2 & B_2 \\ k_s & k_\ell & k_B \end{Bmatrix} \begin{Bmatrix} s_1' & l_1' & B_1 \\ s_2' & l_2' & B_2 \\ k_{s'} & k_{\ell'} & k_B \end{Bmatrix} \rho_{k_s n_s}(s_1 s_2)\, \rho_{k_\ell n_\ell}(l_1 l_2)$$

$$\cdot \epsilon_{k_{s'} n_{s'}}^{*}(s_1' s_2')\, \epsilon_{k_{\ell'} n_{\ell'}}^{*}(l_1' l_2') \langle B_1 s_1' l_1' \mid R_c \mid B_1 \rangle \langle B_2 s_2' l_2' \mid R_c \mid B_2 \rangle^{*} \tag{2.10}$$

The tensor parameters that arise from a plane wave state of particles are called radiation parameters (Ferguson 1965). In our reaction scheme, Eqn. 2.10 can be simplified for practical purposes by choosing appropriate parameters for $\rho_{k_s n_s}$, $\rho_{k_\ell n_\ell}$, $\epsilon_{k_{s'} n_{s'}}^{*}$ and $\epsilon_{k_{\ell'} n_{\ell'}}^{*}$. Here, for simplicity, only the final results for these radiation parameters are listed.

$$\rho_{k_s n_s}(s_1 s_2) = \frac{\hat{s}_1}{(\hat{A}\hat{i}_p)^2}\ \delta_{s_1 s_2}\ \delta_{A_1 A_2}\ \delta_{i_{p_1} i_{p_2}} \cdot \delta_{k_s 0}\ \delta_{n_s 0}\ \delta_{k_A 0}\ \delta_{n_A 0}\ \delta_{k_{i_p} 0}\ \delta_{n_{i_p} 0} \tag{2.11}$$

$$\rho_{k_\ell n_\ell}(l_1 l_2) = \frac{\hat{l}_1 \hat{l}_2}{4\pi}\ (-1)^{l_2}\ (l_1 0 l_2 0 | k_\ell 0)\ \delta_{n_\ell 0} \tag{2.12}$$

$$\epsilon^{*}_{k_{\ell'} n_{\ell'}}(l_1' l_2') = \frac{\hat{l}_1' \hat{l}_2'}{\sqrt{4\pi}\ \hat{k}_{\ell'}}\ (-1)^{l_2'}\ (l_1' 0 l_2' 0 | k_{\ell'} 0)\ Y^{*}_{k_{\ell'} n_{\ell'}}(\theta) \tag{2.13}$$

$$\epsilon^{*}_{k_{s'} n_{s'}}(s_1' s_2') = \hat{s}'\ \delta_{s_1' s_2'}\ \delta_{c_1 c_2}\ \delta_{i_{p_1'} i_{p_2'}}\ \delta_{k_{s'} 0}\ \delta_{n_{s'} 0} \cdot \delta_{k_{c0}}\ \delta_{n_{c0}}\ \delta_{k_{i_p' 0}}\ \delta_{n_{i_p' 0}} \tag{2.14}$$

Substituting these four radiation parameters back into Eqn. 2.10, we find the general formula for proton inelastic scattering in the channel spin representation. $W(\theta_{p'})$ and $W(\theta_\gamma)$ in the channel spin representation and the angular momentum representation are (Dittrich 1975):

1) Channel Spin Representation:

$$W(\theta_{p'}) = \sum (-1)^{s+s'-2B_2+1/2(l_2-l_1+l_2'-l_1')} (4\pi \hat{A} \hat{i}_p)^{-2}$$
$$\cdot Z(l_1 B_1 l_2 B_2; sk)\, Z(l_1' B_1 l_2' B_2; s'k)\, P_k(\theta_{p'})$$
$$\cdot \langle B_1 s' l_1' | R_c | B_1 \rangle \langle B_2 s' l_2' | R_c | B_2 \rangle^* \qquad (2.15)$$

$$W(\theta_\gamma) = \sum (-1)^{s-B_2-B_1-s_1'-s_2'-2C_2+D+l'+i_{p'}+L_2-L_1-1+1/2(l_2-l_1+7k)}$$
$$\cdot \frac{\hat{B}_1 \hat{B}_2 \hat{s}_1' \hat{s}_2' \hat{C}_1 \hat{C}_2 \hat{L}_1 \hat{L}_2}{8\pi (\hat{A} \hat{i}_p \hat{i}_{p'})^2} Z(l_1 B_1 l_2 B_2; sk)\, W(B_2 s_2' B_1 s_1'; l'k)$$
$$\cdot W(s_2' C_2 s_1' C_1; i_{p'} k)\, W(L_2 C_2 L_1 C_1; Dk)\, (L_1 1 L_2 - 1 | k0)\, P_k(\theta_\gamma)\, J_k$$
$$\cdot \langle B_1 s_1' l' | R_c | B_1 \rangle \langle B_2 s_2' l' | R_c | B_2 \rangle^*$$
$$\cdot \langle C_1 | R_D | C_1 D L_1 \rangle^* \langle C_2 | R_D | C_2 D L_2 \rangle \qquad (2.16)$$

2) Angular Momentum Representation:

$$W(\theta_{p'}) = \sum (-1)^{A-2B_2+C-2j_1-2j_1'+i_p+i_p'+3k+1/2(l_1-l_2+l_1'-l_2')}$$
$$\cdot (\hat{B}_1 \hat{B}_2)^2 (\hat{A} \hat{i}_p \hat{i}_{p'} 4\pi)^{-2} Z(l_1 j_1 l_2 j_2; i_p k)\, W(j_2 B_2 j_1 B_1; Ak)$$
$$\cdot Z(l_1' j_1' l_2' j_2'; i_{p'} k)\, W(j_2' B_2 j_1' B_1; ck)\, P_k(\theta_{p'})$$
$$\cdot \langle B_1 C_1 j_1' | R_c | B_1 \rangle \langle B_2 C_2 j_2' | R_c | B_2 \rangle^* \qquad (2.17)$$

$$W(\theta_\gamma) = \sum (-1)^{A-B_1-B_2-2C_2+D+i_p-2j_1+j'-L_1+L_2+(7/2)k+(1/2)(l_1-l_2)}$$
$$\cdot \frac{\hat{C}_1 \hat{C}_2 \hat{L}_1 \hat{L}_2 (\hat{B}_1 \hat{B}_2)^2}{8\pi (\hat{A} \hat{i}_p \hat{i}_{p'})^2} Z(l_1 j_1 l_2 j_2; i_p k) W(j_2 B_2 j_1 B_1; A k)$$
$$\cdot W(B_2 C_2 B_1 C_1; j' k) W(L_2 C_2 L_1 C_1; D k) (L_1 1 L_2 -1 | k 0) P_k(\theta_\gamma)$$
$$\cdot J_k \langle B_1 C_1 j' | R_c | B_1 \rangle \langle B_2 C_2 j' | P_c | B_2 \rangle^*$$
$$\cdot \langle C_1 | P_D | C_1 D L_1 \rangle^* \langle C_2 | P_D | C_2 D L_2 \rangle \qquad (2.18)$$

2.A.4 Matrix Element, Phase Shift, and Mixing Ratios

Considering the incident channel s_1 and l_1, the matrix element $\langle B_1 s_1' l_1' | R | B_1 \rangle$ in Eqn. 2.15 is equivalent to $\langle B_1 s_1' l_1' | R | B_1 s_1 l_1 \rangle$, which is given by Wigner and Eisenbud (1947) as:

$$\langle B_1 s_1' l_1' | R | B_1 s_1 l_1 \rangle \sim e^{i(\xi(l_1)+\xi(l_1'))} \frac{i \cdot a(s_1 l_1) g(s_1' l_1')}{E_0 - E - i\Gamma/2} \qquad (2.19)$$

where $a(s_1 l_1)$, $a(s_1' l_1')$ are real and equal to $\pm(\Gamma(s_1 l_1))^{1/2}$, $\pm(\Gamma(s_1' l_1'))^{1/2}$, respectively, $\Gamma(s_1 l_1)$ and $\Gamma(s_1' l_1')$ are the partial laboratory widths, Γ is the total width, and E_0 is the "effective" resonance energy. $\xi(l)$ is an energy dependent phase shift which contains a

Coulomb phase shift and a hard sphere phase shift, and is given by:

$$\xi(l) = -\tan^{-1}(F_\ell / G_\ell) + \sum_{m=1}^{l} \tan^{-1}(\eta/m) \qquad (2.20)$$

where F_ℓ, G_ℓ are respectively the regular and irregular radial wave functions associated with the particle, and η is the Coulomb parameter

$$\eta = 0.1574\ Z_0 Z_1 (m_1/E)^{1/2} \qquad (2.21)$$

where Z_0 and Z_1 are the charge numbers of the target nucleus and the incident particle, m_1 is the mass of the incident particle in atomic mass units, and E is the incident energy in the laboratory system in MeV. Therefore

$$\langle R_1 s_1' l_1' | R | B_1 s_1 l_1 \rangle \langle B_2 s_2' l_2' | R | B_2 s_2 l_2 \rangle^* \sim \frac{\cos(\xi(l_1) + \xi(l_2) - \xi(l_1') - \xi(l_2'))}{(E_0 - E)^2 + \Gamma^2/4} \cdot g(s_1 l_1) g(s_2 l_2) g(s_1' l_1') g(s_2' l_2') \qquad (2.22)$$

and

$$Y=\frac{\langle B_1 s_1' l_1' | R | B_1 s_1 l_1 \rangle}{\langle B_2 s_2' l_2' | R | B_2 s_2 l_2 \rangle}$$

$$=\cos(\xi(l_1)+\xi(l_1')-\xi(l_2)-\xi(l_2'))\cdot\frac{g(s_1 l_1)g(s_1' l_1')}{g(s_2 l_2)g(s_2' l_2')} \qquad (2.23)$$

Now $\Gamma_{\ell c}=2P_\ell \gamma_{\ell c}^2$, where P_ℓ is the Coulomb barrier penetrability and $\gamma_{\ell c}^2$ is the channel reduced width. Hence, if $l_1=l_2$ and $l_1'=l_2'$, then Y is equivalent to the mixing ratio δ which is defined as the ratio of two channel amplitude reduced widths, i.e.,

$$\delta=\frac{\gamma(s'l')}{\gamma(s'l')} \quad .$$

If $l_1=l_2$ and $l_1'\neq l_2'$, then

$$Y=\cos(\xi(l_1')-\xi(l_2'))\cdot\left(\frac{P(l_1')}{P(l_2')}\right)^{1/2}\cdot\delta$$

$$=\text{Phase}\cdot(\text{Pen}(l_1',l_2'))^{1/2}\cdot\delta$$

$$=(P\&P)\cdot\delta \qquad (2.24)$$

where $\text{Phase}=\cos(\xi(l_1')-\xi(l_2'))$, $\text{Pen}(l_1',l_2')=P(l_1')/P(l_2')$ and (P&P) denotes the product of the corresponding phase and the square root of the penetrability ratio, namely, the ratio between Y and δ.

Notice that $|Y|^2=\frac{g^2(s_1 l_1)\ g^2(s_1' l_1')}{g^2(s_2 l_2)\ g^2(s_2' l_2')}$ is independent of the phase shift. The values of Phase and Pen(0,2) for d-wave resonance energies in ^{49}V are listed in Table 2.1,

where the resonance numbers are taken from the previous elastic scattering work of Prochnow (1971), and the missing numbers mean the resonances are either too weak to be analyzed or omitted due to interference effects.

Table 2.1

Values of Resonance Phase Factor and Penetrability Ratio

Res. No.	E_r (MeV)	Phase $\cos(\xi(0)-\xi(2))$	Pen(0,2) Pen(0)/Pen(2)
5	2.2981	-0.63	19.00
8	2.3204	-0.62	18.79
9	2.3340	-0.62	18.65
10	2.3637	-0.61	18.37
14	2.4203	-0.60	17.84
17	2.4464	-0.59	17.60
19	2.4694	-0.59	17.39
20	2.4903	-0.58	17.20
22	2.5176	-0.58	16.96
24	2.5468	-0.57	16.70
25	2.5547	-0.57	16.63
26	2.5713	-0.57	16.49
28	2.5943	-0.56	16.29
29	2.5962	-0.56	16.28
32	2.6313	-0.55	15.98
33	2.6437	-0.55	15.88
35	2.6560	-0.55	15.77
36	2.6764	-0.55	15.60
37	2.6824	-0.54	15.56
39	2.6885	-0.54	15.51

Table 2.1 (continued)

Res. No.	E_p (MeV)	Phase $\cos(\xi(0)-\xi(2))$	Pen(0,2) Pen(0)/Pen(2)
40	2.6983	-0.54	15.43
41	2.7051	-0.54	15.37
43	2.7226	-0.54	15.23
44	2.7383	-0.53	15.10
50	2.7674	-0.53	14.87
51	2.7736	-0.53	14.82
52	2.7834	-0.52	14.75
53	2.7878	-0.52	14.71
54	2.7964	-0.52	14.65
55	2.8037	-0.52	14.59
56	2.8072	-0.52	14.56
58	2.8225	-0.52	14.44
59	2.8288	-0.52	14.40
60	2.8322	-0.52	14.37
63	2.8422	-0.51	14.29
65	2.8671	-0.51	14.10
67	2.8687	-0.51	14.09
68	2.8737	-0.51	14.05
69	2.8859	-0.51	13.96
70	2.8964	-0.50	13.89

Table 2.1 (continued)

Res. No.	E_p (MeV)	Phase $\cos(\xi(0) - \xi(2))$	Pen(0,2) Pen(0)/Pen(2)
71	2.9082	-0.50	13.80
72	2.9186	-0.50	13.72
74	2.9227	-0.50	13.69
75	2.9244	-0.50	13.68
76	2.9284	-0.50	13.65
77	2.9292	-0.50	13.64
78	2.9378	-0.50	13.58
79	2.9505	-0.49	13.49
80	2.9557	-0.49	13.45
82	2.9661	-0.49	13.38
83	2.9687	-0.49	13.36
84	2.9716	-0.49	13.34
85	2.9780	-0.49	13.29
86	2.9796	-0.49	13.28
87	2.9825	-0.49	13.26
88	2.9930	-0.49	13.18
89	2.9950	-0.49	13.17
90	2.9981	-0.49	13.15
91	3.0012	-0.49	13.12
92	3.0215	-0.48	12.98

Table 2.1 (continued)

Res. No.	E_p (MeV)	Phase $\cos(\xi(0) - \xi(2))$	Pen(0,2) Pen(0)/Pen(2)
93	3.0234	-0.48	12.97
94	3.0256	-0.48	12.95
95	3.0289	-0.48	12.93
96	3.0300	-0.48	12.92
97	3.0311	-0.48	12.91
98	3.0367	-0.48	12.88
99	3.0375	-0.48	12.87
100	3.0383	-0.48	12.86
101	3.0442	-0.48	12.82
102	3.0454	-0.48	12.82
103	3.0485	-0.48	12.79
104	3.0527	-0.48	12.76
105	3.0559	-0.48	12.74
106	3.0605	-0.48	12.71
107	3.0628	-0.48	12.70
108	3.0754	-0.47	12.61
109	3.0784	-0.47	12.59
110	3.0815	-0.47	12.57
111	3.0843	-0.47	12.55
112	3.0880	-0.47	12.52

2.A.5. The Coupling Scheme and D-Wave Angular Correlation Expressions

The angular momentum coupling scheme for the reaction $^{48}Ti(p,p\gamma)^{48}Ti$ with $l_p=2$ is shown in Fig. 2.1. There are three transitions involved in this reaction. The first transition is a process in which the target nucleus ^{48}Ti (in ground state 0^+) captures the incident proton and forms the compound nucleus ^{49}V. There are excited states with different angular momenta which can be formed in the compound nucleus. Wells (1978) performed a similar study on p-wave ($l_p=1$) resonances in ^{49}V; the present work is focussed on d-wave ($l_p=2$) resonances. The second transition is a de-excitation process in which the compound nucleus decays by proton emission and leaves the target nucleus in its first excited state (2^+). There are three outgoing inelastic channels open for $l_p' \leq 2$. Channels corresponding to $l_p'=4$ are neglected due to the very low Coulomb barrier penetrability. The first excited state then decays by gamma-ray emission and completes the third transition.

For convenience, the matrix elements and the amplitude reduced matrix elements are denoted as $\langle al'j' \rangle$ and $\langle a,l',j' \rangle$, respectively, where a corresponds to either angular momentum representation j or channel spin

Figure 2.1 Energy Level Scheme and Angular Momentum Coupling Scheme for the reaction $^{48}Ti(p,p'\gamma)^{48}Ti$.

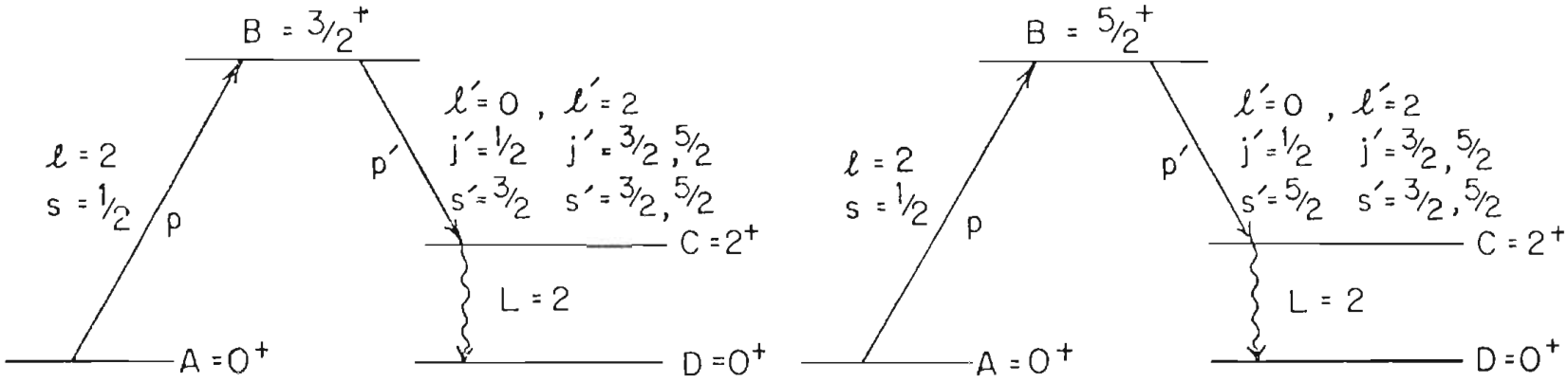

	ENTRANCE CHANNEL	EXIT CHANNEL
CHANNEL SPIN REPRESENTATION	$\vec{s} = \vec{A} + \vec{i}_p$ $\vec{B} = \vec{s} + \vec{\ell}$	$\vec{s}' = \vec{C} + \vec{i}_p$ $\vec{B} = \vec{s}' + \vec{\ell}'$
ANGULAR MOMENTUM REPRESENTATION	$\vec{j} = \vec{\ell} + \vec{i}_p$ $\vec{B} = \vec{A} + \vec{j}$	$\vec{j}' = \vec{\ell}' + \vec{i}_p$ $\vec{B} = \vec{C} + \vec{j}'$

representation s, l' is the orbital angular momentum of the outgoing inelastically scattered protons, and j' is twice the value of the channel total angular momentum. Namely

$$\langle B\ C\ j' | R | B \rangle = \langle jl'(2j') \rangle$$

$$\langle B\ l's' | R | B \rangle = \langle sl'(2s') \rangle \qquad (2.25)$$

and

$$\gamma(l',j') = g(l',j')/(2P(l'))^{1/2} = \langle j,l',2j' \rangle$$

$$\gamma(l',s') = g(s',l')/(2P(l'))^{1/2} = \langle s,l',2s' \rangle \qquad (2.26)$$

For instance, in the angular momentum representation, the matrix elements for three outgoing inelastic channels of a 5/2+ compound state are <j01>, <j23>, <j25>, and the corresponding amplitude reduced matrix elements are <j,0,1>, <j,2,3>, <j,2,5>. In the channel spin representation, the matrix elements are <s05>, <s23>, <s25>, and the amplitude reduced width matrix elements are <s,0,5>, <s,2,3>, <s,2,5>.

a) Angular Distributions for $5/2^+$ Compound States

1) Angular Momentum Representation:

$$W(\theta_{p'}) = (3/32\pi^2)\,(|\langle j01\rangle|^2+|\langle j23\rangle|^2+|\langle j25\rangle|^2)$$
$$-(3/280\pi^2)\cdot\{|\langle j23\rangle|^2-|\langle j25\rangle|^2$$
$$-(24/7)\,(\langle j23\rangle\langle j25\rangle^*+\langle j25\rangle\langle j23\rangle^*)$$
$$-2\sqrt{14}\,(\langle j01\rangle\langle j23\rangle^*+\langle j23\rangle\langle j01\rangle^*)$$
$$+(3\sqrt{14}/2)\,(\langle j01\rangle\langle j25\rangle^*+\langle j25\rangle\langle j01\rangle^*)\}\cdot P_2(\cos\theta_{p'})$$
$$-9/224\pi^2\cdot\{|\langle j25\rangle|^2+12/7\cdot(\langle j23\rangle\langle j25\rangle^*$$
$$+\langle j25\rangle\langle j23\rangle^*)\}\cdot P_4(\cos\theta_{p'}) \qquad (2.27)$$

$$W(\theta_\gamma) = \{(-3/16\pi)\,(|\langle j01\rangle|^2+|\langle j23\rangle|^2+|\langle j25\rangle|^2)\cdot J_0$$
$$-(3/28\pi)\,(|\langle j01\rangle|^2+5/14\cdot(|\langle j23\rangle|^2-|\langle j25\rangle|^2))$$
$$\cdot J_2\cdot P_2(\cos\theta_\gamma)$$
$$+(3/28\pi)\,(|\langle j01\rangle|^2-9/7|\langle j23\rangle|^2+9/14|\langle j25\rangle|^2)$$
$$\cdot J_4\cdot P_4(\cos\theta_\gamma)\}$$
$$\cdot\langle C_1|P_D|C_1 D\,L_1\rangle^*\langle C_2|P_D|C_2 D L_2\rangle \qquad (2.28)$$

Two independent mixing ratios δ_1 and δ_2 are defined as

$$\delta_1 = \frac{\langle j,1,1\rangle}{\langle j,2,3\rangle}\ , \qquad \delta_2 = \frac{\langle j,2,5\rangle}{\langle j,2,3\rangle}$$

Then

$$W(\theta_{p'}) \sim 1 - \frac{4}{35} \frac{1 - \delta_2^2 - (48/7)\delta_2 - 4\sqrt{14}\cdot(P\&P)\delta_1 + 3\sqrt{14}\cdot(P\&P)\delta_1\delta_2}{1 + pen(0,2)\delta_1^2 + \delta_2^2} P_2(\cos\theta_{p'})$$

$$- \frac{3}{7} \frac{\delta_2^2 + (24/7)\delta_2}{1 + pen(0,2)\delta_1^2 + \delta_2^2} P_4(\cos\theta_{p'}) \qquad (2.29)$$

$$W(\theta_\gamma) \sim 1 + \frac{(4/7)(pen(0,2)\delta_1^2 + (5/14)\cdot(1-\delta_2^2))}{1 + pen(0,2)\delta_1^2 + \delta_2^2} Q_2 P_2(\cos\theta_\gamma)$$

$$+ \frac{(-4/7)(pen(0,2)\delta_1^2 - 8/7 + (9/14)\delta_2^2)}{1 + pen(0,2)\delta_1^2 + \delta_2^2} Q_4 P_4(\cos\theta_\gamma) \qquad (2.30)$$

where $Q_{kL} = J_{kL}/J_o$ is the attenuation factor. For the charged particle detectors, $Q_{kL} \approx 1$, and is therefore not included in the angular distribution expressions for inelastically scattered protons. The attentuation factors for 3"x3" NaI(Tl) gamma-ray detectors are tabulated in Ferguson(1965). The factors Pen(0,2) and (P&P) are defined in sec. 2.A.4.

2) Channel Spin Representation:

$$W(\theta_{p'}) = 3/16\pi^2 (|\langle s05\rangle|^2 + |\langle s23\rangle|^2 + |\langle s25\rangle|^2)$$
$$+ \{(15/196\pi^2)|\langle s23\rangle|^2 - (15/196\pi^2)|\langle s25\rangle|^2$$
$$- (3\sqrt{14}/56\pi^2)(\langle s05\rangle\langle s25\rangle^* + \langle s25\rangle\langle s05\rangle^*)\} P_2(\cos\theta_{p'})$$
$$+ \{(-9/49\pi^2)|\langle s23\rangle|^2 + (81/784\pi^2)|\langle s25\rangle|^2\} P_4(\cos\theta_{p'}) \qquad (2.31)$$

$$W(\theta_\gamma) = (3/16\pi)(|\langle s05\rangle|^2 + |\langle s23\rangle|^2 + |\langle s25\rangle|^2) \cdot J_0$$
$$+ \{(3/28\pi)|\langle s05\rangle|^2 - (3/280\pi)|\langle s23\rangle|^2 + (3/280\pi)|\langle s25\rangle|^2$$
$$- (9/245\pi)(\langle s23\rangle\langle s25\rangle^* + \langle s25\rangle\langle s23\rangle^*)\} \cdot J_2 P_2(\cos\theta_\gamma)$$
$$+ \{-(3/28\pi)|\langle s05\rangle|^2 + (3/56\pi)|\langle s25\rangle|^2$$
$$- (9/99\pi)(\langle s23\rangle\langle s25\rangle^* + \langle s25\rangle\langle s23\rangle^*)\} \cdot J_4 P_4(\cos\theta_\gamma) \qquad (2.32)$$

Two independent mixing ratios δ_1, δ_2 are defined as:

$$\delta_1 = \frac{\langle s,0,5\rangle}{\langle s,2,3\rangle} \quad , \quad \delta_2 = \frac{\langle s,2,5\rangle}{\langle s,2,3\rangle}$$

Then

$$W(\theta_{p'}) \sim 1 + \frac{20/49 - 20/49 \cdot \delta_2^2 - (4\sqrt{14}/7) \cdot (2\mathcal{P}) \delta_1 \delta_2}{1 + \text{pen}(0,2)\delta_1^2 + \delta_2^2} P_2(\cos\theta_{p'})$$

$$+ \frac{(-48/49)(\text{pen}(0,2)\delta_1^2) + (27/49)\delta_2^2}{1 + \text{pen}(0,2)\delta_1^2 + \delta_2^2} P_4(\cos\theta_{p'}) \qquad (2.33)$$

$$W(\theta_\gamma) \sim 1 + \frac{(4/7)\,\text{pen}(0,2)\delta_1^2 + 2/35 \cdot (\delta_2^2 - 1) - 96/245 \cdot \delta_2}{1 + \text{pen}(0,2)\delta_1^2 + \delta_2^2} \cdot Q_2 P_2(\cos\theta_\gamma)$$

$$+ \frac{(-4/7)\,\text{pen}(0,2)\delta_1^2 + (2/7)\delta_2^2 - (48/49)\delta_2}{1 + \text{pen}(0,2)\delta_1^2 + \delta_2^2} \cdot Q_4 P_4(\cos\theta_\gamma) \qquad (2.34)$$

b) Angular Distributions for 3/2+ Compound States

1) Angular Momentum Representation:

$$\begin{aligned} W(\theta_{p'}) = {} & 1/16\pi^2 \cdot (|\langle j01\rangle|^2 + |\langle j23\rangle|^2 + |\langle j25\rangle|^2) \\ & + 1/8\pi^2 \cdot \{-(3/10) \cdot |\langle j23\rangle|^2 - (2/35) \cdot |\langle j25\rangle|^2 \\ & + 21/35 \cdot (\langle j23\rangle\langle j25\rangle^* + \langle j25\rangle\langle j23\rangle^*) \\ & - 1/5 \cdot (\langle j01\rangle\langle j23\rangle^* + \langle j23\rangle\langle j01\rangle^*) \\ & - 21/10 (\langle j01\rangle\langle j25\rangle^* + \langle j25\rangle\langle j01\rangle^*)\} P_2(\cos\theta_{p'}) \end{aligned}$$

(2.35)

$$W(\theta_\gamma) = -1/8\pi \cdot (|\langle j01\rangle|^2 + |\langle j23\rangle|^2 + |\langle j25\rangle|^2) \cdot J_0$$
$$-1/8\pi\,(1/2) \cdot |\langle j01\rangle|^2 - (5/14) \cdot |\langle j25\rangle|^2) \cdot J_2\, P_2(\cos\theta_\gamma) \tag{2.36}$$

Two independent mixing ratios δ_1, δ_2 are defined as:

$$\delta_1 = \frac{\langle j,0,1\rangle}{\langle j,2,3\rangle} \quad , \quad \delta_2 = \frac{\langle j,2,5\rangle}{\langle j,2,3\rangle}$$

Then

$$W(\theta_{p'}) \sim 1 + \frac{ZZ}{1+\text{pen}(0,2)\,\delta_1^2+\delta_2^2}\, P_2(\cos\theta_{p'}) \tag{2.37}$$

where

$$ZZ = -(4/35)\,\delta_1^2 - 2\sqrt{21}/5 \cdot (P\&P)\,\delta_1\,\delta_2 - 4/5 \cdot (P\&2)\,\delta_1$$
$$+ (4\sqrt{21}/35) \cdot \delta_2 - 3/5$$

$$W(\theta_\gamma) \sim 1 + \frac{(1/2) \cdot \text{pen}(0,2)\,\delta_1^2 - (5/14) \cdot \delta_2^2}{1+\text{pen}(0,2)\,\delta_1^2+\delta_2^2}\, P_2(\cos\theta_\gamma) \tag{2.38}$$

2) Channel Spin Representation:

$$W(\theta_{p'}) = 1/8\pi^2 \cdot (|\langle s03\rangle|^2 + |\langle s23\rangle|^2 + |\langle s25\rangle|^2) - 1/8\pi^2 \cdot \{(\langle s03\rangle\langle s23\rangle^* + \langle s23\rangle\langle s03\rangle^*) + 5/7 \cdot |\langle s25\rangle|^2\} P_2(\cos\theta_{p'}) \quad (2.39)$$

$$W(\theta_\gamma) = 1/8\pi \cdot (|\langle s03\rangle|^2 + |\langle s23\rangle|^2 + |\langle s25\rangle|^2) \cdot J_0 + 1/16\pi \cdot \{(|\langle s23\rangle|^2 - 3/5 \cdot |\langle s23\rangle|^2 - 4/35 \cdot |\langle s25\rangle|^2 - 2\sqrt{21}/35 \cdot (\langle s23\rangle\langle s25\rangle^* + \langle s25\rangle\langle s23\rangle^*)\} \cdot J_2 P_2(\cos\theta_\gamma) \quad (2.40)$$

Two independent mixing ratios δ_1, δ_2 are defined as:

$$\delta_1 = \frac{\langle s,0,5\rangle}{\langle s,2,3\rangle} \quad , \quad \delta_2 = \frac{\langle s,2,5\rangle}{\langle s,2,3\rangle}$$

Then

$$W(\theta_{p'}) \sim 1 + \frac{-(5/7)\delta_2^2 - 2 \cdot (P\&P) \cdot \delta_1}{1 + \text{pen}(0,2)\delta_1^2 + \delta_2^2} P_2(\cos\theta_{p'}) \quad (2.41)$$

$$W(\theta_\gamma) \sim 1 + \frac{1/2 \cdot (\text{pen}(0,2)\delta_1^2) - 3/10 - 2/35 \cdot \delta_2^2 - 2\sqrt{21}/35 \cdot \delta_2}{1 + \text{pen}(0,2)\delta_1^2 + \delta_2^2} \cdot Q_2 P_2(\cos\theta_\gamma) \quad (2.42)$$

2.A.6 Transformation Equations

The relation between any reduced matrix element in the channel spin representation and the corresponding reduced matrix elements in the angular momentum representation is given by Satchler(1955) and Goldfarb(1959).

$$\langle C|s'|B\rangle=\sum_{j'}\langle C|j'|B\rangle(-1)^{l'+i_{p'}-j'}\hat{s}'\hat{j}'W(c\ i_{p'}B\ l';s'j') \tag{2.43}$$

i) For B=5/2+ compound states, Eqn. 2.43 reduces to

$$\langle s,2,3\rangle = 3/5\cdot\langle j,2,3\rangle+4/5\cdot\langle j,2,5\rangle \tag{2.44}$$

$$\langle s,2,5\rangle=-4/5\cdot\langle j,2,3\rangle+3/5\cdot\langle j,2,5\rangle \tag{2.45}$$

Define $\delta_{s'_{35}} = \dfrac{\langle s,2,3\rangle}{\langle s,2,5\rangle}$, $\delta_{j'_{35}} = \dfrac{\langle j,2,3\rangle}{\langle j,2,5\rangle}$

Then Eqn. 2.44 and Eqn. 2.45 yield

$$\delta_{s'_{35}} = \tan(\tan^{-1}\delta_{j'_{35}}+\tan^{-1}(4/3))$$

Therefore

$$\tan^{-1}\delta_{s'_{35}}=\tan^{-1}\delta_{j'_{35}}+\tan^{-1}(4/3)$$

This is equivalent to

$$\phi_{s'_{35}}=\phi_{j'_{35}}+53.13^{\circ}$$

Hence, there is a linear relation between $j\text{-}\phi_{53}$ and $s\text{-}\phi_{53}$.

ii) For $B=3/2^+$ compound states, Eqn. 2.43 reduces to

$$\langle s,0,3\rangle=\langle j,0,1\rangle \tag{2.46}$$

and

$$\langle s,2,3\rangle= \sqrt{2}/5\langle j,2,3\rangle +\sqrt{21}/5\langle j,2,5\rangle \tag{2.47}$$

$$\langle s,2,5\rangle=-\sqrt{21}/5\langle j,2,3\rangle+2/5\langle j,2,5\rangle \tag{2.48}$$

Define $\delta_{s'_{35}}=\dfrac{\langle s,2,3\rangle}{\langle s,2,5\rangle}$, $\delta_{j'_{35}}=\dfrac{\langle j,2,3\rangle}{\langle j,2,5\rangle}$

Then Eqn. 2.47 and Eqn. 2.48 yield

$$\delta_{s'_{35}}=\tan(\tan^{-1}\delta_{j'_{35}}+\tan^{-1}(\sqrt{21}/2))$$

Therefore

$$\tan^{-1}\delta_{s'_{35}}=\tan^{-1}\delta_{j'_{35}}+\tan^{-1}(\sqrt{21}/2)$$

This is equivalent to

$$\phi_{s'_{35}}=\phi_{j'_{35}}+66.42^\circ$$

This is the linear relation between $j\text{-}\phi_{35}$ and $s\text{-}\phi_{35}$.

2.A.7. Properties of $5/2^+$ Compound States

a) Physical Range of a_{2g} and a_{4g}

In the angular momentum representation, we denote the mixing ratios $\delta_{31}, \delta_{51}, \delta_{53}$ as follows:

$$\delta_{31} = \frac{\langle j,2,3\rangle}{\langle j,0,1\rangle} \qquad \delta_{51} = \frac{\langle j,2,5\rangle}{\langle j,0,1\rangle} \qquad \delta_{53} = \frac{\langle j,2,5\rangle}{\langle j,2,3\rangle}$$

Only two are independent. Following Eqn. 2.28, we may rewrite a_{2g}, a_{4g} in terms of δ_1 and δ_2, thus

$$a_{2g} = \frac{4/7\,(1+(5/14)\,\delta_{31}^2-(5/14)\,\delta_{51}^2)}{1+\delta_{31}^2+\delta_{51}^2}$$

$$a_{4g} = \frac{-4/7\,(1-(8/7)\,\delta_{31}^2+(9/14)\,\delta_{51}^2)}{1+\delta_{31}^2+\delta_{51}^2} \qquad (2.49)$$

Solving δ_{31}, δ_{51} in terms of a_{2g}, a_{4g}, we obtain

$$\delta_{31} = \pm \sqrt{\frac{5a_{2g} + 19a_{4g} + 8}{5(5a_{2g} - 2a_{4g} + 2/7)}}$$

$$\delta_{51} = \pm \sqrt{\frac{-3(10a_{2g} + 3a_{4g} - 4)}{5(5a_{2g} - 2a_{4g} + 2/7)}}$$

$$\delta_{35} = \pm \sqrt{\frac{-3(10a_{2g} + 3a_{4g} - 4)}{5a_{2g} + 19a_{4g} + 8}} \qquad (2.50)$$

Since $\delta_{31}^2 \geq 0$, $\delta_{51}^2 \geq 0$, $\delta_{35}^2 \geq 0$, there are three restrictions on the physical region of a_{2g} and a_{4g}:

$$(5a_{2g} + 19a_{4g} + 8)(5a_{2g} - 2a_{4g} + 2/7) \geq 0$$

$$-(10a_{2g} + 3a_{4g} - 4)(5a_{2g} - 2a_{4g} + 2/7) \geq 0$$

$$-(10a_{2g} + 3a_{4g} - 4)(5a_{2g} + 19a_{4g} + 8) > 0 \qquad (2.51)$$

The physical region that satisfies the above restrictions is shown by a triangle in Fig. 2.2. Obviously the three edges of this triangle (lines $5a_{2g} - 2a_{4g} + 2/7 = 0$, $5a_{2g} + 19a_{4g} + 8 = 0$ and $10a_{2g} + 3a_{4g} - 4 = 0$) represent $\langle j,0,1\rangle = 0$, $\langle j,2,3\rangle = 0$ and $\langle j,2,5\rangle = 0$, respectively. The intersection point $(4/7, -4/7)$ of lines $\langle j,2,3\rangle = 0$ and $\langle j,2,5\rangle = 0$ represents 100% $1' = 0$, i.e., the $1' = 2$ admixture ϵ^2 is zero.

Figure 2.2 The Physical Region of Legendre Polynomial Coefficients a_2, a_4 in the Angular Momentum Representation.

ANGULAR MOMENTUM REPRESENTATION

$D-5/2^{+}$ – STATES

AMPLITUDE REDUCED MATRIX

$\langle a, \ell', 2j' \rangle$

a = j - spin

ℓ' = ORBITAL ANGULAR MOMENTUM

j' = TOTAL ANGULAR MOMENTUM

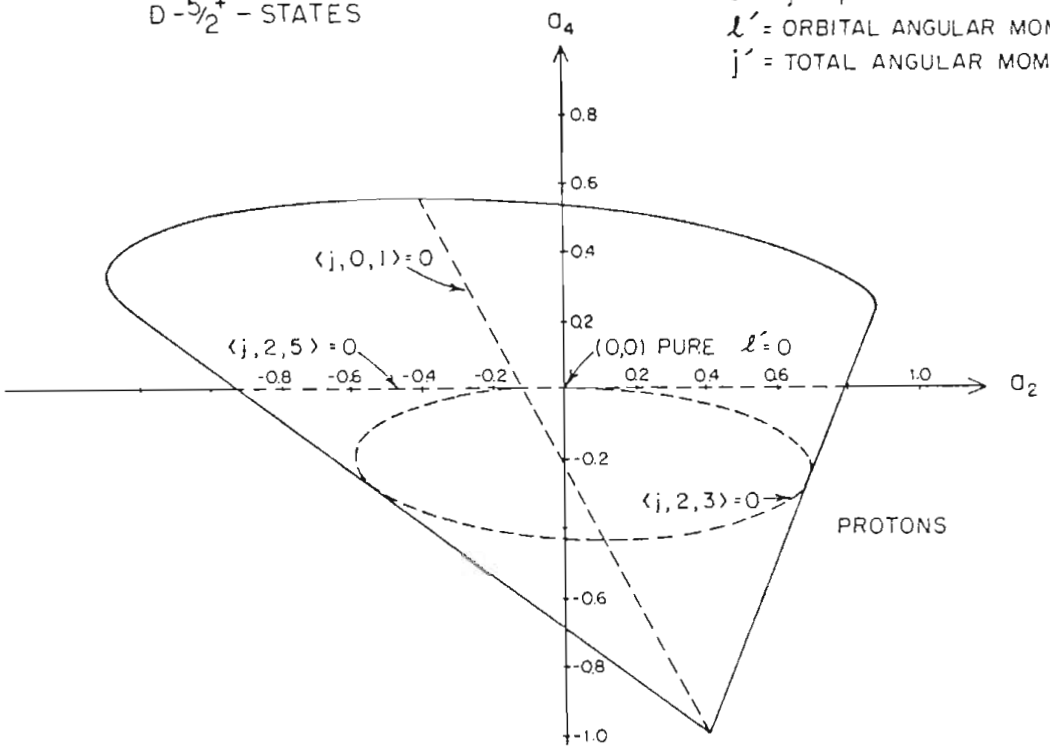

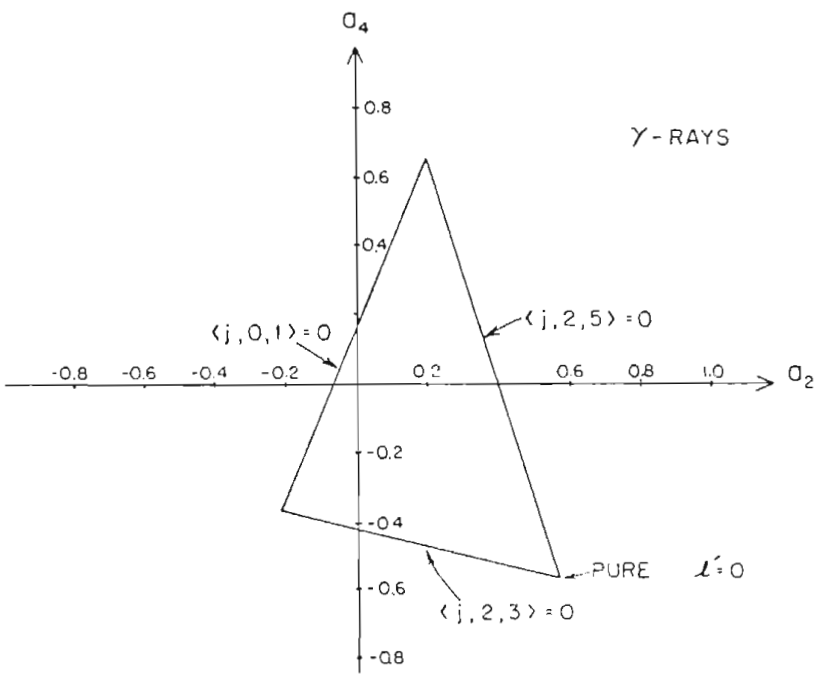

In the channel spin representation, the measured values of a_{2g} and a_{4g} are obviously the same as in the angular momentum representation. However, the lines which represent $\langle s,2,5\rangle=0$ and $\langle s,2,3\rangle=0$ will be quite different from the lines representing limiting cases in the angular momentum representation.

To find the line for $\langle s,0,5\rangle=0$, we may set the corresponding matrix element $\langle s05\rangle=0$ in the angular distribution Eqn. 2.32 This yields

$$W(\theta_\gamma) \sim (3/16\pi)(|\langle s23\rangle|^2+|\langle s25\rangle|^2)\cdot J_0$$
$$+\{(-3/280\pi)|\langle s23\rangle|^2+(3/280\pi)|\langle s25\rangle|^2$$
$$-(\sqrt{6}/245\pi)(\langle s23\rangle\langle s25\rangle^*+\langle s25\rangle\langle s23\rangle^*)\}\cdot J_2 P_2(\cos\theta_\gamma)$$
$$+\{(3/56\pi)|\langle s25\rangle|^2-(9/98\pi)(\langle s23\rangle\langle s25\rangle^*$$
$$+\langle s25\rangle\langle s23\rangle^*)\}\cdot J_4 P_4(\cos\theta_\gamma) \qquad (2.52)$$

Define $\delta=\dfrac{\langle s,2,5\rangle}{\langle s,2,3\rangle}$, then the Legendre polynomial coefficients a_{2g}, a_{4g} are

$$a_{2g} = \frac{-2/35+(2/35)\zeta^2-(96/245)\zeta}{1+\zeta^2}$$

$$a_{4g} = \frac{(2/7)\zeta^2-(48/49)}{1+\zeta^2} \qquad (2.53)$$

This is equivalent to

$$(a_{2g}-2/35)\zeta^2+(96/245)\zeta+(a_{2g}+2/35)=0$$

$$(a_{4g}-2/7)\zeta^2+(48/49)\zeta+a_{4g}=0 \qquad (2.54)$$

Eliminating the linear term from the above two equations, we obtain

$$(-a_{2g}+(2/5)a_{4g}-2/35)(\zeta^2+1)=0 \qquad (2.55)$$

Since $\zeta^2+1\neq 0$ then $-a_{2g}+(2/5)a_{4g}-2/35=0$. Hence the line $35a_{2g}-14a_{4g}+2=0$ represents the amplitude $\langle s,2,5\rangle=0$ as well as $\langle j,0,5\rangle=0$. Following the same procedure, we find that line $35a_{2g}+21a_{4g}-8=0$ and line $70a_{2g}+77a_{4g}+4=0$ correspond to $\langle s,2,3\rangle=0$ and $\langle s,2,5\rangle=0$, respectively. The allowed physical region of a_{2g} and a_{4g} for the channel spin representation is shown in Fig 2.3.

The Coulomb barrier penetrability ratio of P(l'=2) to P(l'=0) for inelastically scattered protons leaving the target nucleus ^{48}Ti in its first excited state (.983 MeV) is about 0.05 at 2 MeV incident proton energy and about 0.08 at 3 MeV. It is therefore expected that most of the

Figure 2.3 Physical Region of Legendre Polynomial Coefficients a_2, a_4 in the Channel Spin Representation.

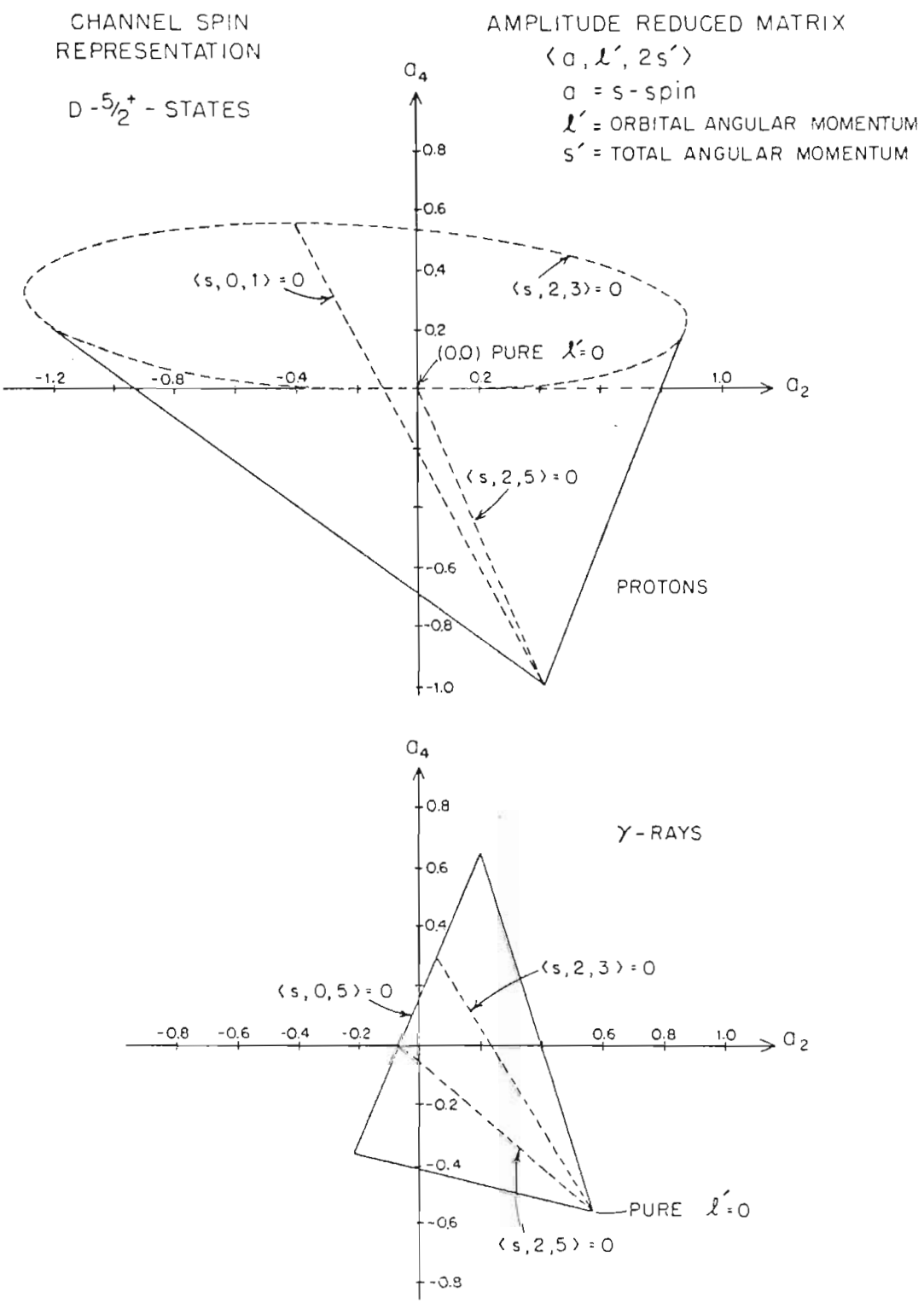
CHANNEL SPIN
REPRESENTATION
D -5/2+ - STATES
AMPLITUDE REDUCED MATRIX
⟨a, ℓ′, 2s′⟩
a = s-spin
ℓ′ = ORBITAL ANGULAR MOMENTUM
s′ = TOTAL ANGULAR MOMENTUM
a4
a2
0.8
0.6
0.4
0.2
-0.2
-0.4
-0.6
-0.8
-1.0
-1.2
1.0
⟨s, 0, 1⟩ = 0
⟨s, 2, 3⟩ = 0
(0,0) PURE ℓ′=0
⟨s, 2, 5⟩ = 0
PROTONS
γ-RAYS
⟨s, 2, 3⟩ = 0
⟨s, 0, 5⟩ = 0
PURE ℓ′=0
⟨s, 2, 5⟩ = 0

resonances will have (a_{2g}, a_{4g}) values falling near the $\epsilon^2=0$ point $(4/7, -4/7)$. The experimental (a_{2g}, a_{4g}) values for 45 5/2+ resonances are plotted in Fig. 2.4.

b) Physical Range of a_{2p} and a_{4p}

Since a_{2p} contains a phase factor which is energy dependent, the physically allowed range of a_{2p} and a_{4p} is also energy dependent.

Define two matrix element mixing ratios δ_1, δ_2 as

$$\delta_1 = \frac{\langle s,0,5\rangle}{\langle s,2,5\rangle} \quad , \quad \delta_2 = \frac{\langle s,2,3\rangle}{\langle s,2,5\rangle}$$

Eqn. 2.31 reduces to

$$a_{2p} = \frac{(20/49)\delta_2^2 - 20/49 - (4\sqrt{14}/7)\cdot(P\&P)\delta_1}{1+\text{pen}(0,2)\delta_1^2+\delta_2^2} \tag{2.56}$$

$$a_{4p} = \frac{-(48/49)\delta_2^2 + 27/49}{1+\text{pen}(0,2)\delta_1^2+\delta_2^2} \tag{2.57}$$

The above two equations are equivalent to

Figure 2.4 The Experimental Legendre Polynomial Coefficients for Forty Five 5/2+ resonances. The Phase^2 factor for the proton physical region is ~ 0.4.

ANGULAR DISTRIBUTIONS FOR INELASTIC SCATTERING FROM $5/2^+$ RESONANCES

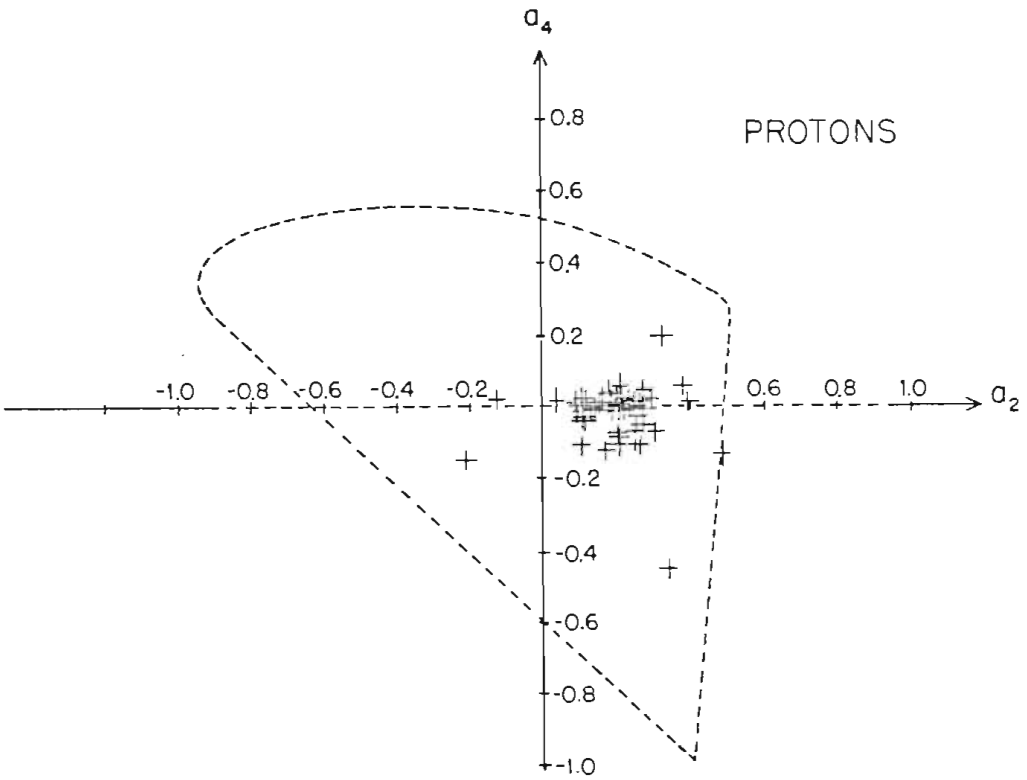

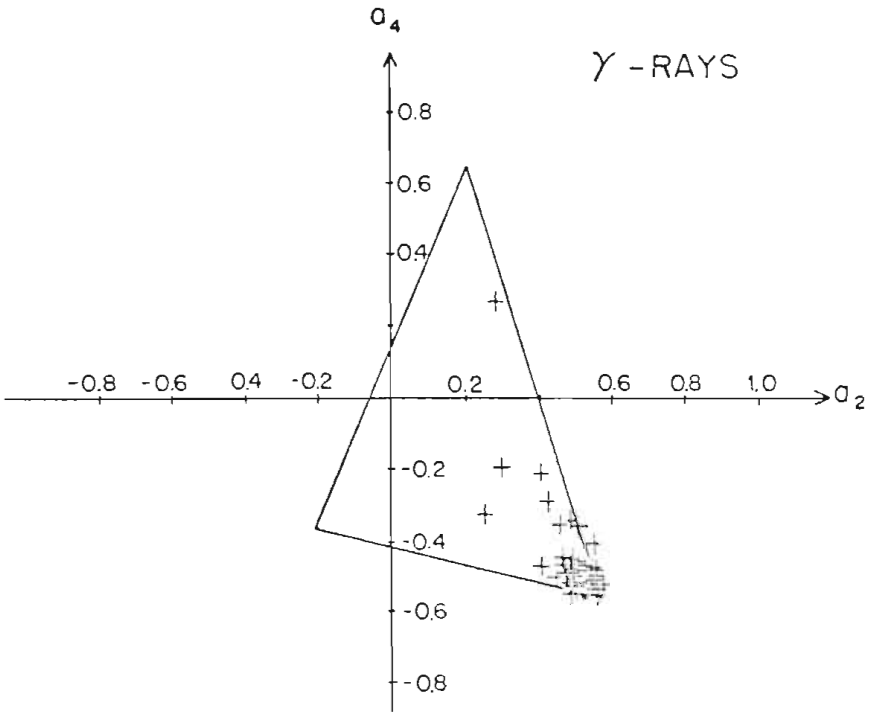

$$\text{pen}(0,2)\, a_{2P}\, \delta_1^2 + (a_{2P} - 20/49)\, \delta_2^2 + 4\sqrt{14}/7 \bullet (P\&P)\, \delta_1 + (a_{2P} + 20/49) = 0$$

$$\text{pen}(0,2)\, a_{4P}\, \delta_1^2 + (a_{4P} + 48/49)\, \delta_2^2 + \quad 0 \quad + (a_{4P} - 27/49) = 0$$

(2.58)

Eliminating from the above two equations, we obtain:

$$A \bullet \delta_1^2 + B \bullet \delta_1 + C = 0 \tag{2.59}$$

where $A = \text{pen}(0,2)\,(48/49 \bullet a_{2P} + 20/49 \bullet a_{4P})$

$B = 4\sqrt{14}/7 \bullet (P\&P)\,(a_{4P} + 48/49)$

$C = 5/49 \bullet (15 a_{2P} + 8 a_{4P} + 12/7)$

Since δ_1 is real, this implies that the discriminant term $B^2 - 4AC \geq 0$. This condition reduces to

$$6300 a_{2P}^2 - (4802 \bullet \text{phase}^2 - 1400) a_{4P}^2 + 5985 a_{2P} a_{4P} + 720 a_{2P}$$
$$- (9408 \bullet \text{phase}^2 - 300) a_{4P} - 4608 \bullet \text{phase}^2 \leq 0 \tag{2.60}$$

If $\text{phase}^2 = 1$, the above condition is equivalent to:

$$(5 a_{2P} - 2 a_{4P} - 4)(140 a_{2P} + 189 a_{4P} + 128) \leq 0 \tag{2.61}$$

Beyond this point, the analytic method for determining the physical region of a_{2P} and a_{4P} encounters difficulties because of the existence of the first order term δ_1 in Eqn. 2.58. Therefore solutions for mixing ratios in terms of a_{2P}, a_{4P} can not be easily obtained, and information about other restrictions on the physical region of a_{2P} and a_{4P} is lost. However, empirically we can generate the physical region of a_{2P} and a_{4P} simply by inserting the limiting values of $\phi_1 = \tan^{-1} \delta_1 (-90^\circ \leq \phi_1 \leq 90^\circ)$ and

$\phi_2 = \tan^{-1}\delta_2 (-90° \leq \phi_2 \leq 90°)$ back into Eqn. 2.56 and 2.57. We found one more restriction which is an elliptical upper limit. For the case of phase^2=1, this ellipse is described by the equation: $81 \cdot a_{2p}^2 + 1264 \cdot a_{4p}^2 + 120 \cdot a_{2p} \cdot a_{4p} - 672 \cdot a_{4p} = 0$. The physical region of a_{2p}, a_{4p} for the case of phase^2=1 is shown in Fig. 2.2 and Fig. 2.3 for the angular momentum representation and channel spin representation, respectively. As the value of phase^2 decreases, the physical region also shrinks; an example for the case of phase$^2 \sim 0.4$ is shown in Fig. 2.4.

The lines or curves representing the vanishing of the three inelastic amplitudes are also of interest. In the angular momentum representation, in order to find the curve for $\langle j,2,3\rangle = 0$ we set the corresponding matrix element $\langle j23\rangle = 0$ in the angular correlation Eqn. 2.27 and $W(\theta_{p'})$ reduces to

$$
\begin{aligned}
W(\theta_{p'}) \sim\ & (3/32\pi^2)\,(|\langle j01\rangle|^2 + |\langle j25\rangle|^2) \\
& - (3/280\pi^2)\,\{-|\langle j25\rangle|^2 + 3\sqrt{14}/2 \cdot (\langle j01\rangle\langle j25\rangle^* \\
& + \langle j25\rangle\langle j01\rangle^*)\}\, P_2(\cos\theta_{p'}) \\
& - (9/224\pi^2)\,|\langle j25\rangle|^2\, P_4(\cos\theta_{p'})
\end{aligned}
\qquad (2.62)
$$

Define $\zeta = \dfrac{\langle j,2,5\rangle}{\langle j,0,1\rangle}$, then the Legendre polynomial coefficients a_{2P}, a_{4P} are

$$a_{2P} = \frac{(4/35)\cdot Pen(0,2)\cdot\zeta^2 - 12\sqrt{14}/35\cdot(P\&P)\cdot\zeta}{1+pen(0,2)\zeta^2}$$

$$a_{4P} = \frac{-(3/7)\cdot pen(0,2)\cdot\zeta^2}{1+pen(0,2)\cdot\zeta^2} \qquad (2.63)$$

Using the above two equations to cancel ζ , we obtain the following relation

$$225a_{2P}^2+(16+2016\cdot phase^2)a_{4P}^2+120a_{2P}a_{4P}+864\cdot phase^2\cdot a_{4P}=0 \qquad (2.64)$$

If $phase^2=1$, this equation reduces to

$$225a_{2P}^2+2032a_{4P}^2+120a_{2P}a_{4P}+864a_{4P}=0 \qquad (2.65)$$

Following the same method, we find the line $a_{4P}=0$ represents $\langle j,2,5\rangle=0$ and the line $3a_{2P}+3/5\cdot a_{4P}+12/35=0$ represents $\langle j,0,1\rangle=0$. These two lines are independent of the phase parameter. The physical region for a_{2P} and a_{4P} and its corresponding curve for $\langle j,0,1\rangle=0$, $\langle j,2,3\rangle=0$ and $\langle j,2,5\rangle=0$ in the angular momentum representation are shown in Fig. 2.3 for case of $phase^2=1$.

In the channel spin representation, the physical

region is the same as in the angular momentum representation; however, the curves or lines corresponding to $\langle s,0,5\rangle=0$, $\langle s,2,3\rangle=0$, and $\langle s,2,5\rangle=0$ must be obtained. In order to derive the curve for $\langle s,2,3\rangle=0$, we set the corresponding matrix element $\langle s23\rangle=0$ in the angular correlation Eqn. 2.31, and obtain

$$W(\theta_{p'}) \sim (3/16\pi^2)\,(|\langle s05\rangle|^2+|\langle s25\rangle|^2) - \{(15/196\pi^2)\,|\langle s25\rangle|^2-(3\sqrt{14}/28\pi^2)\cdot\langle s05\rangle\langle s25\rangle^*\} \cdot P_2(\cos\theta_{p'}) + (81/784\pi^2)\,|\langle s25\rangle|^2\,P_4(\cos\theta_{p'}) \qquad (2.66)$$

Defining $\delta = \dfrac{\langle s,0,5\rangle}{\langle s,2,5\rangle}$, the Legendre polynomial coefficients are therefore

$$a_{2p} = \frac{-20/49-8/\sqrt{14}\cdot(p\&p)\,\delta}{1+pen(0,2)\,\delta^2}$$

$$a_{4p} = \frac{27/49}{1+pen(0,2)\,\delta^2} \qquad (2.67)$$

Cancelling δ in the above two equations, we obtain the following equation

$$729a_{2p}^2+(400+10976\cdot phase^2)\,a_{4p}^2+1080a_{2p}\,a_{4p}-6048\cdot phase^2\cdot a_{4p}=0 \qquad (2.68)$$

For the case of phase^2=1, this equation reduces to

$$81a_{2P}^2+1264a_{4P}^2+120a_{2P}a_{4P}-672a_{4P}=0 \qquad (2.69)$$

Following the same method, we find that the corresponding lines for $\langle s,0,5\rangle=0$ and $\langle s,2,5\rangle=0$ are $105a_{2P}+56a_{4P}+12=0$ and $12a_{2P}+5a_{4P}=0$. These two lines are independent of the phase parameter. The physical region for a_{2P} and a_{4P} and the corresponding curves or lines for $\langle s,0,5\rangle=0$, $\langle s,2,3\rangle=0$ and $\langle s,2,5\rangle=0$ in the channel spin representation are shown in Fig. 2.3. The intersection point of $\langle s,2,5\rangle=0$ and $\langle s,0,5\rangle=0$ is the origin (0,0) which represents 100% $1'=0$. Hence, we expect most of the resonances will have values of (a_{2P},a_{4P}) located near the origin. The experimental results of (a_{2P},a_{4P}) are shown in Fig. 2.4, where the proton physical region corresponds to phase$^2\sim 0.4$.

B. Data Analysis

Since the experimentally measurable quantities are the W's and θ's, the angular distribution equations are normally rewritten in a form

$$W_i(\theta_{p'}) = a_{op}\,(1 + a_{2p}\,P_2(\cos\theta_{p'}) + a_{4p}\,P_4(\cos\theta_{p'}))$$
$$W_i(\theta_\gamma) = a_{oq}\,(1 + a_{2q}\,P_2(\cos\theta_\gamma) + a_{4q}\,P_4(\cos\theta_\gamma)) \qquad (2.70)$$

where $a_{2p}, a_{4p}, a_{2q}, a_{4q}$ are functions of mixing ratios ($\delta_1^2, \delta_2^2, \delta_1\delta_2, \delta_1, \delta_2, c$), i is the index for detectors located at different angles, and $a_{4p} = a_{4q} = 0$ for 3/2+ states.

For each angular distribution studied (inelastically scattered proton and the subsequent gamma-ray decay), five detectors were located at angles ranging from $(\cos\theta)^2 = 0$ to $(\cos\theta)^2 \sim 1$. The measured counts from each detector provide one data point on the distribution curve $W(\theta)$. For each resonance, with five data points for each of the two angular distribution curves, values of (a_{op}, a_{2p}, a_{4p}) and (a_{oq}, a_{2q}, a_{4q}) can be extracted by a Lengendre polynomial fit with two degrees of freedom.

2.B.1. Spin Assignment for the D-wave Compound State

As mentioned before, compound states formed by the $l_p=2$ incident protons have two possible spins, 3/2+ and 5/2+. The spin assignments for these compound states can be obtained by examination of the characteristic angular distribution curves $W(\theta)$. The obvious difference between the angular distributions for these two states is that $W(\theta)$ is a linear function of $\cos^2\theta$ for 3/2+ states and a second order polynomial of $\cos^2\theta$ for 5/2+ states. In other words, on the angular distribution curves the 3/2+ state corresponds to a straight line while the 5/2+ state may be a parabola or a straight line (if $a_4=0$).

Therefore, for each resonance the appearance of a parabola in the proton or gamma-ray distribution curve ($a_{4p}\neq 0$ or $a_{4\gamma}\neq 0$) ensures that it is a 5/2+ state. For resonances with straight lines in both distributions, a second check on the values of a_{2p} and $a_{2\gamma}$ is necessary to distinguish between the two states.

For 5/2+ states, a_{4p} and $a_{4\gamma}$ are quadratic functions of δ_1 and δ_2. If $a_{4p}=a_{4\gamma}=0$, then (δ_1,δ_2) are confined to certain sets of values. Replacing these values back into the expressions for a_{2p} and $a_{2\gamma}$, then these coefficients in turn are restricted to certain fixed values. For instance, if phase^2=1, then $(a_{2p},a_{2\gamma})=(.4,-.003)$ or

(-.8 ,-.003).

For resonances with a_{4p} and a_{4g} = 0, if the values of (a_{2p} ,a_{2g}) do not agree with one of the calculated values that correspond to a_{4p} =a_{4g}=0 for 5/2+ states, these resonances are assigned as 3/2+ states. If (a_{2p} ,a_{2g}) does agree with either of these calculated values, then the resonance can be either a 3/2+ or a 5/2+ state. However, since a_{4g}=0 for 5/2+ states corresponds to high l'=2 admixture ($\epsilon_\pi^2 \geq 47\%$), within our laboratory energy range such combinations appear very unlikely. None were found in our experimental results. In all we analyzed 80 resonances, of which 45 are assigned as 5/2+ states, and 35 are assigned as 3/2+ states.

2.B.2. Mixing Ratios

Three channels are open for inelastically scattered protons from a d-wave compound state. The relative sign and strength between each two channel width amplitudes are represented by mixing ratios (only two of them are independent). From these two mixing ratios, the total width can be subdivided into each channel width.

By measuring the angular distributions of both the inelastically scattered proton and the subsequent gamma-

ray decay, mixing ratio values for 5/2+ states can be uniquely determined. However, there are two solutions for a 3/2+ state. With the present experimental information, we are not able to select the true solution. We therefore shall simply list both solutions without any further analysis.

The reason that mixing ratios for 5/2+ states can be uniquely determined may be briefly stated as follows: From the Legendre polynomial fit to the proton angular distribution, two independent equations involving mixing ratios δ_1, δ_2 are obtained.

$$a_{2p} = f_{a_{2p}}(\delta_1^2, \delta_2^2, \delta_1, c)$$
$$a_{4p} = f_{a_{4p}}(\delta_1^2, \delta_2^2, c) \qquad (2.71)$$

Where δ_1, δ_2 are defined as:

$$\delta_1 = \frac{\langle s,0,5\rangle}{\langle s,2,5\rangle} \quad , \quad \delta_2 = \frac{\langle s,2,3\rangle}{\langle s,2,5\rangle}$$

thus a_{2p} and a_{4p} are symmetric about δ_2. Solving (δ_1, δ_2) in terms of a_{2p} and a_{4p}, we obtain a maximum of four solutions which follow a pattern such as: $(\delta_1, \delta_2) = (A, \pm B)$ or $(C, \pm D)$. The ± sign in front of B and D results from of the symmetry properties of a_{2p}, a_{4p} as a function of δ_2. To select the right solution, we need the additional information supplied by the gamma-ray angular distribution. In the same manner, we have

$$a_{2q} = f_{a_{2q}}(\delta_1^2, \delta_2^2, \delta_2, c)$$

$$a_{4q} = f_{a_{4q}}(\delta_1^2, \delta_2^2, c) \qquad (2.72)$$

The four solutions obtained by solving these two independent equations follow a pattern: $(\delta_1, \delta_2) = (\pm A', B')$ or $(\pm C', D')$, where the $\pm$ sign in front of A' and C' is a result of the symmetry properties of a_{2q}, a_{4q} as a function of δ_1.

Comparing these two sets of solutions, it is apparent that the sign of δ_1 is decided by the inelastically scattered proton distribution, and the sign of δ_2 is decided by the gamma-ray distribution. A unique solution for (δ_1, δ_2) can therefore be determined.

For $3/2^+$ states, because $a_{4p} = a_{4q} = 0$, from each experiment there is only one equation for two independent variables:

$$a_{2p} = f_{a_{2p}}(\delta_1^2, \delta_2^2, \delta_1\delta_2, \delta_1, \delta_2, c)$$

$$a_{2q} = f_{a_{2q}}(\delta_1^2, \delta_2^2, \delta_1\delta_2, \delta_1, \delta_2, c) \qquad (2.73)$$

Combining these two equations with the constraint that δ_1, δ_2 are real, there will still be two solutions for the mixing ratios (δ_1, δ_2).

2.B.3. χ^2 search

Various methods can be adopted to solve for the mixing ratios. For convenience, the infinitely ranged variables (δ_1, δ_2) are transformed into finitely ranged variables (ϕ_1, ϕ_2) by the transformation $\phi_1 = \tan^{-1}\delta_1$, $\phi_2 = \tan^{-1}\delta_2$. One measure of the quality of the fit of any solution (ϕ_1, ϕ_2) is provided by the value of χ^2, defined as:

$$\chi^2(\phi_1,\phi_2) = \sum_{i=1}^{5}\left(\frac{W_{p'}(\phi_1,\phi_2;\theta_i) - W_{p'}(\theta_i)}{\Delta W_{p'}(\theta_i)}\right)^2 + \sum_{i=1}^{5}\left(\frac{W_{\gamma}(\phi_1,\phi_2;\theta_i) - W_{\gamma}(\theta_i)}{\Delta W_{\gamma}(\theta_i)}\right)^2 \tag{2.74}$$

where $W_{p'}(\theta_i)$ and $W_{\gamma}(\theta_i)$ are the experimentally measured counts at each angle, $\Delta W_{p'}(\theta_i)$ and $\Delta W_{\gamma}(\theta_i)$ are the corresponding errors, and $W_{p'}(\phi_1,\phi_2;\theta_i)$ and $W_{\gamma}(\phi_1,\phi_2;\theta_i)$ are the calculated values corresponding to the solution (ϕ_1, ϕ_2).

If a three-dimensional plot of χ^2 versus ϕ_1, ϕ_2 is drawn, then the value of (ϕ_1, ϕ_2) that corresponds to the absolute minimum point of χ^2 will be the best choice. Four χ^2 plots are shown in Fig. 2.5 through Fig. 2.8 for $5/2^+$ and $3/2^+$ resonances in j-spin and s-spin representations. The absolute peak value therefore represents the best solution.

Figure 2.5 χ^2 Plot for a $5/2^+$ Resonance (No. 102) in the Angular Momentum Representation. The highest peak (absolute minimum point of χ^2) represents the best solution for mixing ratios $(\phi_{3/}, \phi_{5/})$, where $\phi_{3/} = \tan^{-1}(\langle s,2,3\rangle/\langle s,0,5\rangle)$ and $\phi_{5/} = \tan^{-1}(\langle s,2,5\rangle/\langle s,0,5\rangle)$, and the background straight lines mean $\chi^2 \geq 30$.

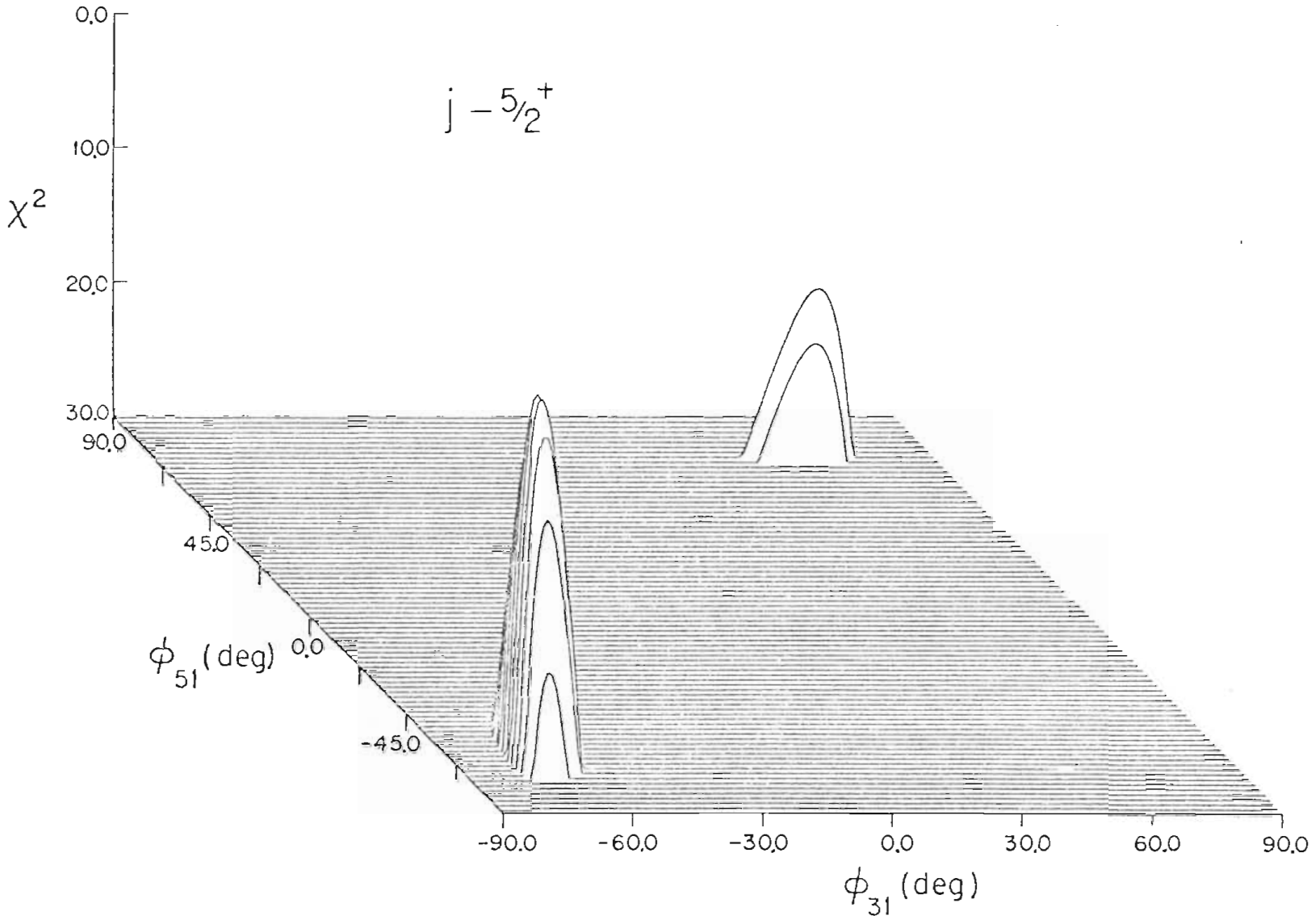
j − 5/2+
χ2
0.0
10.0
20.0
30.0
90.0
45.0
0.0
-45.0
φ51 (deg)
-90.0
-60.0
-30.0
0.0
30.0
60.0
90.0
φ31 (deg)

Figure 2.6 χ^2 Plot for a $5/2^+$ Resonance (No. 106) in the Channel Spin Representation. The peak (absolute minimum point of χ^2) represents the best solution for (ϕ_{31}, ϕ_{51}), where $\phi_{31} = \tan^{-1}(\langle s,2,3\rangle / \langle s,0,5\rangle)$ and $\phi_{51} = \tan^{-1}(\langle s,2,5\rangle / \langle s,0,5\rangle)$, and the background straight lines mean $\chi^2 \geq 30$.

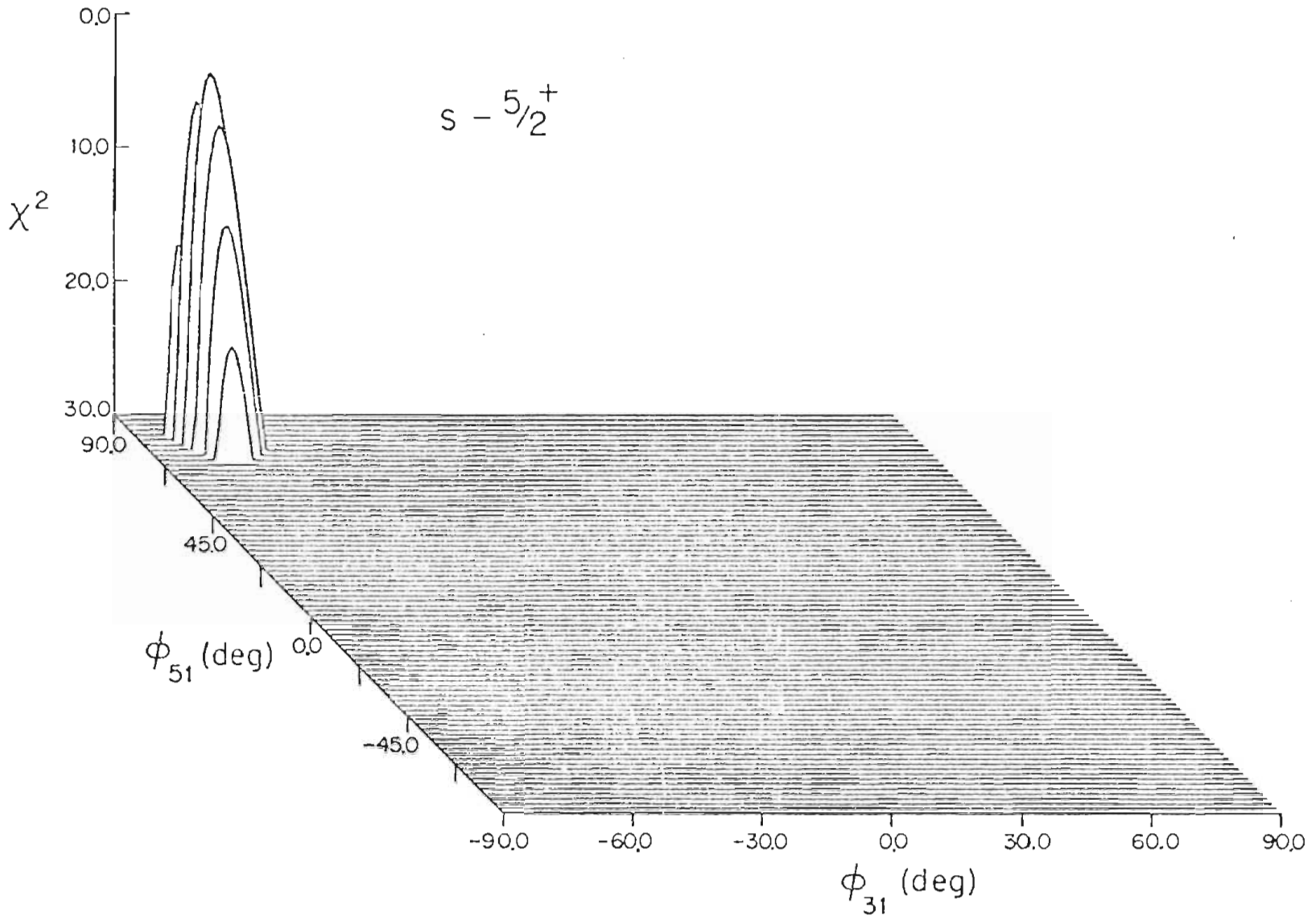
0.0
10.0
20.0
30.0
χ^2
$s - 5/2^+$
90.0
45.0
0.0
-45.0
ϕ_{51} (deg)
-90.0
-60.0
-30.0
0.0
30.0
60.0
90.0
ϕ_{31} (deg)

Figure 2.7 χ^2 Plot for a $3/2^+$ Resonance (No. 74) in the Angular Momentum Representation. The two peaks (with the same χ^2 value) represent the two acceptable solutions for (ϕ_{3l}, ϕ_{5l}), where $\phi_{3l} = \tan^{-1}(\langle j,2,3\rangle / \langle j,0,3\rangle)$ and $\phi_{5l} = \tan^{-1}(\langle j,2,5\rangle / \langle j,0,3\rangle)$, and the background straight lines mean $\chi^2 \geq 30$.

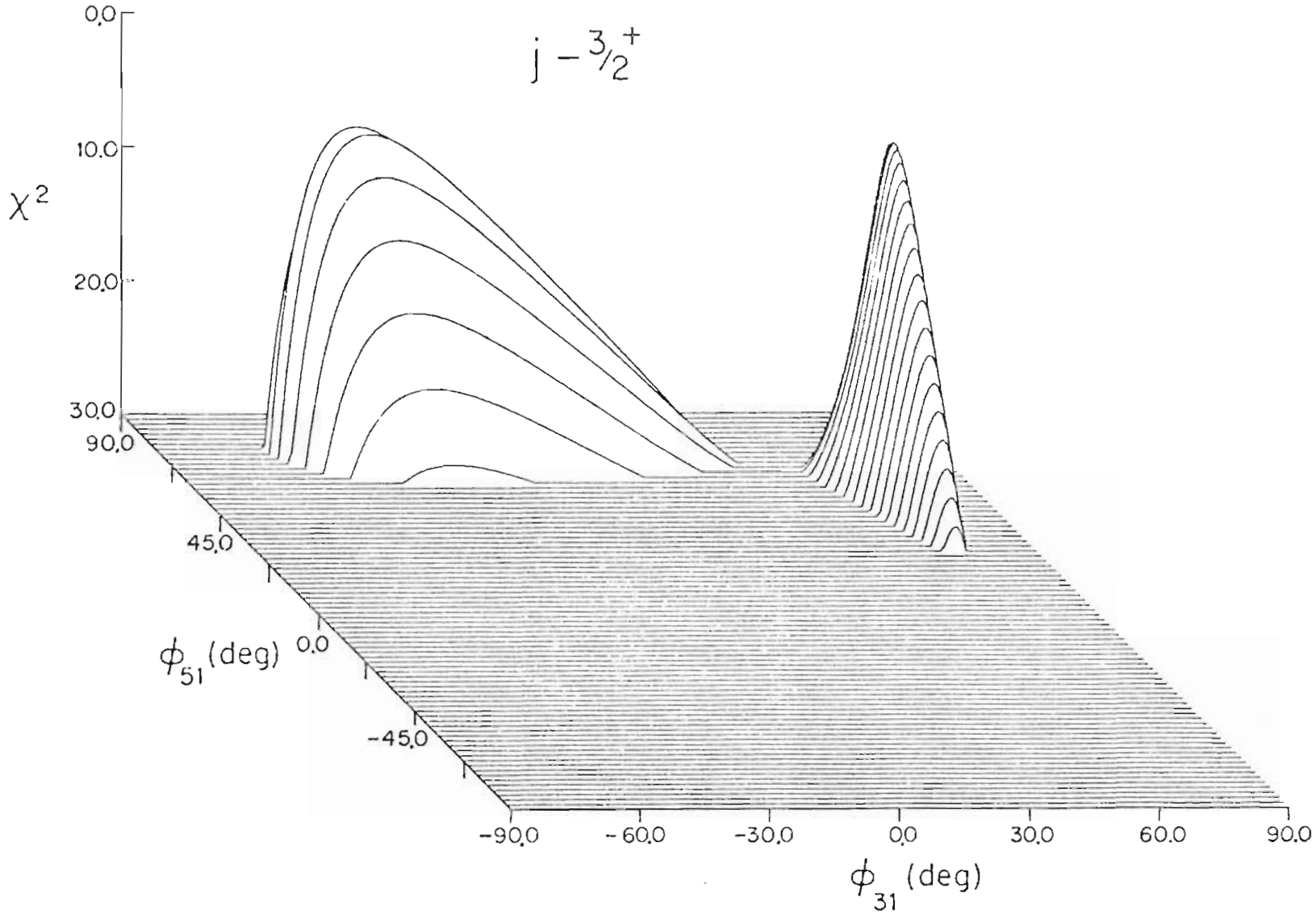
j − 3/2+
χ2
0.0
10.0
20.0
30.0
90.0
45.0
0.0
-45.0
φ51 (deg)
-90.0
-60.0
-30.0
0.0
30.0
60.0
90.0
φ31 (deg)

Figure 2.8 χ^2 Plot for a $3/2^+$ Resonance (No. 67) in the Channel Spin Representation. The two peaks (with the same χ^2 value) represent the two acceptable solutions for $(\phi_{3/}, \phi_{5/})$, where $\phi_{3/} = \tan^{-1}(\langle s,2,3\rangle / \langle s,0,3\rangle)$ and $\phi_{5/} = \tan^{-1}(\langle s,2,5\rangle / \langle s,0,3\rangle)$, and the background straight lines mean $\chi^2 \geq 30$.

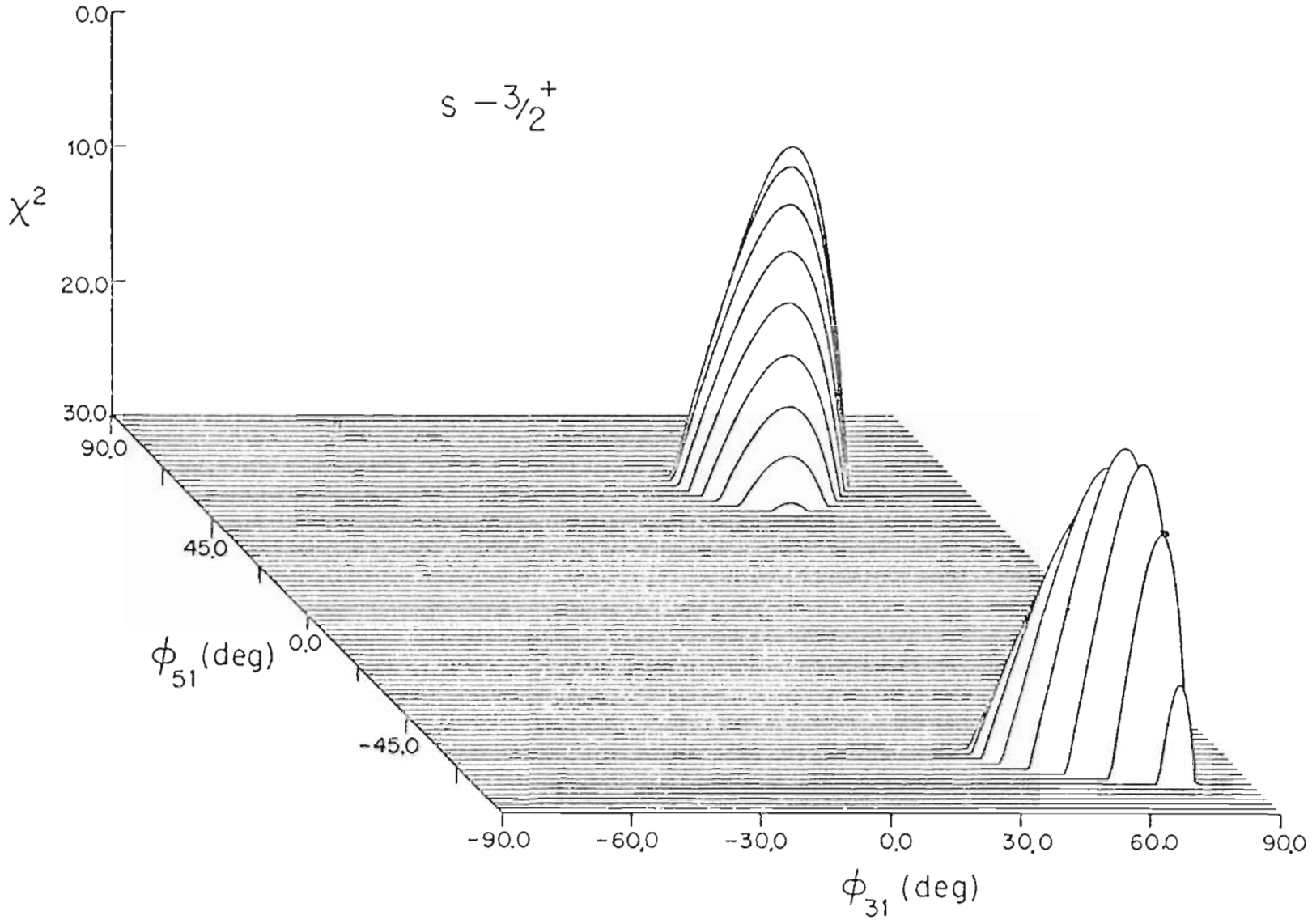
0.0
10.0
20.0
30.0
χ^2
S $-3/2^+$
90.0
45.0
0.0
-45.0
ϕ_{51} (deg)
-90.0
-60.0
-30.0
0.0
30.0
60.0
90.0
ϕ_{31} (deg)

In processing the data, a χ^2 (Ø space) gradient search program called Rocord was used to find the solution efficiently. The a_2, a_4 values obtained from the Legendre polynomial fit are listed in Table 2.2. The mixing ratio values and corresponding ϵ_r^2, ϵ_m^2, and χ^2 values for 5/2+ resonances are listed in Table 2.3 and Table 2.4 for j-spin and s-spin representation, respectively, where $\delta_{31}=\tan\emptyset_{31}=\langle j,2,3\rangle/\langle j,0,3\rangle$, $\delta_{53}=\tan\emptyset_{53}=\langle j,2,5\rangle/\langle j,2,3\rangle$, and $\delta_{51}=\tan\emptyset_{51}=\langle j,2,5\rangle/\langle j,0,3\rangle$ in the j-spin representation and $\delta_{31}=\tan\emptyset_{31}=\langle s,2,3\rangle/\langle s,0,5\rangle$, $\delta_{53}=\tan\emptyset_{53}=\langle s,2,5\rangle/\langle s,2,3\rangle$, and $\delta_{51}=\tan\emptyset_{51}=\langle s,2,5\rangle/\langle s,0,5\rangle$ in the s-spin representation. The two mixing ratios and corresponding ϵ_r^2, ϵ_m^2, and χ^2 values for 3/2+ resonances are listed in Table 2.5 and Table 2.6 for j-spin and s-spin representation, respectivelv, where $\delta_{31}=\tan\emptyset_{31}=\langle j,2,3\rangle/\langle j,0,3\rangle$, $\delta_{53}=\tan\emptyset_{53}=\langle j,2,5\rangle/\langle j,2,3\rangle$, and $\delta_{51}=\tan\emptyset_{51}=\langle j,2,5\rangle/\langle j,0,3\rangle$ in the j-spin representation and $\delta_{31}=\tan\emptyset_{31}=\langle s,2,3\rangle/\langle s,0,3\rangle$, $\delta_{53}=\tan\emptyset_{53}=\langle s,2,5\rangle/\langle s,2,3\rangle$, and $\delta_{51}=\tan\emptyset_{51}=\langle s,2,5\rangle/\langle s,0,3\rangle$ in the s-spin representation. The parameter ϵ_r^2 represents the $l'=2$ admixture for reduced widths, and ϵ_m^2 is the $l'=2$ admixture for matrix element. Over one third of the resonances (17 out of 45) have $\chi^2\leq 1$, and over one half of the resonances (27 out of 45) have $\chi^2\leq 2$. These extremely small χ^2 values reflect the excellent correspondence between fit and data.

The error bar on the mixing ratios can be obtained in two ways: One is the empirical method, where a χ^2 cut-off value is defined and then all the solutions (δ_1, δ_2) whose corresponding χ^2 values are smaller than the cut-off value are accepted. The other method is purely mathematical, and uses an error matrix (Bevington, 1969). Since the empirical method has an ambiguity in choosing the standard χ^2-cutoff, the error bars for the mixing ratios in Table 2.3 through Table 2.6 were determined by the error matrix calculation.

Table 2.2

Legendre Polynomial Coefficients for l=2 Resonances in ^{49}V

Res. No.	Exp.	a_0	a_2	a_4
5	P	3990 ± 86	0.230 ± 0.044	0.014 ± 0.059
	G	27103 ± 519	0.525 ± 0.034	-0.520 ± 0.050
8	P	7476 ± 168	-0.206 ± 0.037	-0.155 ± 0.053
	G	50544 ± 919	0.566 ± 0.032	-0.533 ± 0.048
9	P	7926 ± 162	0.142 ± 0.040	-0.001 ± 0.054
	G	72023 ± 1309	0.535 ± 0.032	-0.528 ± 0.048
10	P	6759 ± 136	0.267 ± 0.041	0.018 ± 0.055
	G	42159 ± 765	0.518 ± 0.032	-0.496 ± 0.048
14	P	3969 ± 85	0.092 ± 0.042	-0.089 ± 0.057
	G	25172 ± 471	0.483 ± 0.040	-0.066 ± 0.055
17	P	6689 ± 136	0.157 ± 0.041	0.023 ± 0.055
	G	39022 ± 730	0.436 ± 0.040	-0.018 ± 0.055
19	P	8562 ± 168	0.092 ± 0.039	0.017 ± 0.051
	G	69729 ± 1267	0.577 ± 0.032	-0.527 ± 0.048
20	P	8091 ± 161	0.176 ± 0.038	-0.127 ± 0.053
	G	61100 ± 1083	0.495 ± 0.031	-0.533 ± 0.046
22	P	5456 ± 111	0.156 ± 0.041	0.036 ± 0.055
	G	81450 ± 1527	0.421 ± 0.040	-0.043 ± 0.055
24	P	6281 ± 137	-0.128 ± 0.039	0.043 ± 0.053
	G	17122 ± 328	0.566 ± 0.033	-0.555 ± 0.050
25	P	6300 ± 125	-0.024 ± 0.037	-0.038 ± 0.050
	G	81754 ± 1517	0.543 ± 0.040	-0.020 ± 0.055
26	P	16334 ± 327	0.121 ± 0.039	0.017 ± 0.053
	G	49432 ± 924	0.549 ± 0.032	-0.552 ± 0.049
28	P	15398 ± 314	0.159 ± 0.040	-0.014 ± 0.054
	G	211154 ± 3636	0.551 ± 0.030	-0.528 ± 0.045

Table 2.2 (continued)

Pes. No.	Exp.	a_0	a_2	a_4
29	P	1891 ± 45	0.287 ± 0.051	0.107 ± 0.065
	G	18056 ± 345	0.201 ± 0.039	-0.029 ± 0.053
32	P	4638 ± 105	-0.444 ± 0.036	0.050 ± 0.049
	G	30182 ± 570	0.320 ± 0.040	-0.008 ± 0.054
33	P	12658 ± 250	0.214 ± 0.041	0.051 ± 0.054
	G	225842 ± 3778	0.553 ± 0.030	-0.516 ± 0.044
35	P	6334 ± 124	0.269 ± 0.041	0.026 ± 0.054
	G	57582 ± 949	0.352 ± 0.035	0.008 ± 0.048
36	P	4936 ± 101	0.337 ± 0.045	0.188 ± 0.057
	G	42025 ± 806	0.259 ± 0.035	-0.334 ± 0.052
37	P	61305 ± 1183	0.202 ± 0.039	-0.009 ± 0.052
	G	252486 ± 4353	0.536 ± 0.030	-0.539 ± 0.045
39	P	9081 ± 186	-0.030 ± 0.038	-0.008 ± 0.051
	G	96100 ± 1614	0.464 ± 0.036	-0.010 ± 0.049
40	P	28171 ± 564	-0.055 ± 0.037	0.013 ± 0.050
	G	289631 ± 4731	0.471 ± 0.035	-0.030 ± 0.048
41	P	16405 ± 361	0.104 ± 0.044	0.058 ± 0.058
	G	67467 ± 1255	0.543 ± 0.033	-0.486 ± 0.049
43	P	9582 ± 281	0.116 ± 0.055	-0.112 ± 0.078
	G	63286 ± 1208	0.559 ± 0.034	-0.494 ± 0.051
44	P	15274 ± 325	0.191 ± 0.043	0.043 ± 0.057
	G	194182 ± 3252	0.525 ± 0.029	-0.524 ± 0.044
50	P	24380 ± 471	0.198 ± 0.039	0.010 ± 0.052
	G	139021 ± 2397	0.539 ± 0.030	-0.533 ± 0.045
51	P	9675 ± 198	0.115 ± 0.040	-0.033 ± 0.054
	G	73736 ± 1341	0.563 ± 0.032	-0.529 ± 0.048

Table 2.2 (continued)

Res. No.	Exp.	a_0	a_2	a_4
52	P	13682 ± 290	0.207 ± 0.042	-0.093 ± 0.057
	G	70810 ± 1289	0.457 ± 0.032	-0.503 ± 0.048
53	P	5585 ± 117	0.307 ± 0.043	-0.001 ± 0.058
	G	65936 ± 1155	0.310 ± 0.036	-0.050 ± 0.050
54	P	16130 ± 317	0.173 ± 0.039	-0.062 ± 0.052
	G	637151 ± 9864	0.413 ± 0.033	-0.053 ± 0.045
55	P	22308 ± 439	0.258 ± 0.039	-0.077 ± 0.054
	G	150533 ± 2668	0.521 ± 0.031	-0.538 ± 0.046
56	P	39309 ± 758	0.207 ± 0.039	-0.010 ± 0.052
	G	138914 ± 2527	0.547 ± 0.032	-0.530 ± 0.048
58	P	6865 ± 149	0.022 ± 0.041	-0.011 ± 0.056
	G	181334 ± 2969	0.446 ± 0.035	-0.048 ± 0.048
59	P	9279 ± 201	0.209 ± 0.044	0.019 ± 0.059
	G	87707 ± 1632	0.534 ± 0.033	-0.489 ± 0.049
60	P	8999 ± 183	0.174 ± 0.040	-0.028 ± 0.054
	G	183483 ± 3012	0.412 ± 0.035	-0.054 ± 0.048
63	P	17042 ± 334	0.277 ± 0.040	-0.058 ± 0.053
	G	92451 ± 1662	0.505 ± 0.034	-0.359 ± 0.050
65	P	21067 ± 452	0.120 ± 0.042	-0.021 ± 0.057
	G	144865 ± 2565	0.523 ± 0.031	-0.521 ± 0.047
67	P	10178 ± 219	0.095 ± 0.042	-0.031 ± 0.056
	G	189995 ± 3166	0.262 ± 0.033	-0.104 ± 0.047
68	P	10304 ± 217	0.297 ± 0.043	-0.051 ± 0.058
	G	110930 ± 1933	0.363 ± 0.036	-0.050 ± 0.050
69	P	3619 ± 86	0.298 ± 0.050	0.018 ± 0.067
	G	47055 ± 892	0.464 ± 0.036	-0.360 ± 0.052

Table 2.2 (continued)

Res. No.	Exp.	a_0	a_2	a_4
70	P	9704 ± 202	0.185 ± 0.042	-0.012 ± 0.056
	G	82507 ± 1431	0.414 ± 0.037	-0.044 ± 0.050
71	P	9225 ± 201	0.187 ± 0.044	0.031 ± 0.059
	G	67094 ± 1186	0.512 ± 0.031	-0.502 ± 0.047
72	P	21739 ± 430	0.115 ± 0.039	-0.031 ± 0.052
	G	80430 ± 1418	0.513 ± 0.032	-0.469 ± 0.047
74	P	10347 ± 212	0.289 ± 0.043	0.011 ± 0.057
	G	98713 ± 1854	0.222 ± 0.040	-0.087 ± 0.056
75	P	16887 ± 350	0.197 ± 0.042	-0.013 ± 0.056
	G	150217 ± 2662	0.531 ± 0.031	-0.536 ± 0.046
76	P	12111 ± 251	0.207 ± 0.042	0.022 ± 0.056
	G	104858 ± 1854	0.546 ± 0.031	-0.512 ± 0.047
77	P	11142 ± 260	0.062 ± 0.043	0.011 ± 0.061
	G	267738 ± 4401	0.402 ± 0.035	-0.056 ± 0.048
78	P	22768 ± 460	0.040 ± 0.039	0.017 ± 0.053
	G	190340 ± 3178	0.501 ± 0.030	-0.479 ± 0.044
79	P	8386 ± 192	-0.139 ± 0.041	0.056 ± 0.056
	G	109752 ± 1887	0.219 ± 0.035	0.007 ± 0.048
80	P	11378 ± 241	0.215 ± 0.043	-0.004 ± 0.057
	G	172060 ± 2850	0.299 ± 0.035	0.030 ± 0.048
82	P	35901 ± 686	0.275 ± 0.040	0.049 ± 0.053
	G	145430 ± 2497	0.509 ± 0.031	-0.482 ± 0.046
83	P	24344 ± 504	0.220 ± 0.042	-0.017 ± 0.056
	G	174568 ± 3000	0.538 ± 0.031	-0.499 ± 0.046
84	P	12008 ± 261	0.209 ± 0.043	-0.076 ± 0.059
	G	67433 ± 1102	0.416 ± 0.031	-0.471 ± 0.046

Table 2.2 (continued)

Pes. No.	Exp.	a_0	a_2	a_4
85	P	15387 ± 323	0.304 ± 0.042	-0.072 ± 0.058
	G	97650 ± 1726	0.487 ± 0.031	-0.497 ± 0.047
86	P	15658 ± 332	0.214 ± 0.043	0.000 ± 0.057
	G	130320 ± 2201	0.416 ± 0.035	-0.078 ± 0.049
87	P	9785 ± 209	0.158 ± 0.042	-0.014 ± 0.057
	G	74105 ± 1285	0.427 ± 0.036	-0.081 ± 0.050
88	P	20731 ± 432	0.159 ± 0.041	-0.021 ± 0.056
	G	97396 ± 1642	0.427 ± 0.036	-0.044 ± 0.049
89	P	38475 ± 741	0.215 ± 0.039	0.011 ± 0.052
	G	112496 ± 1935	0.550 ± 0.030	-0.514 ± 0.045
90	P	18034 ± 361	0.299 ± 0.042	0.011 ± 0.055
	G	85746 ± 1455	0.354 ± 0.035	-0.043 ± 0.049
91	P	16986 ± 345	0.190 ± 0.041	0.006 ± 0.055
	G	129061 ± 2060	0.404 ± 0.034	-0.057 ± 0.046
92	P	18393 ± 398	0.051 ± 0.042	-0.007 ± 0.056
	G	66632 ± 1154	0.445 ± 0.037	-0.059 ± 0.050
93	P	12189 ± 266	0.161 ± 0.044	0.011 ± 0.058
	G	61928 ± 1152	0.471 ± 0.033	-0.468 ± 0.049
94	P	18789 ± 399	0.382 ± 0.046	0.051 ± 0.060
	G	74297 ± 1344	0.497 ± 0.033	-0.448 ± 0.048
95	P	21762 ± 435	0.115 ± 0.039	-0.044 ± 0.053
	G	96516 ± 1738	0.552 ± 0.034	-0.410 ± 0.049
96	P	40632 ± 800	0.055 ± 0.038	0.011 ± 0.051
	G	120974 ± 2041	0.422 ± 0.036	-0.047 ± 0.049
97	P	14457 ± 328	-0.233 ± 0.039	0.003 ± 0.054
	G	67078 ± 1211	0.283 ± 0.036	-0.121 ± 0.051

Table 2.2 (continued)

Res. No.	Exp.	a_0	a_2	a_4
98	P	11540 ± 239	0.422 ± 0.044	-0.048 ± 0.058
	G	72975 ± 1235	0.111 ± 0.033	-0.038 ± 0.046
99	P	14167 ± 315	-0.249 ± 0.038	0.026 ± 0.053
	G	77688 ± 1331	0.252 ± 0.035	-0.039 ± 0.048
100	P	27058 ± 566	-0.028 ± 0.039	-0.031 ± 0.053
	G	91947 ± 1578	0.235 ± 0.035	-0.031 ± 0.048
101	P	22276 ± 491	0.252 ± 0.045	-0.035 ± 0.060
	G	76667 ± 1377	0.432 ± 0.035	-0.286 ± 0.050
102	P	7803 ± 173	0.344 ± 0.039	-0.459 ± 0.057
	G	59993 ± 1083	0.307 ± 0.035	-0.205 ± 0.050
103	P	8708 ± 185	-0.388 ± 0.033	0.015 ± 0.047
	G	54944 ± 1185	0.005 ± 0.041	-0.072 ± 0.057
104	P	11853 ± 249	0.272 ± 0.043	-0.010 ± 0.058
	G	172909 ± 2896	0.494 ± 0.029	-0.520 ± 0.044
105	P	16051 ± 343	0.139 ± 0.042	-0.024 ± 0.057
	G	165558 ± 2714	0.429 ± 0.035	-0.060 ± 0.047
106	P	8705 ± 188	0.266 ± 0.043	-0.106 ± 0.059
	G	61868 ± 1084	0.293 ± 0.040	0.273 ± 0.051
107	P	5181 ± 134	0.497 ± 0.053	-0.138 ± 0.073
	G	39067 ± 737	0.412 ± 0.037	-0.215 ± 0.053
108	P	9553 ± 201	0.094 ± 0.041	0.005 ± 0.055
	G	78324 ± 1297	0.313 ± 0.034	-0.051 ± 0.047
109	P	18944 ± 382	0.247 ± 0.041	0.006 ± 0.055
	G	100170 ± 1683	0.499 ± 0.029	-0.554 ± 0.043
110	P	15095 ± 310	0.088 ± 0.040	-0.035 ± 0.054
	G	91851 ± 1551	0.410 ± 0.036	-0.053 ± 0.049

Table 2.2 (continued)

Res. No.	Exp.	a_0	a_2	a_4
111	P	13365 ± 277	0.398 ± 0.044	0.035 ± 0.058
	G	116976 ± 2105	0.490 ± 0.034	-0.359 ± 0.050
112	P	25358 ± 543	0.134 ± 0.042	-0.016 ± 0.057
	G	106054 ± 1776	0.570 ± 0.030	-0.531 ± 0.044

Table 2.3

Values of Mixing Ratios, ϵ^2, ϵ^2, and ^{2} for 5/2+ Resonances in ^{49}V (j-spin)

Res. No.	j- δ_{31}	j- δ_{53}	j- δ_{51}	j-ϕ_{31}	j-ϕ_{53}	j-ϕ_{51}	ϵ^2_γ	ϵ^2_m	χ^2
5	-1.04± 0.31	0.01± 0.50	-0.01± 0.19	-46.2°+ 9.9° - 7.3°	0.6°+ 26.6° - 26.8°	-0.6°+ 10.7° - 10.7°	0.52	0.05	1.0
8	1.14± 0.23	0.18± 0.21	0.21± 0.27	48.8°+ 5.1° - 6.4°	10.3°+ 10.9° - 11.7°	11.8°+ 13.7° - 15.2°	0.57	0.07	8.9
9	-0.86± 0.22	0.43± 0.33	-0.37± 0.35	-40.8°+ 8.2° - 6.6°	23.4°+ 14.0° - 17.6°	-20.5°+ 19.1° - 15.4°	0.47	0.05	1.0
10	-1.20± 0.27	-0.07± 0.43	0.08± 0.42	-50.2°+ 7.4° - 5.6°	-3.8°+ 23.6° - 22.4°	4.7°+ 22.0° - 23.4°	0.59	0.07	2.2
19	-0.49± 0.33	0.24± 0.82	-0.12± 0.47	-26.2°+ 17.2° - 13.3°	13.6°+ 33.0° - 43.5°	-6.7°+ 25.9° - 23.6°	0.20	0.02	0.7
20	0.49± 0.21	3.01± 1.15	1.46± 0.19	26.0°+ 8.8° - 10.4°	71.6°+ 4.9° - 9.9°	55.7°+ 3.1° - 3.7°	0.70	0.12	1.5
24	0.36± 0.51	-0.56± 2.64	-0.20± 0.66	19.6°+ 21.2° - 28.2°	-29.1°+ 93.5° - 43.5°	-11.2°+ 36.2° - 29.6°	0.14	0.01	1.0
26	-0.10± 0.47	-5.68±30.65	0.59± 0.53	-5.9°+ 26.0° - 23.9°	-80.0°+167.7° - 8.4°	30.5°+ 17.7° - 27.2°	0.26	0.02	1.3
28	-0.82± 0.23	0.23± 0.40	-0.19± 0.37	-39.3°+ 8.7° - 6.9°	13.0°+ 19.4° - 22.8°	-10.8°+ 20.8° - 18.3°	0.41	0.04	0.4
33	-0.79± 0.32	-0.43± 0.76	0.34± 0.48	-38.4°+ 13.1° - 9.6°	-23.1°+ 41.5° - 26.8°	18.7°+ 20.6° - 26.8°	0.43	0.05	1.1
36	-2.18± 0.28	-1.49± 0.23	3.26± 0.35	-65.4°+ 3.1° - 2.5°	-56.2°+ 4.5° - 3.6°	73.0°+ 1.6° - 1.9°	0.94	0.50	2.7
37	-0.25± 0.35	-3.67± 6.36	0.91± 0.35	-13.9°+ 19.7° - 16.9°	-74.8°+144.4° - 9.6°	42.3°+ 9.3° - 13.1°	0.47	0.05	0.7

Table 2.3 (continued)

Res. No.	$J-\delta_{31}$	$J-\delta_{53}$	$J-\delta_{51}$	$J-\phi_{31}$	$J-\phi_{53}$	$J-\phi_{51}$	ϵ_r^2	ϵ_m^2	χ^2
41	-0.76± 0.22	0.42± 0.38	-0.31± 0.34	-37.1° + 8.9° - 7.2°	22.6° + 16.0° - 20.7°	-17.5° + 18.8° - 15.6°	0.40	0.04	3.5
43	-0.88± 0.20	0.70± 0.32	-0.62± 0.30	-41.3° + 7.0° - 5.8°	35.1° + 10.6° - 14.2°	-31.7° + 14.1° - 10.8°	0.54	0.07	2.7
44	-0.41± 0.52	-1.93± 3.63	0.80± 0.53	-22.4° + 28.5° - 20.5°	-62.6° + 122.1° - 17.2°	38.6° + 14.5° - 23.9°	0.45	0.05	1.4
50	-0.41± 0.51	-1.83± 3.65	0.75± 0.57	-22.1° + 28.3° - 20.5°	-61.4° + 122.6° - 18.3°	36.7° + 16.0° - 26.7°	0.42	0.05	0.3
51	-0.69± 0.21	0.43± 0.39	-0.30± 0.33	-34.6° + 9.1° - 7.5°	23.2° + 16.2° - 21.2°	-16.5° + 18.4° - 15.5°	0.36	0.04	0.3
52	0.36± 0.25	4.44± 2.92	1.60± 0.18	19.8° + 11.4° - 13.2°	77.3° + 5.0° - 20.6°	58.0° + 2.7° - 3.2°	0.73	0.15	1.3
55	-0.17± 0.28	-7.49±13.15	1.27± 0.23	-9.6° + 15.8° - 14.5°	-82.4° + 162.4° - 4.8°	51.7° + 4.6° - 5.7°	0.62	0.10	4.2
56	-0.84± 0.35	-0.20± 0.77	0.16± 0.58	-39.9° + 13.7° - 9.8°	-11.0° + 41.0° - 33.0°	9.2° + 27.5° - 32.0°	0.42	0.05	0.4
59	-1.03± 0.23	-0.02± 0.42	0.02± 0.23	-45.8° + 7.2° - 5.7°	-0.9° + 22.7° - 22.5°	1.2° + 12.8° - 13.0°	0.51	0.07	0.6
63	-1.70± 0.17	0.23± 0.16	-0.40± 0.27	-59.6° + 2.6° - 2.3°	13.1° + 8.2° - 8.7°	-21.6° + 14.3° - 12.0°	0.75	0.18	0.1
65	-0.85± 0.17	0.58± 0.30	-0.49± 0.28	-40.3° + 6.2° - 5.2°	30.2° + 11.1° - 14.3°	-26.3° + 14.3° - 11.5°	0.49	0.06	1.1
69	-1.80± 0.20	-0.02± 0.28	0.04± 0.20	-60.9° + 3.0° - 2.5°	-1.2° + 15.8° - 15.6°	2.2° + 11.2° - 11.4°	0.76	0.19	4.6

Table 2.3 (continued)

Res. No.	j- δ_{31}	j- δ_{53}	j- δ_{51}	j-ϕ_{31}	j-ϕ_{53}	j-ϕ_{51}	ϵ^z_γ	ϵ^z_m	χ^2
71	-1.00± 0.22	0.05± 0.46	-0.05± 0.26	-44.9°+ 7.0° - 5.6°	2.9°+ 24.1° - 25.1°	-3.0°+ 14.7° - 14.3°	0.50	0.07	2.0
72	-0.97± 0.15	0.69± 0.24	-0.67± 0.23	-44.1°+ 4.9° - 4.2°	34.5°+ 8.2° - 10.2°	-33.7°+ 10.3° - 8.3°	0.58	0.09	2.0
75	-0.25± 0.35	-3.72± 6.37	0.92± 0.32	-13.9°+ 20.0° - 17.1°	-75.0°+144.3° - 9.4°	42.6°+ 8.6° - 11.8°	0.48	0.06	0.7
76	-0.83± 0.32	-0.32± 0.76	0.27± 0.55	-39.9°+ 12.7° - 9.3°	-17.8°+ 41.7° - 29.5°	15.0°+ 24.4° - 31.0°	0.43	0.05	0.2
78	-0.73± 0.15	1.12± 0.31	-0.82± 0.22	-36.3°+ 6.0° - 5.2°	48.1°+ 6.8° - 9.2°	-39.3°+ 8.2° - 6.7°	0.55	0.08	5.3
82	-0.96± 0.34	-0.85± 0.78	0.82± 0.49	-43.9°+ 12.2° - 8.7°	-40.5°+ 36.2° - 18.0°	39.5°+ 13.3° - 21.1°	0.62	0.11	0.4
83	-1.02± 0.21	-0.02± 0.41	0.02± 0.14	-45.4°+ 6.5° - 5.3°	-1.2°+ 22.3° - 22.0°	0.9°+ 8.2° - 8.2°	0.51	0.07	0.7
84	0.38± 0.28	4.57± 3.43	1.74± 0.18	20.8°+ 12.8° - 15.4°	77.7°+ 5.2° - 28.9°	60.1°+ 2.3° - 2.7°	0.76	0.19	5.8
85	-0.33± 0.32	-4.52± 4.79	1.49± 0.22	-18.2°+ 17.7° - 14.8°	-77.5°+ 92.8° - 6.4°	56.1°+ 3.6° - 4.4°	0.70	0.15	3.4
89	-0.82± 0.32	-0.37± 0.77	0.31± 0.53	-39.4°+ 12.6° - 9.3°	-20.5°+ 42.0° - 28.3°	17.1°+ 22.8° - 29.6°	0.44	0.06	0.7
93	-1.15± 0.17	0.46± 0.26	-0.53± 0.30	-49.0°+ 4.5° - 3.8°	24.7°+ 11.0° - 13.3°	-27.9°+ 14.9° - 11.8°	0.62	0.11	4.7
94	-1.21± 0.29	-0.86± 0.52	1.04± 0.42	-50.5°+ 7.8° - 5.9°	-40.6°+ 21.7° - 13.3°	46.1°+ 9.4° - 14.3°	0.72	0.17	3.5

Table 2.3 (continued)

Res. No.	$j-\delta_{31}$	$j-\delta_{53}$	$j-\delta_{51}$	$j-\phi_{31}$	$j-\phi_{53}$	$j-\phi_{51}$	ϵ_γ^2	ϵ_m^2	χ^2
95	-0.99± 0.16	0.61± 0.22	-0.61± 0.22	-44.8° + 4.9° - 4.2°	31.4° + 8.2° - 9.9°	-31.2° + 10.2° - 8.4°	0.58	0.10	3.8
101	-1.98± 0.19	0.24± 0.17	-0.47± 0.33	-63.3° + 2.4° - 2.1°	13.4° + 8.9° - 9.6°	-25.3° + 17.0° - 13.3°	0.81	0.25	4.2
102	-2.77± 0.21	0.83± 0.10	-2.30± 0.25	-70.2° + 1.5° - 1.3°	39.6° + 3.3° - 3.7°	-66.5° + 2.5° - 2.1°	0.93	0.50	2.2
104	-0.49± 0.31	-2.48± 1.94	1.22± 0.25	-26.2° + 16.1° - 12.6°	-68.0° + 39.6° - 9.2°	50.7° + 5.2° - 6.6°	0.63	0.12	1.1
106	-5.68± 0.52	0.08± 0.05	-0.47± 0.30	-80.0° + 1.0° - 0.8°	4.7° + 2.9° - 2.9°	-25.3° + 15.4° - 12.3°	0.97	0.72	1.9
107	-2.57± 0.20	0.31± 0.12	-0.81± 0.30	-68.8° + 1.6° - 1.4°	17.4° + 5.9° - 6.3°	-38.9° + 11.9° - 9.0°	0.88	0.36	12.
109	-0.39± 0.27	-2.85± 2.34	1.12± 0.23	-21.5° + 14.5° - 12.1°	-70.6° + 43.9° - 8.5°	48.3° + 5.3° - 6.7°	0.59	0.10	0.8
111	-1.74± 0.20	-0.25± 0.26	0.44± 0.42	-60.2° + 3.1° - 2.6°	-14.1° + 14.5° - 12.9°	23.7° + 17.0° - 22.6°	0.76	0.21	4.6
112	-0.62± 0.24	0.05± 0.63	-0.03± 0.22	-31.8° + 11.1° - 9.0°	2.7° + 31.3° - 32.8°	-2.0° + 12.4° - 12.2°	0.28	0.03	0.4

Table 2.4

Values of Mixing Ratios, ϵ^2, ϵ^2, and ^{2} for 5/2+ Resonances in ^{49}V (s-spin)

Res. No.	s-δ_{31}	s-δ_{53}	s-δ_{51}	s-ϕ_{31}	s-ϕ_{53}	s-ϕ_{51}	ϵ^2_γ	ϵ^2_m	χ^2
5	-0.63± 0.58	-1.30± 1.36	0.83± 0.18	-32.4°+ 29.4° - 18.2°	-52.5°+ 55.5° - 16.9°	39.6°+ 5.7° - 6.8°	0.52	0.05	1.0
8	0.85± 0.34	-0.93± 0.37	-0.79± 0.10	40.5°+ 9.5° - 13.3°	-42.8°+ 13.7° - 9.5°	-38.3°+ 3.7° - 3.3°	0.57	0.07	8.9
9	-0.82± 0.39	-0.57± 0.37	0.47± 0.14	-39.3°+ 16.1° - 11.1°	-29.7°+ 18.3° - 13.5°	25.0°+ 6.4° - 7.2°	0.47	0.05	1.0
10	-0.66± 0.54	-1.54± 1.42	1.01± 0.19	-33.3°+ 26.4° - 16.7°	-56.9°+ 50.5° - 14.4°	45.3°+ 4.9° - 6.0°	0.59	0.07	2.2
19	-0.39± 0.56	-0.83± 1.30	0.32± 0.13	-21.4°+ 31.2° - 22.3°	-39.5°+ 64.8° - 25.2°	17.9°+ 6.3° - 6.8°	0.20	0.02	0.7
20	1.46± 0.24	0.33± 0.13	0.49± 0.15	55.7°+ 3.9° - 4.8°	18.5°+ 6.3° - 6.8°	26.1°+ 6.4° - 7.2°	0.70	0.12	1.5
24	0.06± 0.81	-7.14± 101.	-0.40± 0.11	3.2°+ 37.6° - 40.1°	-82.0°+171.4° - 7.5°	-22.0°+ 5.6° - 5.2°	0.14	0.01	1.0
26	0.41± 0.68	1.05± 1.89	0.43± 0.14	22.4°+ 25.2° - 37.7°	46.5°+ 24.8° - 86.3°	23.5°+ 6.6° - 7.3°	0.26	0.20	1.3
28	-0.64± 0.40	-0.84± 0.66	0.54± 0.15	-32.7°+ 19.3° - 13.6°	-40.1°+ 29.5° - 16.2°	28.4°+ 6.3° - 7.1°	0.41	0.04	0.4
33	-0.21± 0.56	-4.08±11.32	0.84± 0.16	-11.6°+ 31.0° - 25.7°	-76.2°+158.4° - 10.1°	40.0°+ 5.0° - 5.8°	0.43	0.05	1.1
36	1.30± 0.30	2.85± 0.64	3.71± 0.34	52.4°+ 5.5° - 7.4°	70.7°+ 3.3° - 5.0°	74.9°+ 1.2° - 1.4°	0.94	0.50	2.7
37	0.58± 0.47	1.29± 1.18	0.74± 0.16	30.1°+ 16.3° - 23.8°	52.1°+ 15.8° - 45.9°	36.7°+ 5.5° - 6.4°	0.47	0.05	0.7

Table 2.4 (continued)

Res. No.	s- δ_{31}	s- δ_{53}	s- δ_{51}	s-ϕ_{31}	s-ϕ_{53}	s-ϕ_{51}	ϵ_r^2	ϵ_m^2	χ^2
41	-0.71± 0.37	-0.59± 0.44	0.42± 0.17	-35.2°+ 16.5° - 11.8°	-30.6°+ 22.0° - 15.3°	22.6°+ 7.6° - 8.6°	0.40	0.04	3.5
43	-1.02± 0.30	-0.33± 0.24	0.33± 0.19	-45.6°+ 9.9° - 7.4°	-18.1°+ 13.0° - 11.3°	18.4°+ 9.3° - 10.4°	0.54	0.07	2.7
44	0.39± 0.73	2.10± 4.22	0.81± 0.19	21.1°+ 27.0° - 40.1°	64.5°+ 16.5° -129.3°	39.0°+ 6.1° - 7.3°	0.45	0.05	1.4
50	0.35± 0.75	2.19± 4.85	0.77± 0.16	19.4°+ 28.3° - 41.0°	65.5°+ 16.4° -134.8°	37.7°+ 5.4° - 6.4°	0.42	0.05	0.3
51	-0.65± 0.36	-0.58± 0.44	0.37± 0.14	-33.0°+ 17.1° - 12.4°	-29.9°+ 22.3° - 15.6°	20.5°+ 6.8° - 7.4°	0.36	0.04	0.3
52	1.49± 0.23	0.45± 0.17	0.67± 0.20	56.2°+ 3.7° - 4.7°	24.3°+ 7.6° - 8.6°	34.0°+ 7.0° - 8.4°	0.73	0.15	1.3
55	0.91± 0.32	0.98± 0.45	0.90± 0.17	42.4°+ 8.5° - 11.6°	44.5°+ 10.6° - 16.6°	41.9°+ 5.1° - 6.0°	0.62	0.10	4.2
56	-0.37± 0.65	-2.05± 3.84	0.77± 0.17	-20.5°+ 36.1° - 25.3°	-64.0°+124.8° - 16.3°	37.5°+ 5.6° - 6.6°	0.42	0.05	0.4
59	-0.60± 0.44	-1.38± 1.21	0.83± 0.20	-31.1°+ 21.9° - 15.1°	-54.0°+ 44.4° - 14.8°	39.8°+ 6.1° - 7.4°	0.51	0.07	0.6
63	-1.34± 0.25	-0.84± 0.25	1.13± 0.20	-53.3°+ 5.8° - 4.5°	-40.0°+ 9.6° - 7.5°	48.4°+ 4.5° - 5.5°	0.75	0.18	0.1
65	-0.90± 0.29	-0.42± 0.26	0.38± 0.16	-42.1°+ 10.4° - 7.9°	-22.9°+ 13.8° - 11.5°	20.9°+ 7.6° - 8.5°	0.49	0.06	1.1
69	-1.05± 0.44	-1.39± 0.83	1.46± 0.31	-46.4°+ 15.1° - 9.8°	-54.3°+ 24.7° - 11.4°	55.6°+ 5.0° - 6.7°	0.76	0.19	4.6

Table 2.4 (continued)

Res. No.	s- δ_{31}	s- δ_{53}	s- δ_{51}	s-ϕ_{31}	s-ϕ_{53}	s-ϕ_{51}	ϵ^2_γ	ϵ^2_m	χ^2
71	-0.64± 0.46	-1.20± 1.12	0.77± 0.22	-32.6° + 22.7° - 15.2°	-50.3° + 45.6° - 16.5°	37.5° + 7.1° - 8.8°	0.50	0.07	2.0
72	-1.11± 0.23	-0.34± 0.18	0.38± 0.16	-48.1° + 6.7° - 5.3°	-18.7° + 9.6° - 8.6°	20.6° + 7.5° - 8.3°	0.58	0.09	2.0
75	0.59± 0.44	1.28± 1.15	0.75± 0.18	30.4° + 15.5° - 22.3°	52.1° + 15.5° - 44.2°	36.9° + 6.1° - 7.3°	0.48	0.06	0.7
76	-0.29± 0.61	-2.90± 6.52	0.83± 0.18	-16.0° + 33.9° - 25.9°	-71.0° +145.5° - 13.0°	39.7° + 5.7° - 6.8°	0.43	0.05	0.2
78	-1.10± 0.22	-0.09± 0.14	0.10± 0.14	-47.6° + 6.4° - 5.1°	-5.0° + 7.9° - 7.7°	5.5° + 8.1° - 8.3°	0.55	0.08	5.3
82	0.08± 0.41	15.94±82.82	1.26± 0.17	4.5° + 21.7° - 23.0°	86.4° + 3.0° -175.6°	51.6° + 3.5° - 4.2°	0.62	0.11	0.4
83	-0.59± 0.42	-1.39± 1.20	0.82± 0.19	-30.6° + 20.8° - 14.7°	-54.3° + 43.2° - 14.6°	39.5° + 5.9° - 7.1°	0.51	0.07	0.7
84	1.62± 0.23	0.46± 0.19	0.74± 0.25	58.3° + 3.3° - 4.0°	24.5° + 8.4° - 9.6°	36.5° + 8.1° - 10.2°	0.76	0.19	5.8
85	0.99± 0.32	1.17± 0.53	1.16± 0.22	44.8° + 8.0° - 11.1°	49.4° + 10.1° - 16.9°	49.2° + 4.8° - 6.0°	0.70	0.15	3.4
89	-0.25± 0.59	-3.41± 8.50	0.84± 0.17	-13.9° + 32.9° - 26.1°	-73.7° +152.5° - 11.5°	40.1° + 5.2° - 6.1°	0.44	0.06	0.7
93	-1.11± 0.27	-0.54± 0.28	0.60± 0.21	-48.1° + 8.0° - 6.1°	-28.4° + 13.6° - 10.8°	31.1° + 7.9° - 9.5°	0.62	0.11	4.7
94	0.09± 0.46	17.36±86.88	1.60± 0.18	5.2° + 23.7° - 25.5°	86.7° + 2.7° -175.9°	57.9° + 2.7° - 3.1°	0.72	0.17	3.5

Table 2.4 (continued)

Res. No.	s- δ_{31}	s- δ_{53}	s- δ_{51}	s-φ_{31}	s-φ_{53}	s-φ_{51}	ϵ^2_r	ϵ^2_m	χ^2
95	-1.09± 0.22	-0.40± 0.18	0.43± 0.16	-47.2°+ 6.6° - 5.3°	-21.7°+ 9.6° - 8.4°	23.3°+ 7.1° - 7.9°	0.58	0.10	3.8
101	-1.57± 0.27	-0.83± 0.27	1.30± 0.27	-57.5°+ 5.0° - 3.9°	-39.7°+ 10.6° - 8.1°	52.5°+ 5.1° - 6.6°	0.81	0.25	4.2
102	-3.50± 0.25	-0.24± 0.06	0.84± 0.21	-74.1°+ 1.2° - 1.0°	-13.5°+ 3.5° - 3.4°	40.1°+ 6.4° - 7.9°	0.93	0.50	2.2
104	0.69± 0.35	1.65± 1.01	1.13± 0.20	34.2°+ 11.7° - 16.0°	58.8°+ 10.6° - 26.2°	48.4°+ 4.5° - 5.5°	0.63	0.12	1.1
106	-3.79± 0.43	-1.13± 0.12	4.26± 0.42	-75.2°+ 1.8° - 1.5°	-48.4°+ 3.1° - 2.8°	76.8°+ 1.1° - 1.4°	0.97	0.72	1.9
107	-2.19± 0.27	-0.72± 0.16	1.57± 0.23	-65.5°+ 3.0° - 2.4°	-35.7°+ 6.6° - 5.7°	57.6°+ 3.5° - 4.3°	0.88	0.36	12.
109	0.66± 0.31	1.49± 0.83	0.99± 0.18	33.5°+ 10.7° - 14.1°	56.2°+ 10.5° - 22.7°	44.6°+ 4.7° - 5.7°	0.59	0.10	0.8
111	-0.70± 0.41	-2.37± 1.60	1.66± 0.22	-34.9°+ 18.9° - 13.0°	-67.2°+ 29.6° - 8.7°	58.9°+ 3.0° - 3.7°	0.76	0.21	4.6
112	-0.40± 0.44	-1.21± 1.54	0.48± 0.16	-21.6°+ 24.0° - 18.2°	-50.5°+ 68.8° - 19.6°	25.6°+ 6.9° - 7.8°	0.28	0.03	0.4

Table 2.5

Values of Mixing Ratios, ϵ^2, e^2, and ^{2} for 3/2+ Resonances in ^{49}V (j-spin)

Res. No.	j- δ_{31}	j- δ_{53}	j- δ_{51}	j-ϕ_{31}	j-ϕ_{53}	j-ϕ_{51}	ϵ^2_r	e^2_m	χ^2
14	-0.07± 0.23	-5.15±15.74	0.37± 0.11	-4.1°+ 13.4° - 12.9°	-79.0°+163.6° - 8.3°	20.3°+ 5.5° - 5.9°	0.12	0.01	6.9
	0.45± 0.12	0.34± 0.37	0.15± 0.23	24.2°+ 5.3° - 5.8°	18.6°+ 16.5° - 20.4°	8.6°+ 12.3° - 13.1°	0.18	0.01	6.9
17	-0.60± 0.70	-1.79± 1.18	1.08± 0.23	-31.1°+ 36.6° - 21.4°	-60.8°+ 29.3° - 10.6°	47.2°+ 5.3° - 6.7°	0.60	0.08	2.2
	1.53± 0.21	0.19± 0.41	0.29± 0.04	56.8°+ 3.3° - 4.0°	10.7°+ 20.2° - 23.1°	16.0°+ 2.2° - 2.3°	0.71	0.12	2.2
22	-0.68± 0.94	-1.72± 1.19	1.17± 0.23	-34.4°+ 48.9° - 24.1°	-59.8°+ 32.1° - 11.2°	49.6°+ 4.9° - 6.1°	0.65	0.10	1.6
	1.68± 0.27	0.19± 0.45	0.31± 0.04	59.3°+ 3.6° - 4.6°	10.5°+ 22.0° - 25.5°	17.4°+ 2.3° - 2.4°	0.75	0.15	1.6
25	-0.06± 0.04	1.25± 1.23	-0.08± 0.27	-3.7°+ 2.5° - 2.5°	51.3°+ 16.7° - 50.3°	-4.7°+ 15.5° - 14.9°	0.01	0.00	4.8
	-0.06± 0.27	1.31± 9.85	-0.08± 0.27	-3.6°+ 15.5° - 15.0°	52.6°+ 32.3° -135.9°	-4.7°+ 15.5° - 14.9°	0.01	0.00	4.8
29	-0.98± 0.16	-2.97± 0.14	2.91± 0.75	-44.4°+ 5.1° - 4.3°	-71.4°+ 0.9° - 0.8°	71.0°+ 3.7° - 5.9°	0.90	0.37	5.2
	3.77± 0.53	0.51± 0.20	1.92± 0.17	75.1°+ 1.8° - 2.3°	27.0°+ 8.3° - 9.7°	62.5°+ 1.9° - 2.2°	0.95	0.52	5.2
32	0.34± 0.03	-5.96± 0.52	-2.04± 0.84	18.9°+ 1.3° - 1.3°	-80.5°+ 0.9° - 0.7°	-63.9°+ 13.6° - 6.9°	0.81	0.21	8.5
	-2.99± 254.	-0.01± 196.	0.05± 0.01	-71.5°+161.3° - 18.3°	-0.7°+ 90.4° - 89.0°	2.7°+ 0.4° - 0.4°	0.90	0.36	8.5

Table 2.5 (continued)

Res. No.	j- δ_{31}	j- δ_{53}	j- δ_{51}	j-ϕ_{31}	j-ϕ_{53}	j-ϕ_{51}	ϵ^2_γ	ϵ^2_m	χ^2
35	-0.53± 0.09	-3.34± 0.35	1.78± 0.29	-28.0°+ 4.0° - 3.7°	-73.3°+ 1.8° - 1.5°	60.7°+ 3.5° - 4.6°	0.78	0.18	0.8
	2.19± 0.20	0.44± 0.17	0.96± 0.09	65.5°+ 1.8° - 2.1°	23.6°+ 7.5° - 8.4°	43.8°+ 2.6° - 2.8°	0.85	0.27	0.8
39	-0.90± 0.12	-0.49± 0.22	0.44± 0.88	-42.0°+ 3.9° - 3.4°	-26.3°+ 10.7° - 9.0°	24.0°+ 28.9° - 47.4°	0.50	0.06	1.0
	0.96± 0.10	-0.37± 0.19	-0.36± 0.76	44.0°+ 2.7° - 3.0°	-20.5°+ 10.0° - 8.9°	-19.8°+ 41.5° - 28.4°	0.51	0.06	1.0
40	0.72± 0.16	-0.57± 0.22	-0.41± 0.27	35.7°+ 5.6° - 6.6°	-29.6°+ 10.5° - 8.7°	-22.2°+ 14.4° - 12.0°	0.41	0.04	0.7
	-0.82± 0.08	-0.34± 0.26	0.28± 5.40	-39.4°+ 2.8° - 2.6°	-18.6°+ 14.0° - 12.0°	15.4°+ 64.6° - 94.4°	0.43	0.05	0.7
53	-0.39± 0.05	-5.12± 0.38	2.02± 0.68	-21.5°+ 2.3° - 2.2°	-79.0°+ 0.9° - 0.8°	63.7°+ 6.0° - 10.3°	0.81	0.22	1.7
	2.30± 0.21	0.56± 0.15	1.30± 0.12	66.5°+ 1.8° - 2.0°	29.4°+ 6.0° - 6.8°	52.4°+ 2.4° - 2.7°	0.87	0.32	1.7
54	-0.53± 0.24	-2.23± 0.57	1.18± 0.16	-27.9°+ 11.6° - 9.6°	-65.9°+ 6.9° - 4.5°	49.8°+ 3.5° - 4.1°	0.63	0.10	4.3
	1.59± 0.14	0.28± 0.26	0.45± 0.06	57.8°+ 2.2° - 2.5°	15.7°+ 12.8° - 14.6°	24.1°+ 2.7° - 2.8°	0.73	0.16	4.3
58	-0.85± 0.19	-0.80± 0.22	0.68± 0.35	-40.3°+ 7.0° - 5.8°	-38.7°+ 8.7° - 7.0°	34.2°+ 11.6° - 15.9°	0.54	0.08	1.4
	1.23± 0.20	-0.13± 0.73	-0.16± 0.08	50.8°+ 4.1° - 5.0°	-7.6°+ 38.4° - 33.2°	-9.2°+ 4.4° - 4.3°	0.60	0.10	1.4

Table 2.5 (continued)

Res. No.	j- δ_{31}	j- δ_{53}	j- δ_{51}	j-ϕ_{31}	j-ϕ_{53}	j-ϕ_{51}	ϵ^2_r	ϵ^2_m	χ^2
60	-0.52± 0.24	-2.27± 0.59	1.19± 0.17	-27.6°+ 11.6° - 9.6°	-66.2°+ 7.0° - 4.5°	49.8°+ 3.7° - 4.4°	0.63	0.11	1.9
	1.58± 0.15	0.29± 0.26	0.46± 0.06	57.7°+ 2.3° - 2.6°	16.1°+ 12.7° - 14.5°	24.5°+ 2.8° - 2.9°	0.73	0.16	1.9
67	-1.43± 0.34	-1.49± 0.15	2.13± 0.26	-55.0°+ 7.7° - 5.6°	-56.1°+ 3.0° - 2.6°	64.8°+ 2.4° - 3.0°	0.87	0.32	5.5
	3.35± 1.10	0.23± 0.53	0.79± 0.07	73.4°+ 4.0° - 7.4°	13.2°+ 24.3° - 29.8°	38.1°+ 2.5° - 2.7°	0.92	0.46	5.5
68	-0.12± 0.02	#12.9± 1.45	1.61± 1.87	-7.1°+ 0.9° - 0.9°	-85.6°+ 0.6° - 0.4°	58.1°+ 15.8° - 72.7°	0.72	0.16	3.0
	1.68± 0.17	0.64± 0.15	1.08± 0.11	59.3°+ 2.3° - 2.7°	32.6°+ 5.8° - 6.6°	47.1°+ 2.8° - 3.1°	0.80	0.22	3.0
70	-0.43± 0.16	-2.72± 0.65	1.17± 0.17	-23.3°+ 7.9° - 7.1°	-69.8°+ 5.6° - 3.7°	49.6°+ 3.8° - 4.5°	0.61	0.10	1.0
	1.50± 0.13	0.34± 0.22	0.51± 0.07	56.3°+ 2.2° - 2.5°	18.8°+ 10.7° - 12.2°	27.1°+ 3.0° - 3.1°	0.72	0.10	1.0
74	-0.60± 0.07	-4.14± 0.22	2.49± 0.98	-31.0°+ 2.8° - 2.7°	-76.4°+ 0.7° - 0.7°	68.1°+ 5.8° - 11.7°	0.87	0.32	3.2
	2.94± 0.33	0.58± 0.15	1.72± 0.16	71.2°+ 1.8° - 2.2°	30.3°+ 6.1° - 6.9°	59.8°+ 2.2° - 2.5°	0.92	0.46	3.2
77	-0.96± 0.28	-1.12± 0.22	1.08± 0.23	-44.0°+ 9.7° - 7.3°	-48.2°+ 6.4° - 5.1°	47.1°+ 5.4° - 6.8°	0.68	0.13	1.9
	1.76± 4.67	0.04± 9.72	0.08± 0.02	60.4°+ 20.7° -131.4°	2.4°+ 81.8° - 86.5°	4.5°+ 0.9° - 0.9°	0.76	0.18	1.9

Table 2.5 (continued)

Res. No.	j- δ_{31}	j- δ_{53}	j- δ_{51}	j-ϕ_{31}	j-ϕ_{53}	j-ϕ_{51}	ϵ_γ^2	ϵ_m^2	χ^2
79	-2.39± 0.19	-0.88± 0.13	2.10± 0.27	-67.3°+ 1.7° - 1.5°	-41.3°+ 4.4° - 3.9°	64.5°+ 2.6° - 3.2°	0.91	0.42	1.7
	4.16± 371.	0.02± 102.	0.07± 0.01	76.5°+ 13.4° -166.3°	1.0°+ 88.5° - 90.4°	4.0°+ 0.6° - 0.6°	0.95	0.56	1.7
80	-0.76± 0.18	-2.58± 0.22	1.97± 0.30	-37.3°+ 7.3° - 6.1°	-68.8°+ 1.8° - 1.5°	63.0°+ 3.2° - 4.1°	0.82	0.25	0.5
	2.57± 0.29	0.41± 0.21	1.05± 0.10	68.8°+ 2.0° - 2.4°	22.3°+ 9.6° - 11.1°	46.5°+ 2.5° - 2.8°	0.89	0.37	0.5
86	-0.20± 0.05	-5.72± 1.21	1.13± 0.22	-11.2°+ 2.8° - 2.7°	-80.1°+ 2.6° - 1.7°	48.5°+ 4.9° - 6.1°	0.57	0.09	3.3
	1.29± 0.12	0.49± 0.18	0.63± 0.08	52.2°+ 2.4° - 2.7°	26.1°+ 7.8° - 9.0°	32.3°+ 3.2° - 3.5°	0.67	0.14	3.3
87	-0.40± 0.20	-2.49± 0.82	1.00± 0.16	-21.9°+ 10.7° - 9.3°	-68.1°+ 9.0° - 5.1°	45.0°+ 4.1° - 4.8°	0.54	0.08	3.2
	1.30± 0.11	0.30± 0.26	0.39± 0.06	52.5°+ 2.3° - 2.6°	16.9°+ 12.6° - 14.5°	21.5°+ 3.0° - 3.1°	0.65	0.12	3.2
88	-0.42± 0.21	-2.44± 0.75	1.03± 0.16	-22.9°+ 10.7° - 9.3°	-67.7°+ 8.4° - 4.9°	45.8°+ 4.0° - 4.7°	0.55	0.09	1.3
	1.35± 0.12	0.30± 0.26	0.41± 0.06	53.4°+ 2.3° - 2.5°	16.8°+ 12.5° - 14.3°	22.1°+ 2.9° - 3.0°	0.66	0.13	1.3
90	-0.10± 0.01	▮16.3± 1.63	1.62± 3.09	-5.7°+ 0.7° - 0.7°	-86.5°+ 0.4° - 0.3°	58.4°+ 19.7° -114.1°	0.73	0.17	1.8
	1.67± 0.17	0.67± 0.15	1.12± 0.11	59.1°+ 2.4° - 2.7°	33.8°+ 5.5° - 6.4°	48.2°+ 2.7° - 3.0°	0.80	0.24	1.8

Table 2.5 (continued)

Res. No.	$j-\delta_{31}$	$j-\delta_{53}$	$j-\delta_{51}$	$j-\phi_{31}$	$j-\phi_{53}$	$j-\phi_{51}$	ϵ_γ^2	ϵ_m^2	χ^2
91	-0.41± 0.12	-2.97± 0.56	1.21± 0.16	-22.2°+ 6.1° - 5.6°	-71.4°+ 4.0° - 2.8°	50.4°+ 3.4° - 4.0°	0.62	0.11	2.0
	1.52± 0.12	0.37± 0.21	0.57± 0.07	56.6°+ 2.0° - 2.3°	20.4°+ 9.6° - 11.0°	29.5°+ 2.9° - 3.1°	0.72	0.17	2.0
92	-0.69± 0.32	-1.03± 0.29	0.71± 0.28	-34.7°+ 14.5° - 10.8°	-45.8°+ 9.5° - 7.1°	35.5°+ 9.4° - 12.2°	0.50	0.07	1.7
	1.18± 8.33	-0.02±37.65	-0.02± 0.01	49.7°+ 34.3° -131.8°	-1.0°+ 89.5° - 87.5°	-1.2°+ 0.4° - 0.4°	0.58	0.10	1.7
96	-0.84± 0.28	-1.09± 0.23	0.92± 0.24	-40.0°+ 11.0° - 8.3°	-47.5°+ 6.6° - 5.3°	42.5°+ 6.7° - 8.5°	0.61	0.11	1.6
	1.50±10.67	0.02±27.31	0.03± 0.01	56.3°+ 29.0° -140.0°	1.3°+ 86.6° - 89.2°	1.9°+ 0.4° - 0.4°	0.69	0.15	1.6
97	-2.45± 0.23	-0.52± 0.24	1.28± 0.48	-67.8°+ 2.1° - 1.6°	-27.6°+ 12.0° - 9.9°	52.1°+ 8.4° - 13.4°	0.88	0.37	5.7
	2.83± 0.56	-0.31± 0.27	-0.87± 1.16	70.5°+ 3.0° - 4.3°	-17.1°+ 14.9° - 12.9°	-41.1°+ 57.3° - 22.8°	0.90	0.41	5.7
98	0.38± 0.02	8.71± 0.19	3.29± 6.71	20.7°+ 0.9° - 0.9°	83.5°+ 0.1° - 0.1°	73.1°+ 11.2° -146.8°	0.92	0.46	2.0
	2.53±47.12	1.21±16.12	3.06± 0.48	68.4°+ 20.4° -157.1°	50.4°+ 36.3° -136.6°	71.9°+ 2.3° - 3.1°	0.94	0.55	2.0
99	-2.65± 0.24	-0.58± 0.22	1.54± 0.36	-69.3°+ 1.9° - 1.6°	-30.1°+ 10.1° - 8.4°	57.0°+ 5.3° - 7.4°	0.90	0.42	1.8
	3.36± 1.31	-0.23± 0.47	-0.77± 1.50	73.4°+ 4.5° - 9.4°	-13.0°+ 26.3° - 21.9°	-37.7°+ 73.7° - 28.6°	0.92	0.48	1.8

Tale 2.5 (continued)

Res. No.	$j-\delta_{31}$	$j-\delta_{53}$	$j-\delta_{51}$	$j-\phi_{31}$	$j-\phi_{53}$	$j-\phi_{51}$	ϵ^2_r	ϵ^2_m	χ^2
100	-1.88± 0.17	-1.11± 0.11	2.09± 0.26	-62.0°+ 2.4° - 2.1°	-48.1°+ 3.0° - 2.7°	64.4°+ 2.5° - 3.0°	0.89	0.38	1.0
	3.74± 5.25	0.13± 1.77	0.47± 0.05	75.0°+ 8.6° -131.5°	7.2°+ 55.0° - 65.9°	25.2°+ 2.4° - 2.4°	0.93	0.53	1.0
103	-4.99± 0.52	-0.87± 0.13	4.35± 0.55	-78.7°+ 1.3° - 1.0°	-41.0°+ 4.6° - 4.0°	77.0°+ 1.4° - 1.8°	0.98	0.77	2.0
	24.91± 554.	0.22± 3.09	5.40± 0.58	87.7°+ 2.2° -177.6°	12.3°+ 60.9° - 83.0°	79.5°+ 1.0° - 1.2°	1.00	0.98	2.0
105	-0.46± 0.31	-2.11± 0.80	0.96± 0.16	-24.6°+ 16.4° - 13.0°	-64.7°+ 12.0° - 6.4°	44.0°+ 4.3° - 5.0°	0.53	0.08	2.2
	1.30± 0.12	0.26± 0.32	0.34± 0.06	52.5°+ 2.4° - 2.7°	14.4°+ 15.6° - 18.1°	18.6°+ 2.8° - 2.9°	0.64	0.12	2.2
108	-1.14± 0.41	-1.49± 0.21	1.70± 0.22	-48.7°+ 12.5° - 8.4°	-56.2°+ 4.2° - 3.4°	59.5°+ 2.9° - 3.6°	0.81	0.25	1.3
	2.61± 0.73	0.21± 0.58	0.56± 0.06	69.0°+ 4.3° - 7.1°	12.0°+ 26.3° - 32.0°	29.0°+ 2.7° - 2.9°	0.88	0.36	1.3
110	-0.78± 0.54	-1.34± 0.38	1.04± 0.21	-37.8°+ 24.4° - 14.9°	-53.2°+ 9.4° - 6.5°	46.0°+ 5.2° - 6.3°	0.63	0.12	1.9
	1.59± 0.57	0.11± 1.26	0.18± 0.03	57.9°+ 7.3° - 12.3°	6.5°+ 47.5° - 55.4°	10.3°+ 1.9° - 1.9°	0.72	0.17	1.9

Table 2.6

Values of Mixing Ratios, ϵ^2, ϵ^2, and ^{2} for 3/2+ Resonances in ^{49}V (s-spin)

Res. No.	s-δ_{31}	s-δ_{53}	s-δ_{51}	s-ϕ_{31}	s-ϕ_{53}	s-ϕ_{51}	ϵ^2_γ	ϵ^2_n	χ^2
14	0.31± 0.19	0.72± 5.50	0.22± 5.14	17.0°+ 9.3° - 10.3°	35.9°+ 44.9° -114.1°	12.5°+ 67.0° - 91.0°	0.12	0.01	6.9
	0.33± 0.25	-1.11± 5.73	-0.35± 1.19	17.7°+ 12.1° - 14.0°	-47.9°+125.7° - 33.7°	-19.4°+ 59.3° - 37.6°	0.18	0.01	6.9
17	0.75± 0.18	1.32± 0.50	0.98± 0.25	36.8°+ 6.1° - 7.2°	52.8°+ 8.4° - 13.5°	44.6°+ 6.4° - 8.2°	0.60	0.08	2.2
	0.87± 0.27	-1.47± 0.47	-1.28± 0.22	41.2°+ 7.8° - 10.1°	-55.8°+ 10.8° - 7.0°	-52.1°+ 5.2° - 4.2°	0.71	0.12	2.2
22	0.80± 0.18	1.37± 0.39	1.10± 0.22	38.8°+ 5.7° - 6.7°	53.8°+ 6.6° - 9.6°	47.6°+ 5.0° - 6.3°	0.65	0.10	1.6
	0.96± 0.28	-1.48± 0.36	-1.42± 0.21	43.8°+ 7.2° - 9.5°	-55.9°+ 7.7° - 5.5°	-54.8°+ 4.4° - 3.6°	0.75	0.15	1.6
25	-0.10± 0.07	-0.25± 7.16	0.03± 0.07	-5.7°+ 4.0° - 4.0°	-13.8°+ 95.5° - 68.5°	1.6°+ 4.0° - 4.0°	0.01	0.00	4.8
	-0.10± 0.07	-0.25± 7.16	0.03± 0.07	-5.7°+ 4.0° - 4.0°	-13.8°+ 95.5° - 68.5°	1.6°+ 4.0° - 4.0°	0.01	0.00	4.8
29	2.27± 0.29	0.91± 0.18	2.06± 0.32	66.3°+ 2.4° - 3.0°	42.2°+ 5.3° - 6.3°	64.1°+ 3.1° - 3.9°	0.90	0.37	5.2
	3.27± 0.48	-0.82± 0.20	-2.66± 0.50	73.0°+ 2.1° - 2.7°	-39.4°+ 7.6° - 6.2°	-69.6°+ 4.1° - 3.0°	0.95	0.52	5.2
32	-1.73± 0.34	0.66± 1.21	-1.15± 0.20	-60.0°+ 5.7° - 4.3°	33.2°+ 28.6° - 62.2°	-48.9°+ 5.6° - 4.6°	0.81	0.21	8.5
	-1.16± 0.21	-2.37± 0.25	2.76± 0.38	-49.3°+ 5.8° - 4.7°	-67.1°+ 2.4° - 2.0°	70.1°+ 2.3° - 2.9°	0.90	0.36	8.5

Table 2.6 (continued)

Res. No.	s-δ_{31}	s-δ_{53}	s-δ_{51}	s-ϕ_{31}	s-ϕ_{53}	s-ϕ_{51}	ϵ_r^2	ϵ_m^2	χ^2
38	1.42± 0.21	0.85± 0.25	1.20± 0.49	50.8°+ 3.6° - 4.4°	40.2°+ 7.3° - 9.3°	50.2°+ 9.2° - 14.8°	0.78	0.18	0.8
	1.76± 0.27	-0.93± 0.16	-1.63± 0.42	60.3°+ 3.4° - 4.3°	-42.8°+ 5.5° - 4.7°	-58.4°+ 8.0° - 5.5°	0.85	0.27	0.8
39	0.04± 0.18	22.66± 9.53	1.00± 0.68	2.5°+ 9.6° - 10.0°	87.5°+ 0.7° - 1.8°	45.1°+ 14.2° - 27.2°	0.50	0.06	1.0
	0.06± 0.24	-18.3± 9.92	-1.03± 0.57	3.2°+ 13.2° - 13.6°	-86.9°+ 3.6° - 1.1°	-45.8°+ 21.2° - 12.2°	0.51	0.06	1.0
40	-0.09± 0.23	9.52± 7.75	-0.82± 0.11	-4.9°+ 12.9° - 12.4°	84.0°+ 2.7° - 23.6°	-39.4°+ 3.9° - 3.5°	0.41	0.04	0.7
	-0.09± 0.18	-11.3± 8.61	0.86± 0.16	-4.3°+ 10.1° - 9.9°	-85.0°+ 6.9° - 1.9°	40.8°+ 4.7° - 5.5°	0.43	0.05	0.7
53	1.69± 0.31	0.85± 0.45	1.17±13.24	59.4°+ 4.0° - 5.2°	34.6°+ 14.1° - 21.0°	49.5°+ 36.6° -134.7°	0.81	0.22	1.7
	2.11± 0.29	-0.75± 0.28	-1.59± 2.96	64.6°+ 2.7° - 3.4°	-37.0°+ 10.8° - 8.4°	-57.8°+111.8° - 19.8°	0.87	0.32	1.7
59	0.87± 0.16	1.10± 0.31	0.96± 0.25	41.1°+ 4.8° - 5.6°	47.7°+ 6.9° - 9.4°	43.8°+ 6.5° - 8.3°	0.63	0.10	4.3
	1.04± 0.23	-1.22± 0.24	-1.27± 0.21	46.2°+ 5.6° - 7.1°	-50.7°+ 6.2° - 4.9°	-51.9°+ 5.1° - 4.2°	0.73	0.16	4.3
58	0.28± 0.16	3.71± 1.08	1.05± 0.09	15.8°+ 8.2° - 8.0°	74.9°+ 3.3° - 5.7°	46.4°+ 2.3° - 2.6°	0.54	0.08	1.4
	0.34± 0.25	-3.48± 1.18	-1.19± 0.10	18.8°+ 11.6° - 13.5°	-74.0°+ 7.5° - 3.9°	-49.9°+ 2.6° - 2.4°	0.60	0.10	1.4

Table 3.6 (continued)

Eos. No.	s-δ_{31}	s-δ_{53}	s-δ_{51}	s-ϕ_{31}	s-ϕ_{53}	s-ϕ_{51}	ϵ^2_r	ϵ^2_m	χ^2
60	0.89± 0.17	1.09± 0.31	0.95± 0.26	41.3°+ 4.9° - 5.8°	47.4°+ 7.1° - 9.7°	43.6°+ 6.9° - 9.0°	0.63	0.11	1.9
	1.05± 0.24	-1.21± 0.24	-1.27± 0.23	46.4°+ 5.8° - 7.4°	-50.3°+ 6.4° - 5.1°	-51.7°+ 5.6° - 4.5°	0.73	0.16	1.9
67	1.38± 0.15	1.57± 0.09	2.16± 0.18	54.0°+ 2.7° - 3.1°	57.4°+ 1.5° - 1.6°	65.1°+ 1.7° - 1.9°	0.87	0.32	5.5
	2.06± 0.32	-1.34± 0.07	-2.76± 0.26	64.1°+ 3.1° - 4.0°	-53.2°+ 1.4° - 1.3°	-70.1°+ 1.9° - 1.6°	0.92	0.46	5.5
69	1.42± 0.47	0.53± 1.52	0.76± 0.27	54.9°+ 7.2° - 11.2°	28.0°+ 36.0° - 72.7°	37.1°+ 8.7° - 11.3°	0.72	0.16	3.0
	1.66± 0.24	-0.67± 0.40	-1.11± 0.54	58.9°+ 3.3° - 4.1°	-33.9°+ 18.7° - 13.1°	-48.1°+ 18.0° - 10.7°	0.80	0.22	3.0
70	0.90± 0.19	0.96± 0.35	0.86± 0.40	42.1°+ 5.2° - 6.2°	43.7°+ 8.8° - 12.5°	40.8°+ 10.8° - 15.8°	0.61	0.10	1.0
	1.07± 0.25	-1.10± 0.26	-1.17± 0.29	46.9°+ 5.9° - 7.6°	-47.6°+ 7.6° - 5.9°	-49.5°+ 8.3° - 6.2°	0.72	0.15	1.0
73	2.01± 0.35	0.76± 0.31	1.55± 0.55	63.9°+ 3.9° - 4.9°	37.2°+ 9.7° - 13.0°	57.1°+ 7.4° - 12.2°	0.87	0.32	3.2
	2.75± 0.41	-0.73± 0.27	-2.01± 0.91	70.0°+ 2.4° - 3.1°	-36.1°+ 11.3° - 8.8°	-63.5°+ 15.9° - 7.6°	0.92	0.46	3.2
77	0.60± 0.15	2.18± 0.34	1.32± 0.12	31.1°+ 6.0° - 6.8°	65.4°+ 3.0° - 3.8°	52.8°+ 2.3° - 2.6°	0.68	0.13	1.9
	0.77± 0.26	-2.06± 0.31	-1.59± 0.14	37.6°+ 8.2° - 10.4°	-64.1°+ 3.9° - 3.0°	-57.8°+ 2.5° - 2.2°	0.76	0.18	1.9

Table 2.6 (continued)

Res. No.	s-δ_{31}	s-δ_{53}	s-δ_{51}	s-θ_{31}	s-θ_{53}	s-λ_{51}	ϵ_r^2	ϵ_m^2	χ^2
79	0.97± 0.12	3.12± 0.08	3.03± 0.60	44.1°+ 3.4° - 3.8°	72.2°+ 0.4° - 0.5°	71.7°+ 2.8° - 4.1°	0.91	0.42	1.7
	1.73± 0.18	-2.19± 0.05	-3.78± 0.75	59.9°+ 4.7° - 6.5°	-65.5°+ 0.5° - 0.5°	-75.2°+ 3.5° - 2.4°	0.95	0.56	1.7
80	1.50± 0.19	0.99± 0.17	1.48± 0.23	56.2°+ 3.1° - 3.7°	44.8°+ 4.5° - 5.4°	56.0°+ 3.7° - 4.6°	0.82	0.25	0.5
	2.00± 0.29	-0.97± 0.14	-1.93± 0.29	63.4°+ 3.0° - 3.8°	-44.1°+ 4.5° - 3.9°	-62.7°+ 4.0° - 3.2°	0.89	0.37	0.5
81	0.96± 0.23	0.66± 0.70	0.63± 1.02	43.8°+ 6.1° - 7.6°	33.4°+ 20.2° - 35.6°	32.3°+ 26.5° - 53.6°	0.57	0.09	3.3
	1.09± 0.23	-0.85± 0.34	-0.93± 1.50	47.6°+ 5.3° - 6.7°	-40.3°+ 13.5° - 9.7°	-42.8°+ 72.8° - 24.8°	0.67	0.14	3.3
97	0.76± 0.17	1.02± 0.44	0.77± 0.36	37.1°+ 5.9° - 6.9°	45.5°+ 10.0° - 15.3°	37.5°+ 10.8° - 15.1°	0.54	0.08	3.2
	0.89± 0.24	-1.17± 0.35	-1.04± 0.26	41.4°+ 7.0° - 8.8°	-49.5°+ 10.0° - 7.1°	-46.0°+ 8.2° - 6.3°	0.65	0.12	3.2
98	0.77± 0.17	1.03± 0.40	0.80± 0.32	37.7°+ 5.6° - 6.6°	45.9°+ 9.2° - 13.6°	38.6°+ 9.7° - 13.2°	0.55	0.09	1.3
	0.91± 0.24	-1.18± 0.31	-1.07± 0.25	42.3°+ 6.7° - 8.4°	-49.7°+ 8.9° - 6.5°	-47.0°+ 7.5° - 5.8°	0.66	0.13	1.3
90	1.45± 0.57	0.51± 2.01	0.74± 0.23	55.4°+ 8.2° - 14.0°	27.1°+ 41.3° - 83.4°	36.5°+ 7.5° - 9.3°	0.73	0.17	1.8
	1.69± 0.23	-0.64± 0.43	-1.08± 0.39	59.4°+ 3.1° - 3.8°	-32.6°+ 20.9° - 14.4°	-47.3°+ 12.7° - 8.6°	0.80	0.24	1.8

Table 2.6 (continued)

Res. No.	s- δ_{31}	s- δ_{53}	s- δ_{51}	s-ϕ_{31}	s-ϕ_{53}	s-ϕ_{51}	ϵ^2_γ	ϵ^2_m	χ^2
91	0.95± 0.17	0.91± 0.33	0.86± 0.42	43.4°+ 4.8° - 5.7°	42.2°+ 8.9° - 12.3°	40.6°+ 11.3° - 16.9°	0.62	0.11	2.0
	1.13± 0.23	-1.03± 0.23	-1.17± 0.30	43.4°+ 5.1° - 6.5°	-46.0°+ 7.0° - 5.6°	-49.4°+ 8.6° - 6.4°	0.72	0.17	2.0
92	0.38+ 0.17	2.44± 0.81	0.92± 0.10	20.7°+ 7.8° - 8.7°	67.7°+ 5.2° - 9.3°	42.7°+ 2.9° - 3.2°	0.50	0.07	1.7
	0.45± 0.25	-2.41± 0.85	-1.09± 0.11	24.4°+ 10.9° - 13.1°	-67.4°+ 10.1° - 5.5°	-47.5°+ 3.0° - 2.7°	0.58	0.10	1.7
96	0.50± 0.15	2.2+ + 0.45	1.14± 0.11	26.7°+ 6.5° - 7.3°	66.1°+ 3.6° - 5.0°	48.6°+ 2.5° - 2.8°	0.61	0.11	1.6
	0.63± 0.25	-2.16± 0.45	-1.36± 0.13	32.2°+ 9.1° - 11.4°	-65.2°+ 5.4° - 3.9°	-53.7°+ 2.7° - 2.4°	0.69	0.15	1.6
97	0.19+ 0.13	14.18± 0.4°	2.76± 7.43	11.0°+ 6.9° - 7.2°	86.0°+ 0.1° - 0.1°	70.1°+ 14.3° -148.0°	0.88	0.37	5.7
	0.33± 0.39	-9.81± 0.74	-2.94± 3.65	18.5°+ 17.5° - 21.8°	-83.5°+ 0.6° - 0.5°	-71.2°+106.5° - 10.1°	0.90	0.41	5.7
98	3.17± 1.02	0.31± 2.42	0.97± 0.07	72.5°+ 4.1° - 7.4°	17.0°+ 52.8° - 81.7°	44.1°+ 1.9° - 2.0°	0.92	0.46	2.0
	3.82+ 1.03	-0.39± 1.78	-1.09± 0.08	75.3°+ 3.0° - 5.1°	-16.0°+ 72.1° - 48.2°	-47.6°+ 2.1° - 2.0°	0.94	0.55	2.0
99	0.35± 0.12	3.70± 0.22	3.04± 3.65	19.3°+ 5.7° - 6.1°	83.4°+ 0.2° - 0.2°	71.8°+ 9.7° -103.3°	0.90	0.42	1.8
	0.64± 0.40	-3.33± 0.30	-3.39± 2.14	32.4°+ 13.5° - 19.1°	-79.4°+ 0.6° - 0.5°	-73.6°+ 22.3° - 6.2°	0.92	0.48	1.8

Table 2.6 (continued)

Res. No.	s- δ_{31}	s- δ_{53}	s- δ_{51}	s-ϕ_{31}	s-ϕ_{53}	s-ϕ_{51}	ϵ^2_γ	ϵ^2_m	χ^2
100	1.16± 0.13	2.20± 0.08	2.56± 0.28	49.4° + 2.9° − 3.3°	65.5° + 0.7° − 0.8°	68.7° + 1.9° − 2.3°	0.89	0.38	1.0
	1.93± 0.35	-1.68± 0.04	-3.24± 0.41	62.6° + 3.7° − 4.9°	-59.2° + 0.7° − 0.7°	-72.9° + 2.3° − 1.8°	0.93	0.53	1.0
103	1.98± 0.12	3.18± 0.02	6.32± 4.73	63.3° + 1.3° − 1.5°	72.6° + 0.1° − 0.1°	81.0° + 3.8° − 23.3°	0.98	0.77	2.0
	14.93±16.45	-1.38± 0.15	#20.6±81.00	86.2° + 2.0° −142.4°	-54.2° + 3.3° − 2.8°	-87.2° +176.3° − 2.2°	1.00	0.98	2.0
105	0.70± 0.16	1.15± 0.02	0.80± 0.24	35.0° + 5.8° − 6.8°	48.9° + 8.5° − 12.8°	38.8° + 7.5° − 9.4°	0.53	0.08	2.2
	0.83± 0.23	-1.28± 0.34	-1.06± 0.20	39.6° + 7.1° − 8.9°	-52.0° + 8.9° − 6.4°	-46.7° + 6.0° − 4.9°	0.64	0.12	2.2
109	1.10± 0.14	1.56± 0.13	1.72± 0.15	47.7° + 3.5° − 4.0°	57.4° + 2.0° − 2.2°	59.8° + 2.0° − 2.3°	0.81	0.25	1.3
	1.55± 0.28	-1.40± 0.09	-2.17± 0.21	57.2° + 4.1° − 5.3°	-54.4° + 1.7° − 1.6°	-65.2° + 2.2° − 1.9°	0.88	0.36	1.3
110	0.64± 0.15	1.76± 0.33	1.13± 0.12	32.6° + 5.7° − 6.6°	60.4° + 4.0° − 5.4°	48.4° + 3.0° − 3.3°	0.63	0.12	1.9
	0.80± 0.25	-1.73± 0.29	-1.39± 0.14	38.8° + 7.7° − 9.8°	-59.9° + 4.8° − 3.7°	-54.2° + 3.0° − 2.6°	0.72	0.17	1.9

2.B.4. The l'=2 admixture ϵ_m^2 for matrix elements

The fraction of the l'=2 admixture for matrix elements in the inelastic decay channels is defined as

$$\epsilon_m^2 = \frac{|\langle l'=2\rangle|^2}{|\langle l'=0\rangle|^2+|\langle l'=2\rangle|^2} = \frac{|\langle s23\rangle|^2+|\langle s25\rangle|^2}{|\langle s05\rangle|^2+|\langle s23\rangle|^2+|\langle s25\rangle|^2} \tag{2.75}$$

Define $\delta_1 = \frac{\langle s05\rangle}{\langle s25\rangle}$, $\delta_2 = \frac{\langle s23\rangle}{\langle s25\rangle}$,

then ϵ_m^2 is equivalent to $\epsilon_m^2 = \frac{1+\delta_2^2}{1+\delta_1^2+\delta_2^2}$ (2.76)

and Eqn. 2.76 yields to

$$\begin{aligned}(a_{2g}-4/7)\,\delta_1^2+(a_{2g}+2/35)\,\delta_2^2+(96/245)\,\delta_2+(a_{2g}-2/35)=0\\ (a_{4g}+4/7)\,\delta_1^2+a_{4g}\qquad\delta_2^2+(48/49)\,\delta_2+(a_{4g}-2/7)=0\end{aligned} \tag{2.77}$$

Cancelling δ_1^2 in the above two equations, we obtain

$$\delta_2^2+1 = \frac{-(a_{2g}-(2/5)\,a_{4g}-4/5)}{a_{2g}-(2/5)\,a_{4g}+2/35} \tag{2.78}$$

Replacing δ_2^2+1 into Eqn. 2.76 , we obtain

$$\epsilon^2 = -(7/6)\,a_{2g}+(7/15)\,a_{4g}+14/15$$

The same equation can be obtained for the angular momentum representation. Therefore, ϵ_m^2 can be determined

with the a_{2g} , a_{4g} values from the gamma-ray angular distribution measurement alone.

2.B.5. Properties of mixing ratios related to line $a_{2g}=-a_{4g}$ and the sign of a_{2p}

Some simple predictions about mixing ratios can be made by examining values of (a_{2g}, a_{4g}). In spite of the complicated equations, one can still obtain some insight into the general trend of the mixing ratios.

Our first simple rule gives the relative strength between amplitude <j,2,3> and <j,2,5> from the values of a_{2g} and a_{4g}.

Define $\delta_1 = \dfrac{\langle j,0,1\rangle}{\langle j,2,3\rangle}$, $\delta_2 = \dfrac{\langle j,2,5\rangle}{\langle j,2,3\rangle}$,

Then Eqn. 2.29 yields

$$a_{2g} = \frac{4/7 \cdot (\mathrm{Pen}(0,2) \cdot \delta_1^2 + 5/14 - 5/14 \cdot \delta_2^2)}{1 + \mathrm{Pen}(0,2)\,\delta_1^2 + \delta_2^2}$$

$$a_{4g} = \frac{-4/7 \cdot (\mathrm{Pen}(0,2) \cdot \delta_1^2 - 8/7 + 9/14 \cdot \delta_2^2)}{1 + \mathrm{Pen}(0,2)\,\delta_1^2 + \delta_2^2} \qquad (2.79)$$

In our laboratory energy range, most of the

resonances show $a_{2g}>0$, $a_{4g}<0$ (low l'=2 admixture). The following derivation is applicable only to resonances with $a_{2g}>0$, $a_{4g}<0$.

1) If $a_{2g}>(-a_{4g})$

This is equivalent to:

$$(Pen(0,2)\cdot\zeta_1^2+5/14-5/14\cdot\zeta_2^2)>-(Pen(0,2)\cdot\zeta_1^2-8/7+9/14\cdot\zeta_2^2) \qquad (2.80)$$

and thus $-1.225<\zeta_2<1.225$

or $-50.77°<\phi_2<50.77°$ (2.81)

2) If $a_{2g}<-a_{4g}$

Then $\zeta_2>1.225$ or $\zeta_2<-1.225$

also $\phi_2>50.77°$ or $\phi_2<-50.77°$ (2.82)

Since $\zeta_2=\dfrac{<j,2,5>}{<j,2,3>}$, the condition $|\zeta_2|>1$ implies that the amplitude $<j,2,5>$ has a larger strength than the amplitude $<j,2,3>$. Therefore line $a_{2g}=-a_{4g}$ can be considered as a border line for $|<j,2,3>|\approx|<j,2,5>|$ and $|\phi_2|\approx 50.77°$. Combining this property with the derived physical region of a_{2g} and a_{4g} in sec. 2.A.5, we may picture this triangle region as a ϕ-space cone where ϕ travels between two extreme edges; $<j,2,3>=0$ where $\phi=90°$ or $\phi=-90°$ and $<j',2,5>=0$ where $\phi=0°$, and the in-between line $a_{2g}=-a_{4g}$ acts as a border line for

$|\langle j,2,3\rangle| \simeq |\langle j,2,5\rangle|$, where $\phi=50.77°$ or $\phi=-50.77°$.

Of the 45 $5/2^+$ resonances analyzed, there are 32 which have $a_{2g} > -a_{4g}$, and 13 which have $a_{2g} < -a_{4g}$. However, the average resonance strengths are unequal, and the total strengths in the $j\text{-}d_{3/2}$ and $j\text{-}d_{5/2}$ channels are approximately equal.

In our experimental results for the mixing ratio distributions, a strong sign correlation exists between amplitudes $\langle s,0,5\rangle$ and $\langle s,2,5\rangle$. Two out of forty-five resonances have negative relative sign between these two channels, the rest of the signs are positive. These two anomalous resonances are the only resonances which have negative values of a_{2p}. It is natural to suspect that there is a correlation between $a_{2p}<0$ and $\delta_1<0$, where the mixing ratios δ_1, δ_2 are defined as

$$\delta_1 = \frac{\langle s,0,5\rangle}{\langle s,2,5\rangle} \quad , \quad \delta_2 = \frac{\langle s,2,3\rangle}{\langle s,2,5\rangle}$$

Substituting δ_1, δ_2 into Eqn. 2.31, we obtain the Legendre polynomial coefficients a_{2p}, a_{4p} as

$$a_{2P} = \frac{(20/49)\delta_2^2 - 20/49 - 8/\sqrt{14} \cdot (P\&P) \cdot \delta_1}{1 + Pen(0,2) \cdot \delta_1^2 + \delta_2^2} \qquad (2.83)$$

$$a_{4P} = \frac{-(48/49)\delta_2^2 + 27/49}{1 + Pen(0,2) \cdot \delta_1^2 + \delta_2^2} \qquad (2.84)$$

On the average, most of the observed resonances have very small values for a_{4P} (because pure $l'=0$ corresponds to $(a_{2P}, a_{4P}) = (0,0)$). As a rough approximation, we set $a_{4P}=0$ in Eqn. 2.84 and obtain $\delta_2^2 \approx 27/48$. The average overall phase factor for $5/2^+$ resonances in ^{49}V with proton energy of 2 to 3 MeV is about -.55 and $Pen(0,2) \sim 14$. Substituting $\delta_2^2 \approx 27/49$ and $(P\&P) \approx 2.06$ in Eqn. 2.83 , we obtain

$$a_{2P} = \frac{-.179 + 4.4\,\delta_1}{1 + Pen(0,2) \cdot \delta_1^2 + \delta_2^2} \qquad (2.85)$$

Clearly, $a_{2P} > 0$ implies $\delta_1 > 0$. In other words the sign between $\langle s,0,5\rangle$ and $\langle s,2,5\rangle$ is positive, and $a_{2P} < 0$ implies a negative value of δ_1, unless $0 < \delta_1 < 0.04$ (which is a very small range).

Chapter 3

Experimental Equipment and Procedure

3.1 3 MV Van de Graaff System

The high-resolution proton inelastic scattering experiment on ^{48}Ti was performed with the 3 MV Van de Graaff accelerator and its associated high resolution system at the Triangle Universities Nuclear Laboratory. The accelerator and the analyzer-homogenizer system was first developed by Parks et al.(1958). A schematic drawing of this experimental system is shown in Fig. 3.1. In the rf ion source (inside the terminal) hydrogen (H_2) gas is ionized into two species, H^+ and HH^+. After acceleration through the constant electrostatic potential between terminal and ground, these two ions are separated by the analyzing magnet into two beams. The proton beam is steered directly into the scattering chamber for performing the experiment, while the molecular beam (HH^+) passes through the electrostatic analyzer into the homogenizer and is utilized to generate a feedback correction signal for beam stabilization.

Figure 3.1 Floor Plan of the 3 MV Van de Graaff Accelerator Laboratory.

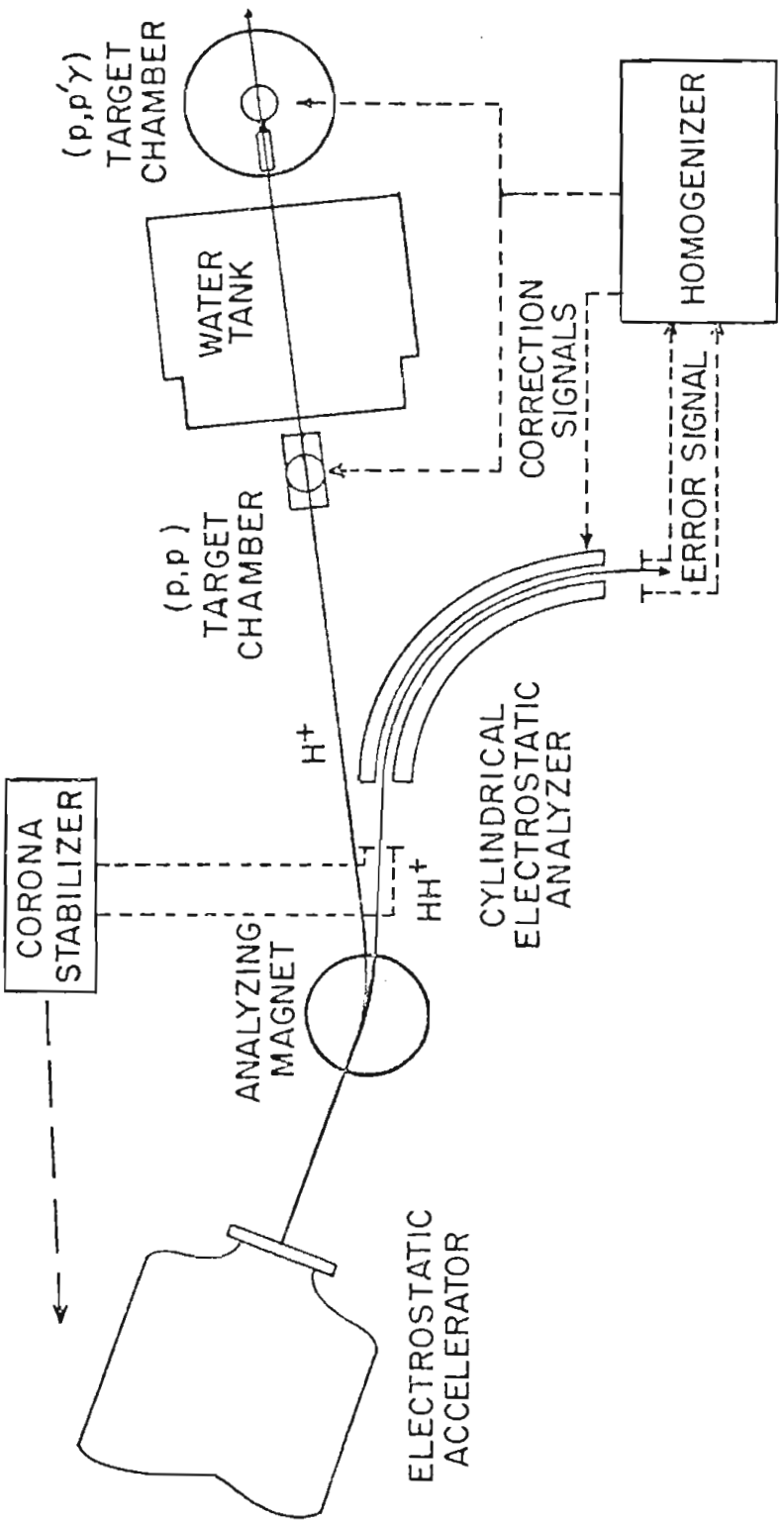
(p,p'γ)
TARGET
CHAMBER
WATER
TANK
(p,p)
TARGET
CHAMBER
CORRECTION
SIGNALS
HOMOGENIZER
ERROR SIGNAL
H+
HH+
CYLINDRICAL
ELECTROSTATIC
ANALYZER
CORONA
STABILIZER
ANALYZING
MAGNET
ELECTROSTATIC
ACCELERATOR

Before entering the analyzer, the HH^+ beam is intercepted by two object slits. The difference signal derived from current on these slits is sent back to the terminal via the corona control circuitry. With the corona control system, large low frequency fluctuations of the terminal voltage are removed, and the beam energy fluctuations are reduced to the order of 1 to 1.5 keV. The finite transit time of the corona discharge causes a phase lag in the correction signal. This phase lag effect and the large capacitance of the dome together limit the effectiveness of the corona control system to low frequencies.

Inside the electrostatic analyzer, the molecular beam (HH^+) is deflected by the large negative voltage applied on the inner plate. The ratio between the voltage needed to center the beam and the beam energy shift is about 1/111 and is purely a function of the analyzer geometry. This voltage is supplied by a Bertan (Model 205A-30N) power supply which can be remotely adjusted in the control room. Through a precision resistance stack, the inner plate voltage is divided by 10,000 and sent to the input of the differential voltmeter (DVM) (see Fig. 3.2). The difference signal between this voltage and the voltage set on the DVM (which is calibrated with respect to the beam energy) is then sent to the homogenizer where this difference signal is summed with the amplified difference

Figure 3.2 The Block Diagram of the Present Electrostatic Analyzer-Homogenizer Circuitry.

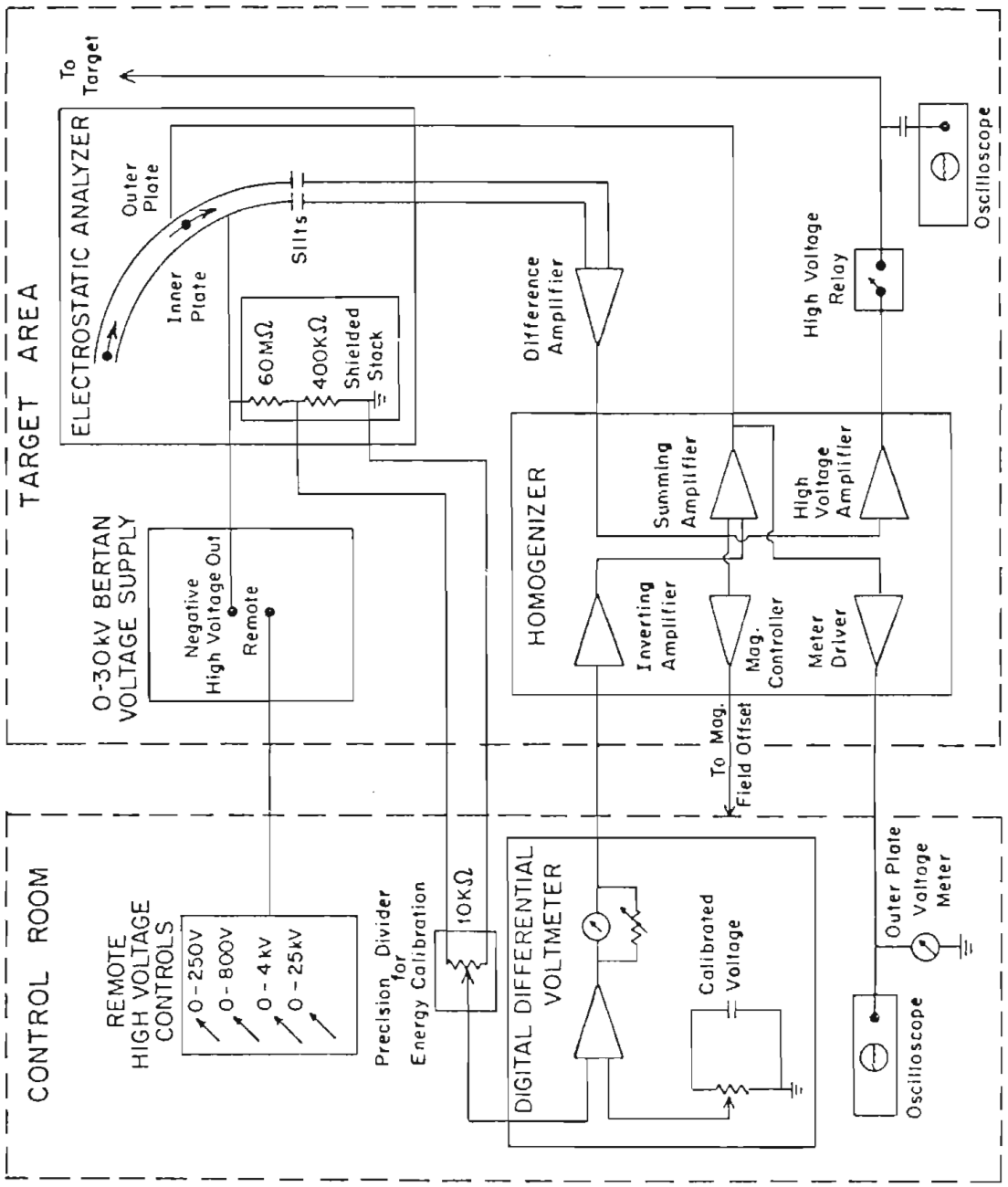
TARGET AREA
To Target
ELECTROSTATIC ANALYZER
Outer Plate
Inner Plate
Slits
60MΩ
400KΩ
Shielded Stack
Difference Amplifier
High Voltage Relay
Oscilloscope
0-30kV BERTAN VOLTAGE SUPPLY
Negative High Voltage Out
Remote
HOMOGENIZER
Summing Amplifier
High Voltage Amplifier
Inverting Amplifier
Mag. Controller
Meter Driver
To Mag. Field Offset
CONTROL ROOM
REMOTE HIGH VOLTAGE CONTROLS
0-250V
0-800V
0-4kV
0-25kV
Precision Divider for Energy Calibration
10KΩ
DIGITAL DIFFERENTIAL VOLTMETER
Calibrated Voltage
Outer Plate Voltage Meter
Oscilloscope

signal from the image slits. The image slits are located at the output of the analyzer. This summed signal is then sent to the outer plate (which is at ground potential) to maintain the beam centered on the image slits. The difference signal from the image slits is also sent to the magnet controller in order to offset the magnet (forcing the corona circuit to track the DVM energy setting), and after amplification is applied to the target rod (cancelling the fast beam energy fluctuations).

The analyzer beam fluctuations caused by the inner plate voltage drifting generate no correction signal to the target rod. Since these drifts cause both a DVM difference signal and a PAR difference signal, they cancel each other in the summing amplifier before being sent to the target rod. With this analyzer-homogenizer system, we are able to correct for most of the energy fluctuations of the proton beam without sacrificing intensity (since there is no need to tightly collimate the beam). The overall energy resolution on a thin solid target with a carbon substrate is about 300 to 450 eV (FWHM).

3.2 Scattering Chambers

The angular distribution measurements of the inelastically scattered proton and the subsequent gamma-ray decay were performed in two scattering chambers: the charged particle scattering chamber and the gamma-ray chamber.

A top view of the charged particle scattering chamber and its collimator assembly is shown in Fig. 3.3. The first two collimators determine the size of the beam spot. The third collimator ensures that the beam will be centered in the chamber, while the last, slightly larger collimator is an anti-scattering collimator which reduces background scattering originating from the previous collimators.

Five silicon surface barrier detectors are mounted at angles of 90°, 120°, 135°, 150°, and 160° with respect to the incident proton beam. A typical spectrum obtained from one of these charged particle detectors is shown in Fig. 3.4. In order to reduce the dead time in the data acquisition system, the carbon peak was gated out electronicaly during the experiment.

The gamma-ray chamber and its collimator assembly are shown in Fig. 3.5. Located outside the chamber are five 3"x3" NaI(Tl) crystal scintillation detectors, which are

Figure 3.3 Top View of the Charged Particle Scattering Chamber and Collimator Assembly.

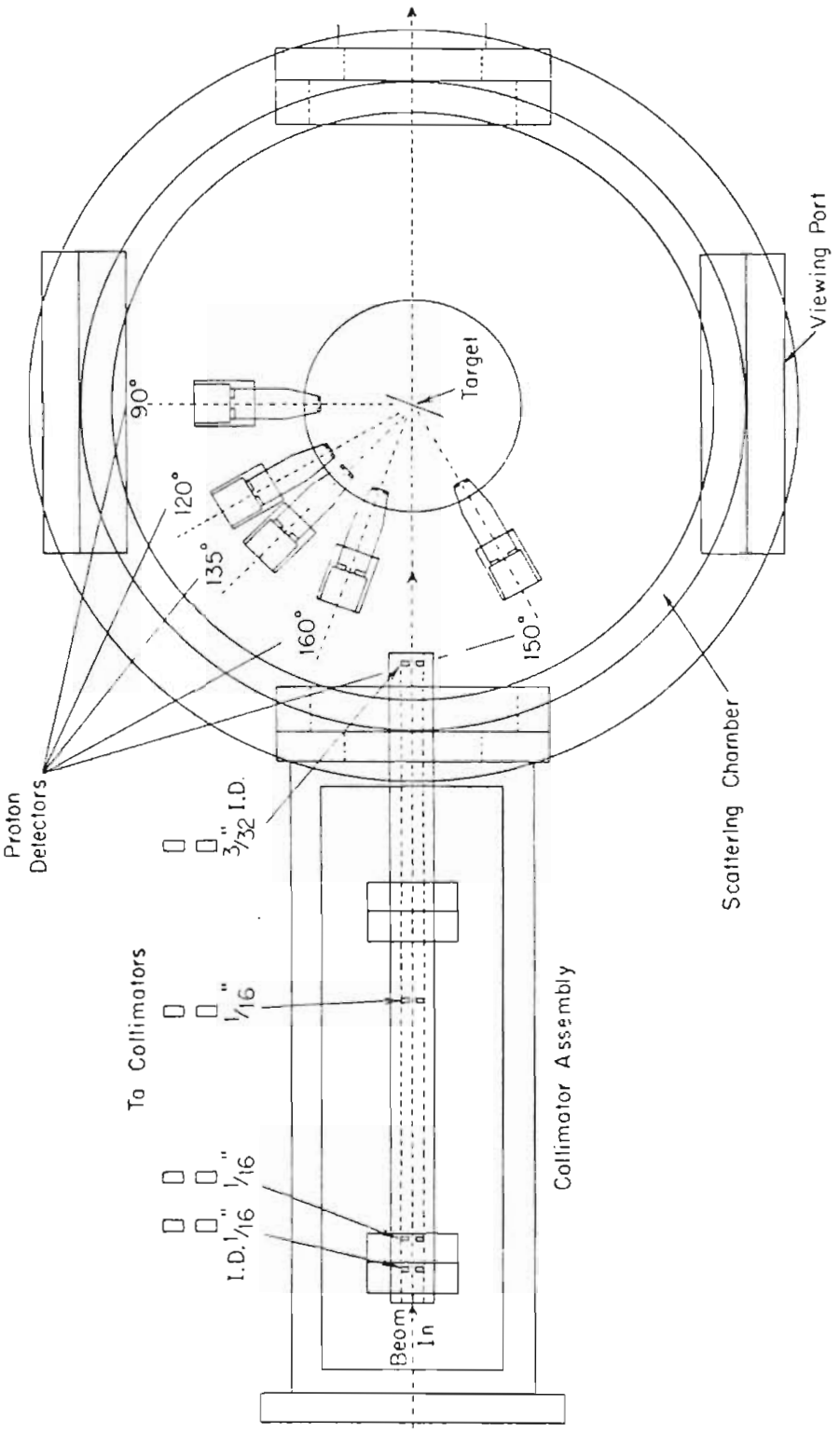
Viewing Port
Target
90°
120°
135°
160°
150°
Proton Detectors
3/32" I.D.
Scattering Chamber
To Collimators
1/16"
I.D. 1/16"
Collimator Assembly
Beam In

Figure 3.4 Typical Spectrum for Protons on ^{48}Ti at E_p =2.9196 MeV. During the experiment the carbon peak was gated out electronically to reduce the dead time. The solid line is a guide to the eye.

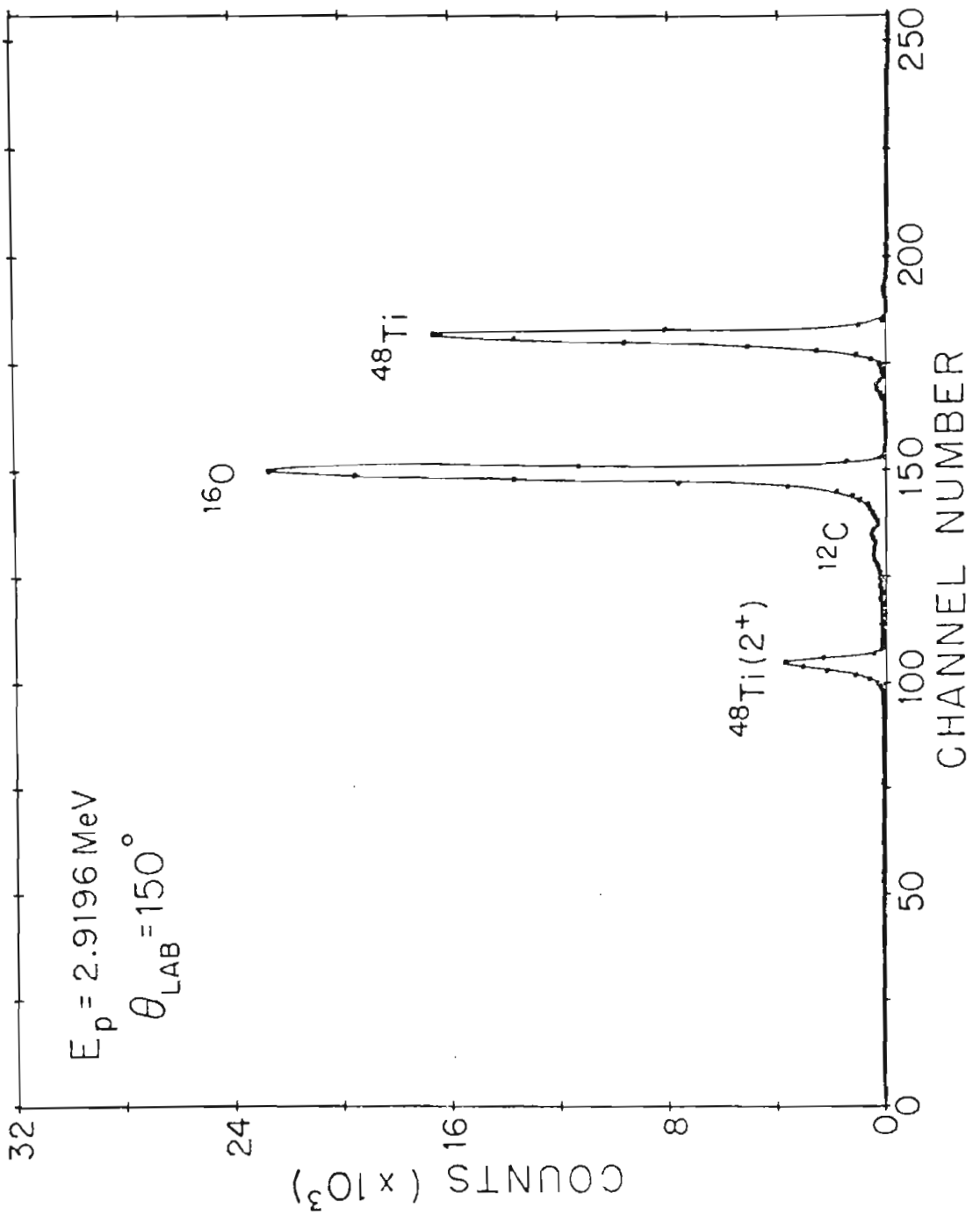
E_p = 2.9196 MeV
θ_{LAB} = 150°
^{16}O
^{48}Ti
^{12}C
$^{48}Ti(2^+)$
COUNTS (x 10^3)
CHANNEL NUMBER
0
8
16
24
32
50
100
150
200
250

Figure 3.5 Gamma-Ray Detection Chamber and Collimator Assembly. The upper part of the drawing is a top view, while the lower part is a side view.

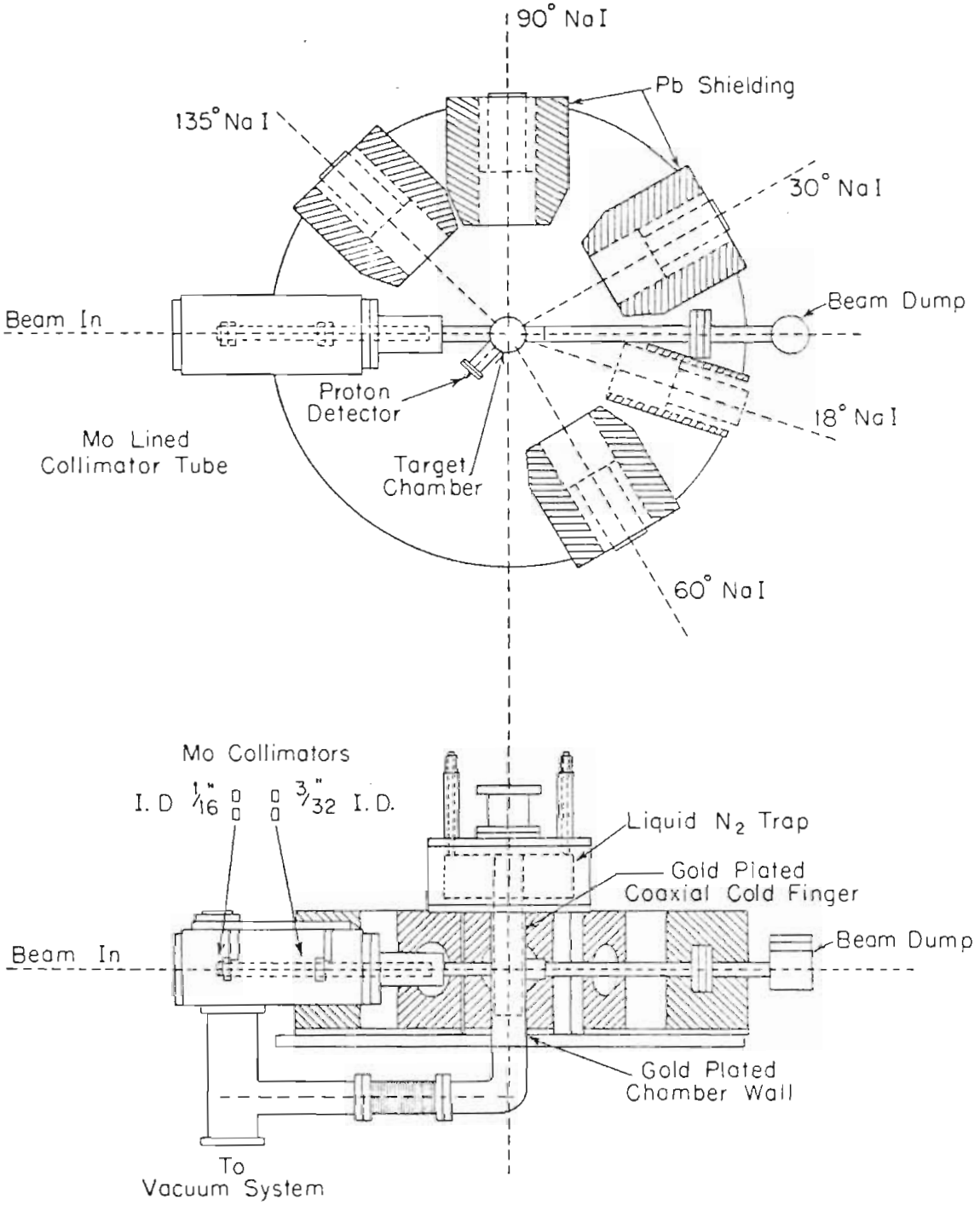
90° NaI
Pb Shielding
135° NaI
30° NaI
Beam In
Beam Dump
Proton Detector
18° NaI
Mo Lined Collimator Tube
Target Chamber
60° NaI
Mo Collimators
I.D 1/16
3/32 I.D.
Liquid N2 Trap
Gold Plated Coaxial Cold Finger
Beam In
Beam Dump
Gold Plated Chamber Wall
To Vacuum System

coupled with RCA 8575 photomultiplier tubes. These detectors are shielded from room background by a two inch thick lead collar and are located at laboratory angles of 90°, 60°, 45°, 30°, and 18°. A typical gamma-ray spectrum is shown in Fig. 3.6. One charged particle detector is mounted inside the chamber at 135° ; this detector is used to determine the resonance energy by measuring the elastic and inelastic cross sections in the vicinity of the resonance. Outside the chamber (not shown on Fig. 3.6), an 80 cc high resolution Ge(Li) detector was used to monitor the spectra and to ensure that there was no unwanted gamma ray in the vicinity of the peak of interest.

In both chambers a vacuum better than 10^{-6} Torr was maintained by a liquid nitrogen trap. This vacuum level greatly reduced the target deterioration due to contamination from buildup of the pump oil vapors.

Figure 3.6 Gamma-Ray Spectrum for $^{48}Ti(p,p'\gamma)\ ^{48}Ti$ at $E_p = 2.7725$ MeV. The peak of interest is the 0.983 MeV gamma ray emitted from the first excited state of ^{48}Ti.

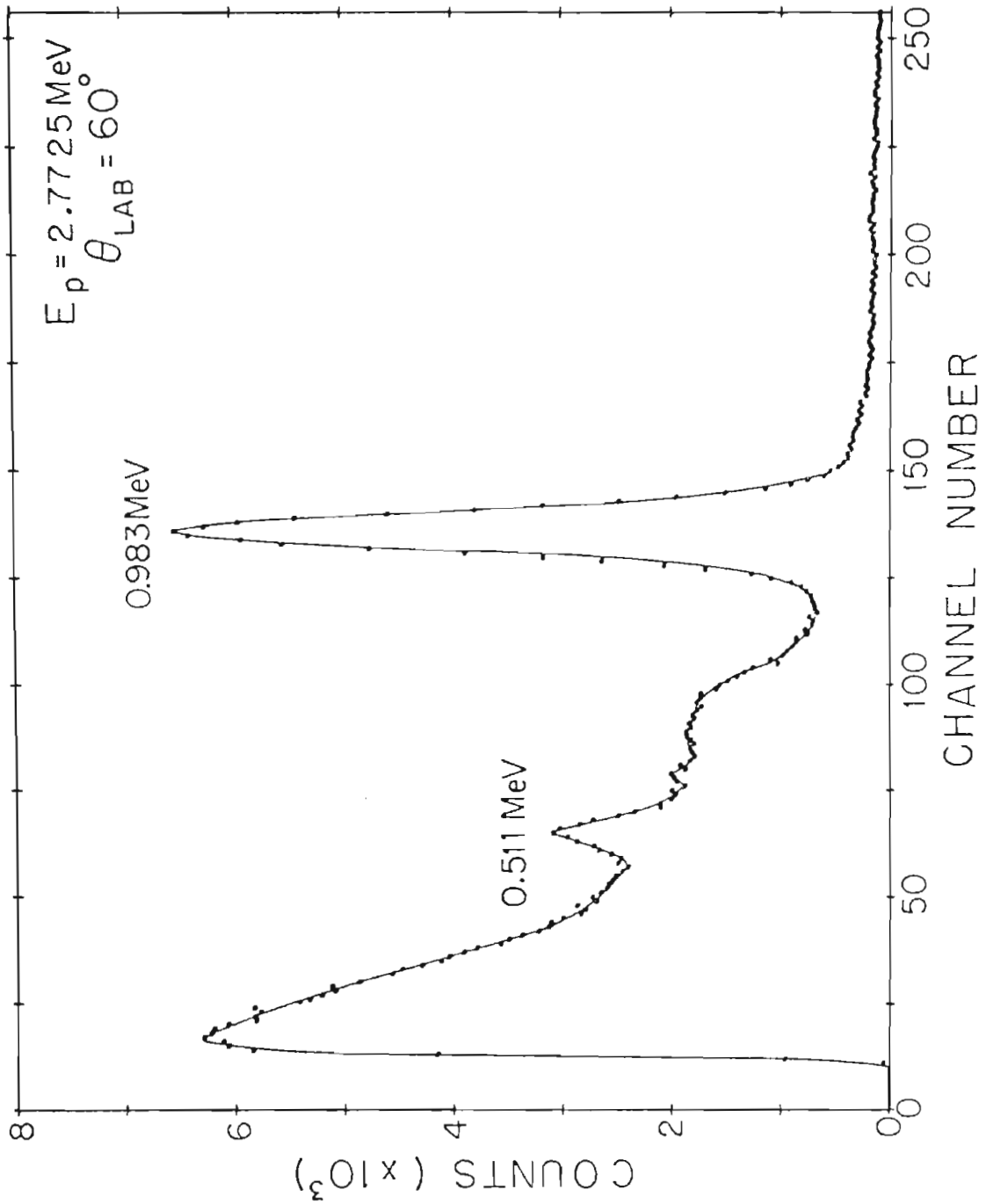
$E_p = 2.7725$ MeV
$\theta_{LAB} = 60°$
0.983MeV
0.511 MeV
COUNTS (x 10^3)
CHANNEL NUMBER
0
2
4
6
8
0
50
100
150
200
250

3.3 Targets

Targets used in this experiment were prepared by evaporating highly enriched (99.1%) ^{48}Ti crystal bar onto 5 $\mu g/cm^2$ carbon foils. Two high current leads were connected to the ends of a tantalum boat which had the ^{48}Ti crystal bar situated in its center. A piece of tantalum plate with a 3/4" hole above the isotope was employed to minimize heating of the target backings by the incandescent boat and to reduce tantalum contamination from any evaporation of the tantalum boat itself. In order to reach the melting point of ^{48}Ti (about 2000°C), approximately 220 A current was required.

A proton spectrum for ^{48}Ti is shown in Fig. 3.4. The thickness was about 2.4 $\mu g/cm^2$ of ^{48}Ti. This compromise thickness gave sufficient counting rate without seriously degrading the energy resolution.

3.4 Electronics

A block diagram of the electronics used for the data acquisition is shown in Fig. 3.7. When a nuclear reaction event is recorded in a detector, an analog pulse proportional to the energy of the particle is produced. This pulse is then amplified by an Ortec Model 109A preamplifier and a Tennelec Model 203 spectroscopy amplifier.

The unipolar outputs from the five spectroscopy amplifiers were then fed into a Dual Sum & Invert (Ortec 433). The combined linear signal was then converted into digital form by an Analog-to-Digital Converter (ADC) and sent to the computer. To ensure that during each ADC conversion only one pulse in this linear signal is digitized, and to identify the angular position of this detected pulse, an eight-input router was used.

The bipolar outputs of each spectroscopy amplifiers were shaped by an Ortec (Model 416A) gate and delay generator and then fed into the eight-input router. The main function of the router was to construct a three bit word which corresponds to the input of the received signal, and to set a fourth bit if more than one input received a signal at the same time. The router also outputs a gate signal to the ADC in a coincidence mode.

Figure 3.7 Block Diagram of the Proton and Gamma-Ray Detection Electronics.

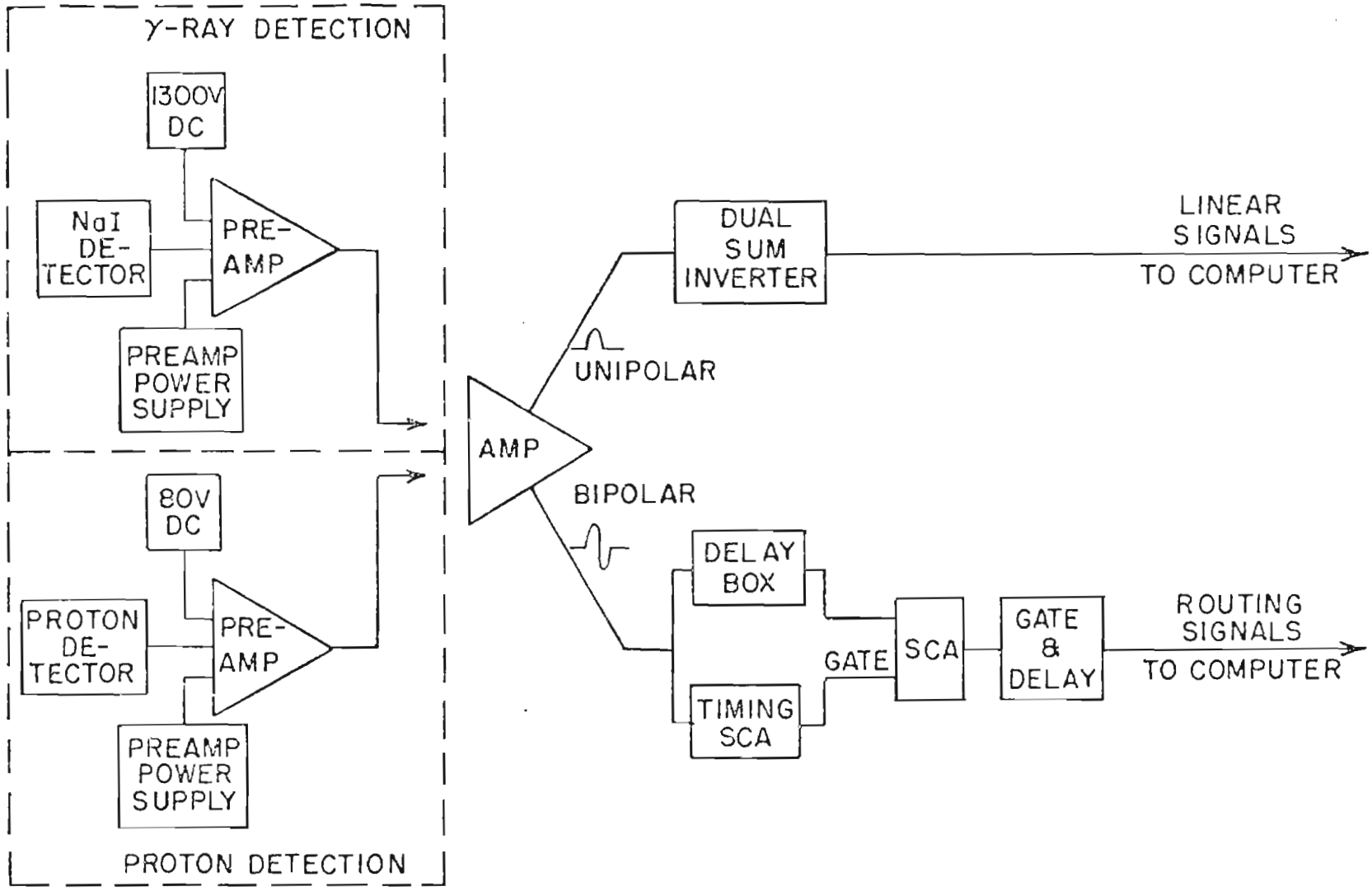
γ-RAY DETECTION
1300V DC
NaI DE-TECTOR
PRE-AMP
PREAMP POWER SUPPLY
80V DC
PROTON DE-TECTOR
PRE-AMP
PREAMP POWER SUPPLY
PROTON DETECTION
AMP
UNIPOLAR
BIPOLAR
DUAL SUM INVERTER
LINEAR SIGNALS TO COMPUTER
DELAY BOX
GATE
SCA
GATE & DELAY
ROUTING SIGNALS TO COMPUTER
TIMING SCA

If the fourth bit is set, the router gate will not be generated and the overlapping pulses therefore will not be digitized by the ADC.

In the proton detection system, the computer dead time (the time that the ADC required to digitize the pulses) can be greatly reduced by gating out the unwanted carbon pulses. The bipolar output of each spectroscopy amplifier was sent into an Ortec (Model 420A) timing single channel analyzer (SCA), where a window was set on the carbon peak. Whenever a carbon pulse is received, a logic pulse is sent to the H.P. SCA which gates off the delayed (.7μs) signal from the bipolar outputs of the spectroscopy amplifier. Since the carbon pulses are not sent to the router, they will not be analyzed by the ADC.

The counting time for each data point is controlled by a Beam Current Integrator (BCI) which digitizes the charge collected on the beam stop. The output of the BCI is sent to a preset scaler. When the scaler reaches the preset value, an interval out signal is sent to the external control of the ADC and Router which stops the data accumulation. The dead time correction for the ADC is controlled by a busy signal sent from the router to the gate of the current digitizer, which stops digitizing the beam current while the ADC is busy.

3.5 Procedure

The $^{48}Ti(p,p)^{48}Ti$ experiment performed by Prochnow (1971) provided resonance information (spin, energy, elastic width) for the d-wave resonances. The resonances were located by measuring a yield curve ($\sim 100\ \mu c$ per point) beginning about 2 keV below the expected resonance. Once the resonance was located, a long spectrum (5,000 μc to 10,000 μc) was taken at the resonance energy. In order to have at least 1% counting statistics, a minimum of 10,000 counts in the inelastic peak was required for most of the resonances.

In the inelastically scattered proton experiment, a gold spectrum ($\sim$ 800 μc) was also taken for each resonance. After correction for Rutherford scattering (in the laboratory system), these yields from the gold target were used as normalization factors to correct for the different solid angles subtended by the detectors. Before the Legendre polynomial coefficients were extracted the data were transformed into the center of mass (C.M.) system. The C. M. angles of these detectors are 91.6°, 121.4°, 136.1°, 150.8°, and 160.5°. A C.M. solid angle correction to the related yield is also necessary (Marion, 1959).

In the gamma-ray experiment, the normalization

factors for the correction of different NaI detector solid angles were obtained by measuring isotropic angular distributions from $1/2^-$ resonances. The experimental results show that normalization factors obtained from the $1/2^-$ resonances are much more reliable than those obtained from radioactive source measurements.

In addition to passing through the collimator assembly, the beam was also tuned through a 1/10" aluminum ring in order to reduce background scattering. For the best results, with an average beam on the beam stop of about 5 A, the beam on the ring was normally kept below 10 nA, while the beam on the collimator was below 30 nA.

Chapter 4

Data and Preliminary Analysis

4.1 Proton Elastic Scattering Experiment

The proton elastic scattering experiment $^{48}Ti(p,p)^{48}Ti$ was performed by Prochnow (1971). The excitation curve at 160° over the incident proton energy range 1.80 MeV to 3.20 MeV is shown in Fig. 4.1. The solid line is a multi-level, multi-channel fit to the data, and the lower half of the plot shows an expanded portion of the region of higher level density. One hundred and twelve d-wave resonances were observed. The main resonance parameters obtained in this experiment are the resonance energies, angular momentum and parity values, and elastic widths.

4.2 Preliminary Analysis

Angular distribution measurements on both the

Figure 4.1 Differential Cross Section of Proton Elastic and Inelastic Scattering on ^{48}Ti at 160°. The expanded region shows data in the high level density region. The solid line is a multi-level, multi-channel fit to the data.

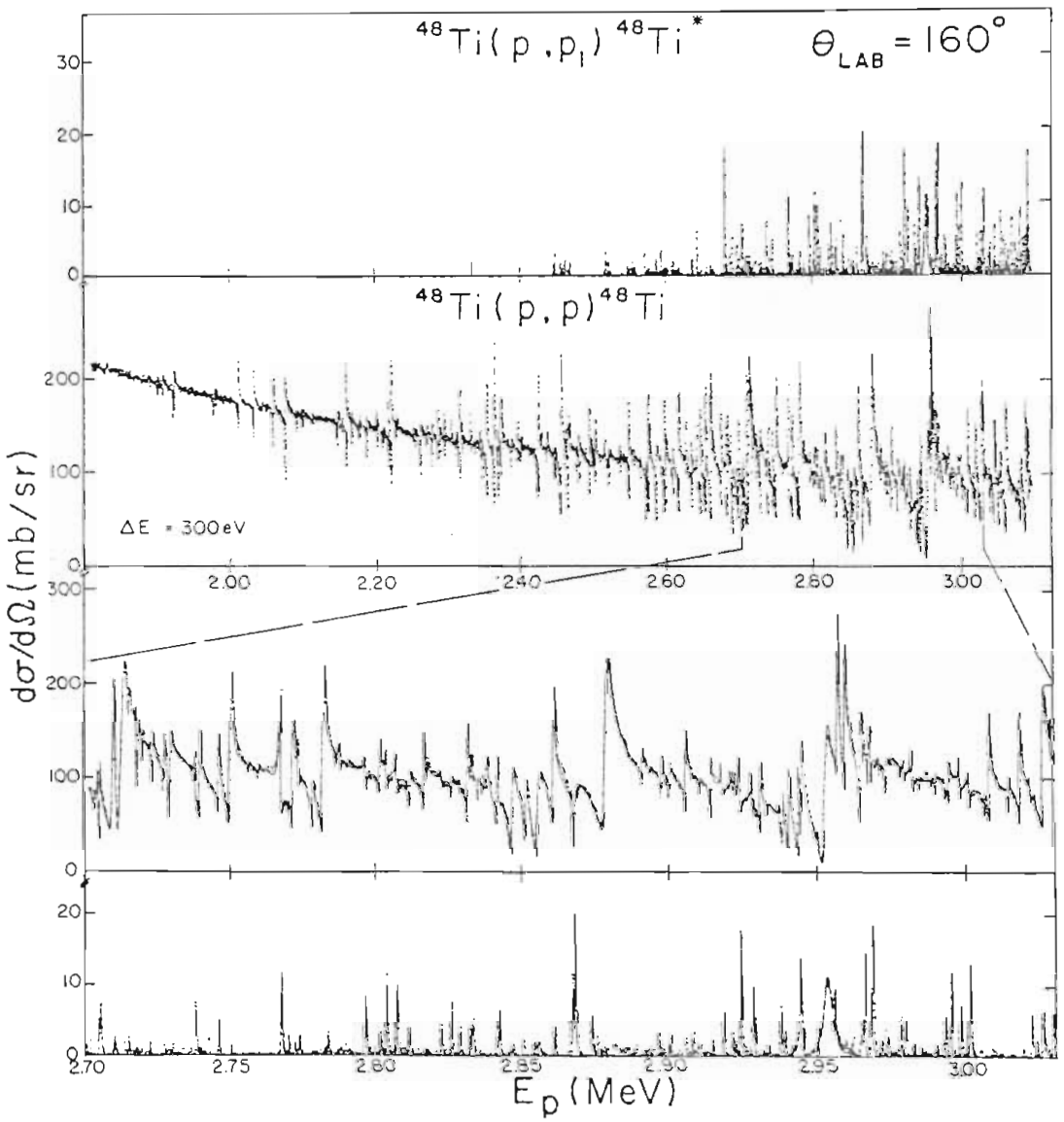
$^{48}Ti(p,p_1)^{48}Ti^*$
$\theta_{LAB} = 160°$
$^{48}Ti(p,p)^{48}Ti$
ΔE = 300eV
dσ/dΩ (mb/sr)
E_p (MeV)

inelastically scattered proton and the gamma ray from the subsequent decay have been performed on all the previously observed d-wave resonances. There are three inelastic channels open for $l_{p'} \leq 2$; channels with $l_{p'}=4$ are neglected because of the low barrier penetrability. Resonances with too small an inelastic strength or resonances showing interference with nearby resonances were omitted from the analysis. Eighty resonances were analyzed, of which thirty-five were assigned as $3/2^+$ states and forty-five were assigned as $5/2^+$ states. For these 80 resonances the following properties are listed in Table 4.1: resonance energy, spin and parity, elastic and total inelastic laboratory width, plus the corresponding reduced widths.

A χ^2 fit was performed (see Eqn. 2.70) where the ten data data points $W_{p'}(\theta_i)$ and $W_{\gamma}(\theta_i)$ are the normalized yields at θ_i. The fractional errors $\Delta W_{p'}(\theta_i)/W_{p}(\theta_i)$ and $\Delta W_{\gamma}(\theta_i)/W_{\gamma}(\theta_i)$ are about 4-6% and 3-5%, respectively.

The absolute minimum point of χ^2 in $\emptyset$-space corresponds to the best solution for the mixing ratios; this minimum is located with a gradient search routine "Record". The mixing ratio values for 45 $5/2^+$ resonances are listed in Table 2.2 and 2.3 for the j-spin and s-spin representations, respectively. The corresponding $\emptyset$-space plots for these 45 $5/2^+$ resonance mixing ratios are shown in Fig 4.2 and Fig 4.3. Since the data points are clustered in regions, these results clearly show that the

Table 4.1

Resonance Parameters for D-Wave Resonances in ^{49}V

Res. No.	E_p (MeV)	J^π	Γ_p (eV)	γ_p^2 (keV)	$\Gamma_{p'}$ (eV)	$\gamma_{p'}^2$ (keV)
5	2.2981	5/2+	10	0.99	0.48	0.57
8	2.3204	5/2+	10	0.93	0.51	0.58
9	2.3340	5/2+	20	1.78	0.97	0.82
10	2.3637	5/2+	10	0.81	0.48	0.43
14	2.4203	3/2+	8	0.52	0.34	
17	2.4464	3/2+	8	0.48	0.94	
19	2.4694	5/2+	20	1.21	1.48	0.38
20	2.4903	5/2+	5	0.29	1.32	0.72
22	2.5176	3/2+	23	1.20	3.37	
24	2.5468	5/2+	3	0.15	1.10	0.17
25	2.5547	3/2+	8	0.36	2.09	
26	2.5713	5/2+	4	0.14	5.96	0.95
28	2.5943	5/2+	12	0.52	5.48	0.96
29	2.5962	3/2+	8	0.33	0.30	
32	2.6313	3/2+	12	0.48	0.59	
33	2.6437	5/2+	35	1.35	5.52	0.78
35	2.6560	3/2+	23	0.84	0.86	
36	2.6764	5/2+	10	0.56	0.69	0.41
37	2.6824	5/2+	65	2.29	23.21	2.95
39	2.6885	3/2+	55	1.91	3.53	

Table 4.1 (continued)

Res. No.	E_p (MeV)	J^π	Γ_p (eV)	γ_p^2 (keV)	$\Gamma_{p'}$ (eV)	$\gamma_{p'}^2$ (keV)
40	2.6983	3/2+	6	0.30	26.00	
41	2.7051	5/2+	35	1.17	5.35	0.55
43	2.7226	5/2+	8	0.26	1.52	0.18
44	2.7383	5/2+	35	1.08	7.40	0.71
50	2.7674	5/2+	85	2.46	19.00	1.55
51	2.7736	5/2+	12	0.34	2.74	0.20
52	2.7834	5/2+	5	0.14	2.98	0.43
53	2.7878	3/2+	12	0.33	0.93	
54	2.7964	3/2+	22	0.54	13.01	
55	2.8037	5/2+	15	0.40	24.00	2.44
56	2.8072	5/2+	15	0.40	18.00	1.25
58	2.8225	3/2+	10	0.26	19.61	
59	2.8288	5/2+	7	0.13	6.65	0.49
60	2.8322	3/2+	22	0.57	6.60	
63	2.8422	5/2+	20	0.49	4.46	0.55
65	2.8671	5/2+	15	0.35	17.00	1.05
67	2.8687	3/2+	30	0.70	9.95	
68	2.8737	3/2+	8	0.11	13.22	
69	2.8859	5/2+	2	0.04	0.73	0.08
70	2.8964	3/2+	4	0.04	3.80	
71	2.9082	5/2+	4	0.06	4.80	0.26

Table 4.1 (continued)

Res. No.	E_p (MeV)	J^π	Γ_p (eV)	γ_p^2 (keV)	$\Gamma_{p'}$ (eV)	$\gamma_{p'}^2$ (keV)
72	2.9186	5/2+	15	0.32	8.34	0.50
74	2.9227	3/2+	8	0.25	3.71	
75	2.9244	5/2+	30	0.62	21.37	1.05
76	2.9284	5/2+	18	0.37	8.89	0.40
77	2.9292	3/2+	8	0.15	15.00	
78	2.9378	5/2+	10	0.20	20.00	1.06
79	2.9505	3/2+	10	0.20	2.78	
80	2.9557	3/2+	15	0.29	5.60	
82	2.9661	5/2+	22	0.42	17.00	0.94
83	2.9687	5/2+	40	0.76	35.41	1.57
84	2.9716	5/2+	6	0.09	5.24	0.41
85	2.9780	5/2+	6	0.09	22.80	1.47
86	2.9796	3/2+	15	0.27	12.91	
87	2.9825	3/2+	30	0.45	2.73	
88	2.9930	3/2+	18	0.33	15.55	
89	2.9950	5/2+	25	0.45	33.66	1.21
90	2.9981	3/2+	33	0.39	12.92	
91	3.0012	3/2+	30	0.52	71.81	
92	3.0215	3/2+	24	0.30	24.48	
93	3.0234	5/2+	5	0.08	3.41	0.16

Table 4.1 (continued)

Res. No.	E (MeV)	J^{π}	Γ_p (eV)	γ_p^2 (keV)	$\Gamma_{p'}$ (eV)	$\gamma_{p'}^2$ (keV)
94	3.0256	5/2+	20	0.34	7.56	0.44
95	3.0289	5/2+	28	0.47	8.95	0.37
96	3.0300	3/2+	30	0.51	63.70	
97	3.0311	3/2+	5	0.05	8.79	
98	3.0367	3/2+	12	0.19	4.73	
99	3.0375	3/2+	6	0.10	10.80	
100	3.0383	3/2+	18	0.30	9.65	
101	3.0442	5/2+	12	0.20	8.36	0.60
102	3.0454	5/2+	15	0.24	1.69	0.21
103	3.0485	3/2+	8	0.12	0.53	
104	3.0527	5/2+	22	0.35	13.25	0.57
105	3.0559	3/2+	12	0.13	15.72	
106	3.0605	5/2+	12	0.19	2.25	0.37
107	3.0628	5/2+	1	0.02	0.69	0.06
108	3.0754	3/2+	8	0.12	6.49	
109	3.0784	5/2+	30	0.46	18.73	0.67
110	3.0815	3/2+	12	0.12	21.89	
111	3.0843	5/2+	10	0.15	9.03	0.49
112	3.0880	5/2+	45	0.67	50.00	1.08

Figure 4.2 Plot of $\phi_{5/}$ versus $\phi_{3/}$ for $5/2^+$ Resonances in the Angular Momentum Representation, with $\phi_{3/} = \tan^{-1}(\langle j,2,3\rangle / \langle j,0,1\rangle)$ and $\phi_{5/} = \tan^{-1}(\langle j,2,5\rangle / \langle j,0,1\rangle)$.

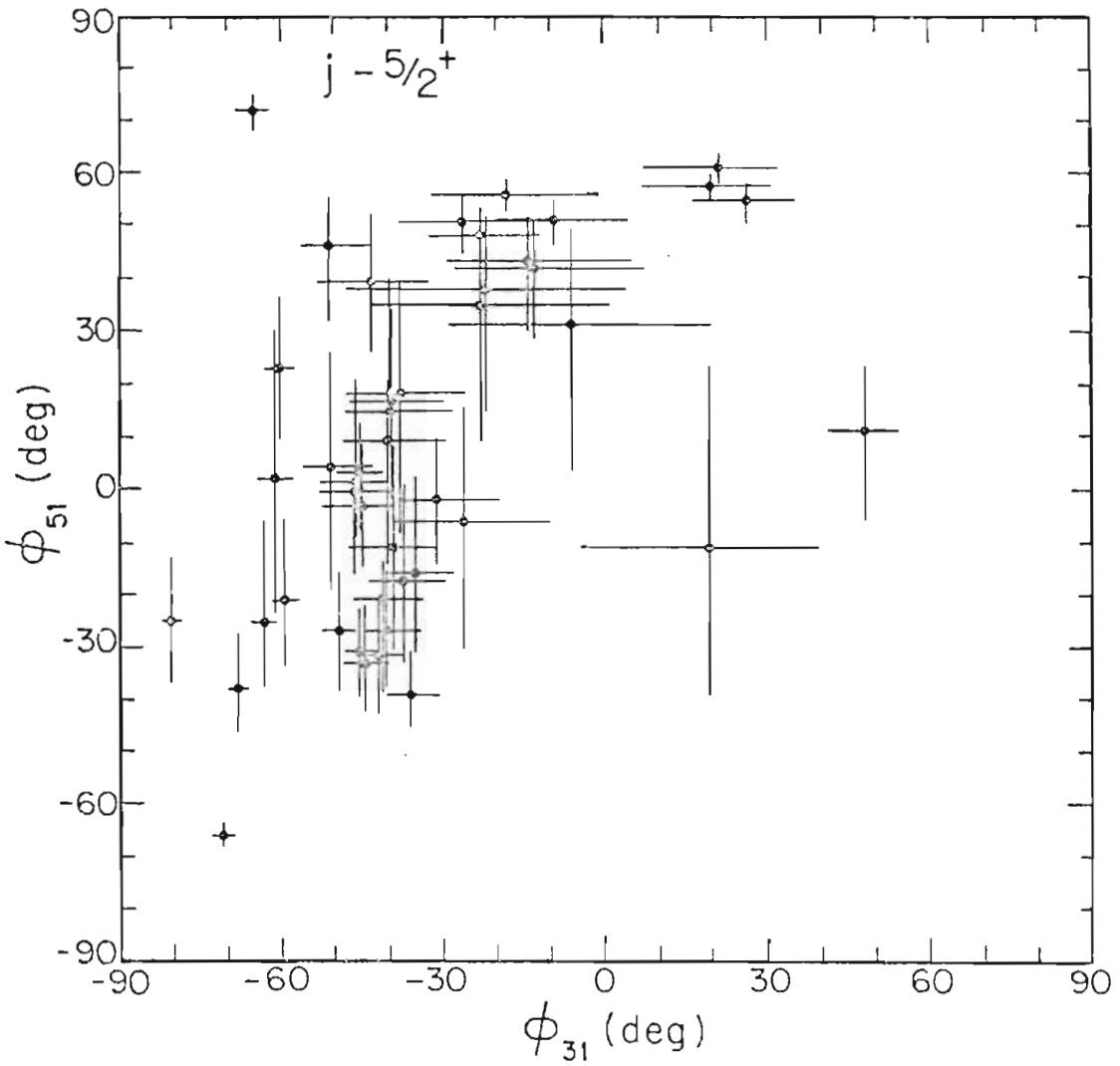
j - 5/2+
90
60
30
0
-30
-60
-90
-90
-60
-30
0
30
60
90
φ51 (deg)
φ31 (deg)

Figure 4.3 Plot of $\phi_{5/}$ versus $\phi_{3/}$ for $5/2^+$ Resonances in the Channel Spin Representation, with $\phi_{3/} = \tan^{-1}(\langle s,2,3\rangle/\langle s,0,5\rangle)$ and $\phi_{5/} = \tan^{-1}(\langle s,2,5\rangle/\langle s,0,5\rangle)$.

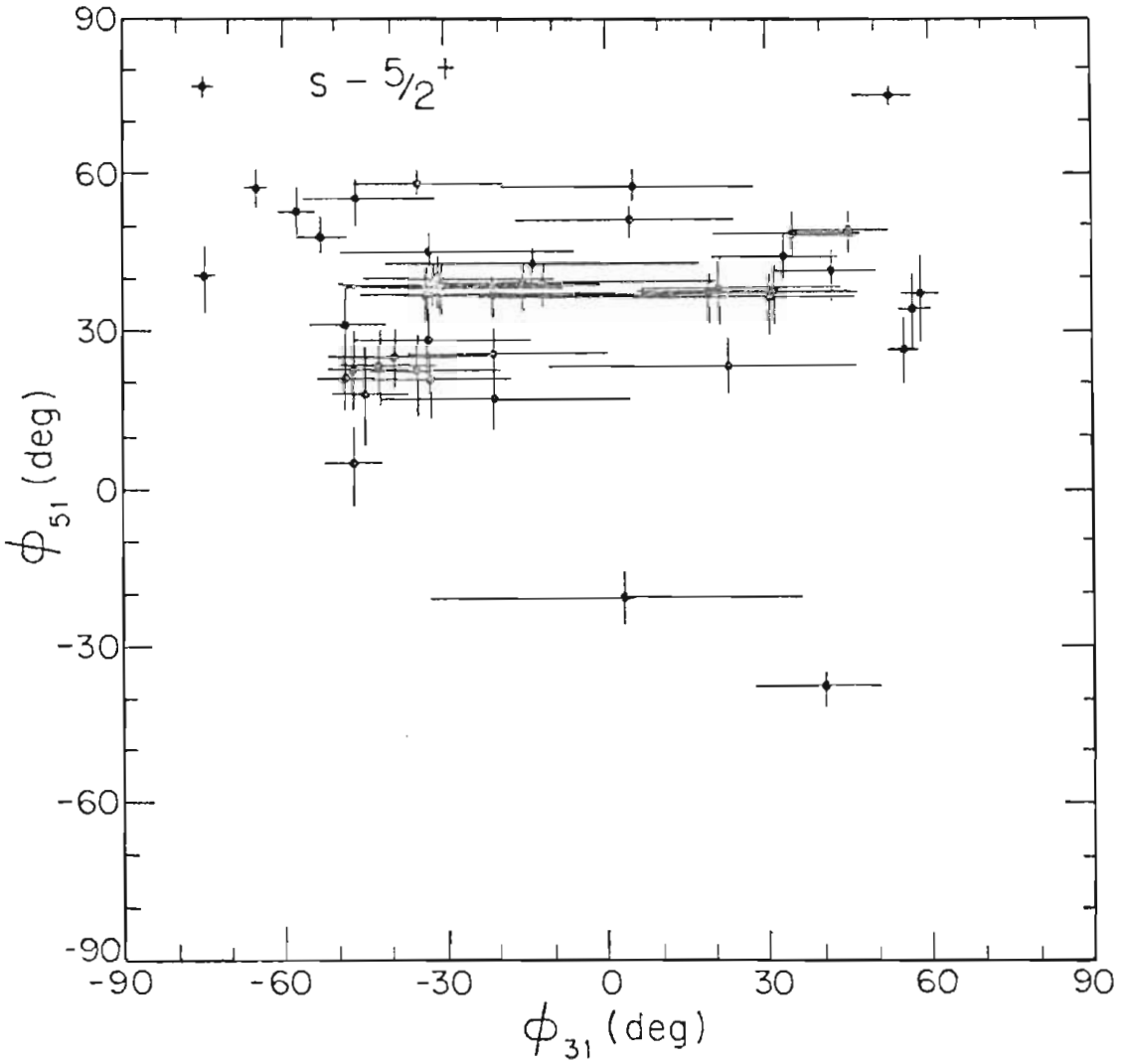
s − 5/2+
90
60
30
0
-30
-60
-90
-90
-60
-30
0
30
60
90
φ51 (deg)
φ31 (deg)

mixing ratios are not statistically distributed. Both acceptable mixing ratios for the 3/2+ resonances are listed in Table 2.4 and Table 2.5 for j-spin and s-spin representations, respectively. The corresponding Ø-space plots for these 35 3/2+ resonance mixing ratios are shown in Fig. 4.4 and Fig. 4.5, where data points marked as "." correspond to the set of solutions with the lower $l_p'=2$ admixture while data points marked as "o" correspond to the set of solutions with the higher $l_p'=2$ admixture. The dashed error bar on certain resonances represents a very large uncertainty in that direction. It seems apparent that some non-statistical phenomenon also exists in the inelastic decay from the 3/2+ states.

4.3 Total Inelastic Width $\Gamma_{p'}$ and Channel Reduced Widths

The total inelastic widths $\Gamma_{p'}$ were determined from the relation

$$\frac{(2J+1)}{(2I_o+1)(2J_o+1)} \frac{\Gamma_p \Gamma_{p'}}{\Gamma} = \frac{2\,Y}{\lambda^2\, t} \qquad \text{(Gove, 1958)} \tag{4.1}$$

where

J : spin of the compound nuclear state

J_o : spin of the target

Figure 4.4 Plot of $\phi_{5/}$ versus $\phi_{3/}$ for $3/2^+$ Resonances in the Angular Momentum Representation, with $\phi_{3/} = \tan^{-1}(\langle j,2,3\rangle / \langle j,0,1\rangle)$ and $\phi_{5/} = \tan^{-1}(\langle j,2,5\rangle / \langle j,0,1\rangle)$. Data points marked as "o" correspond to the solution set with higher $l_p' = 2$ admixture, while data points marked as "." correspond to the solution set with lower $l_p' = 2$ admixture.

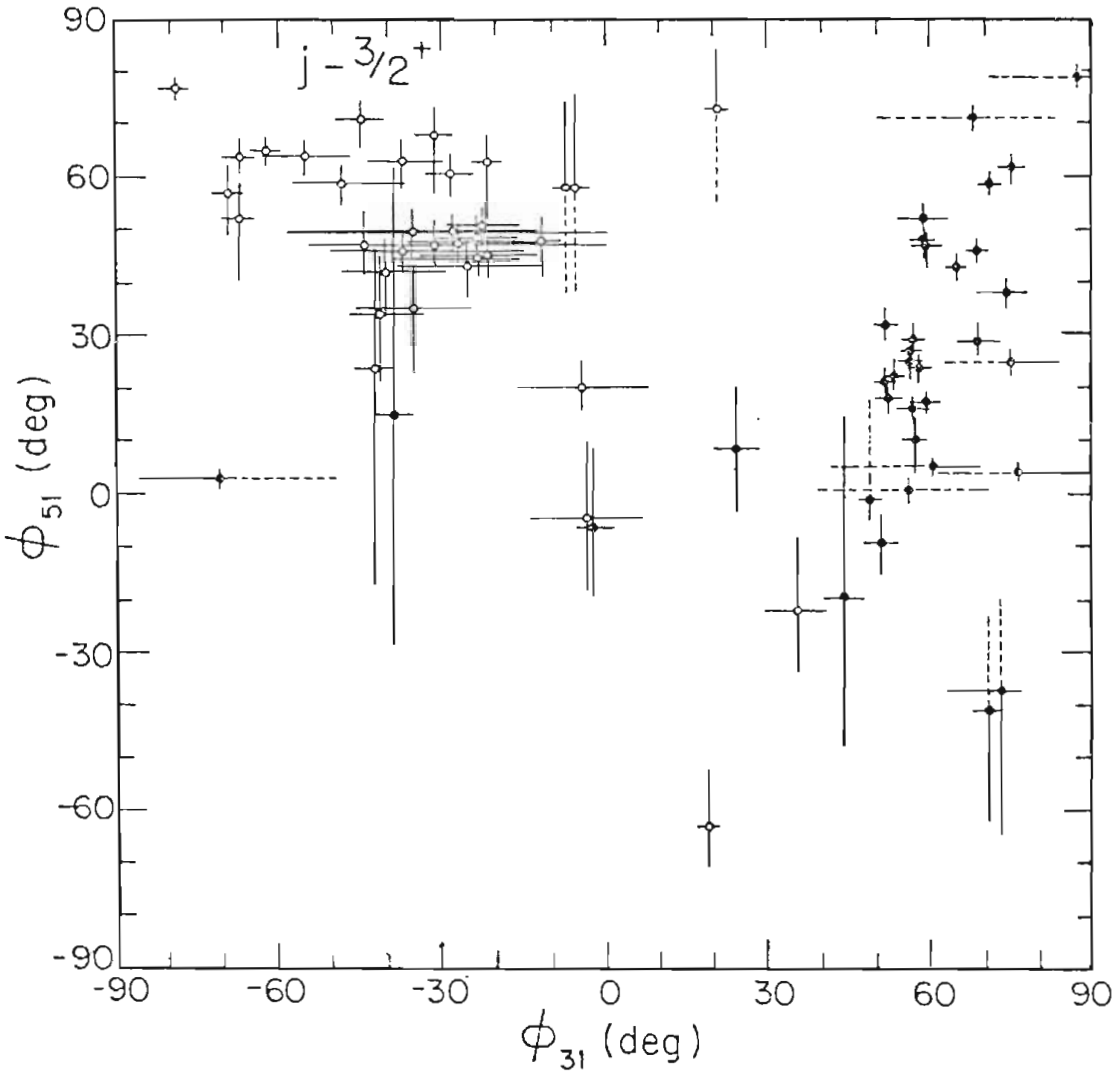
j - 3/2+
90
60
30
0
-30
-60
-90
-90
-60
-30
0
30
60
90
φ51 (deg)
φ31 (deg)

Figure 4.5 Plot of $\phi_{5/}$ versus $\phi_{3/}$ for $3/2^+$ Resonances in the Channel Spin Representation, with $\phi_{3/} = \tan^{-1}$ (<s,2,3>/<s,0,5>) and $\phi_{5/} = \tan^{-1}$ (<s,2,5>/<s,0,1>). Data points marked as "o" correspond to the solution set with higher $1'_p = 2$ admixture, while data points marked as "." correspond to the solution set with lower $1'_p = 2$ admixture.

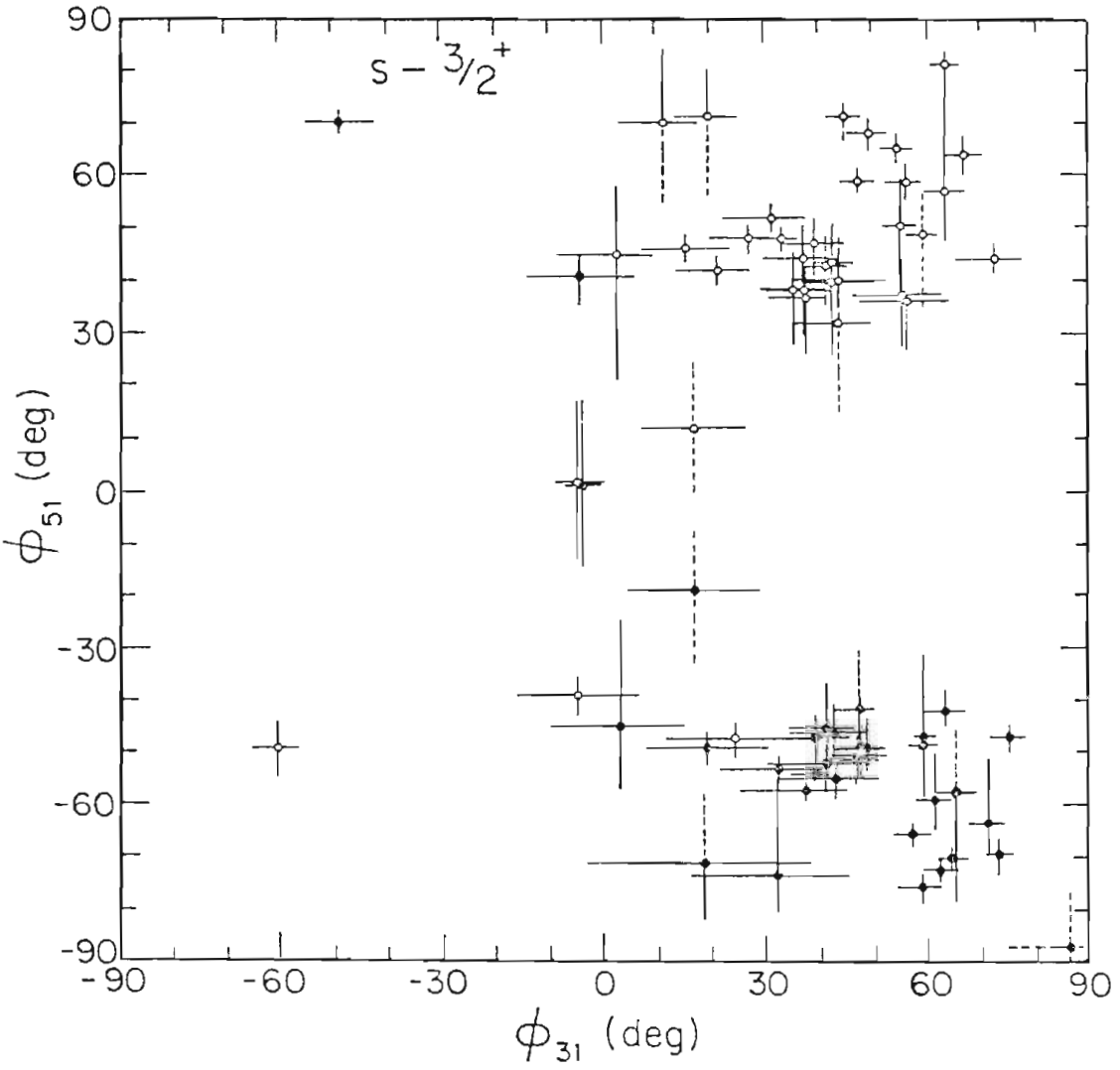
S − 3/2+
90
60
30
0
-30
-60
-90
-90
-60
-30
0
30
60
90
φ51 (deg)
φ31 (deg)

I_o: spin of the incident proton

Γ_p: proton elastic width

$\Gamma_{p'}$: total inelastic width

Γ: total width

t : target thickness in atoms per square centimeters

λ : center of mass wavelength of the incident protons in centimeters.

Y : area of the resonance yield curve in unit of reactions times energy per incident particle.

Neglecting all other channels, the total width can be approximated as $\Gamma \approx \Gamma_p + \Gamma_{p'}$, and Eqn. 4.1 is therefore equivalent to

$$\Gamma_{p'} = \frac{\Gamma_p Y'}{\Gamma_p - Y'} \quad , \quad \text{where } Y' = \frac{2Y(2I_o+1)(2J_o+1)}{\lambda^2 t (2J+1)}$$

Since $\Gamma_{p'}$ is always positive, this indicates that Γ_p is larger than Y'; in other words, Y' is a lower bound for the elastic width Γ_p. Y' is determined from the present experiment, while Γ_p is normally taken from the previous elastic scattering work of Prochnow(1971). Resonances with Y' larger than Γ_p, were refitted using a multi-level, multi-channel R-matrix computer program MULTI, written by D.L. Sellin (1969).

The channel width for 5/2+ resonances can be calculated by dividing the total width into three channels

according to the mixing ratios. The channel reduced width is then calculated from equation

$$\gamma_p^2 = \frac{\Gamma_p}{2P}$$

where P is the Coulomb barrier penetrability. The penetrability was calculated at a channel radius $1.25(A^{1/3}+1)$ F, where A is the mass number of the target. The total inelastic reduced width is the summation of the three channel reduced widths.

The values of the total inelastic width Γ_p, for 80 d-wave resonances and the total inelastic reduced width for $5/2^+$ resonances are listed in Table 4.1. The three channel reduced widths and the three products of channel reduced width amplitudes are listed for each resonance in Table 4.2 and 4.3 for the j-spin and s-spin representations, respectively. The corresponding plots for reduced widths versus energy and the sum of reduced widths versus energy are shown in Fig. 4.6 and Fig 4.7. Plots for the product of two channel reduced width amplitudes versus energy and the sum of the product versus energy are shown in Fig. 4.8 and Fig. 4.9 for the j-spin and s-spin representations, respectively. Clearly, a strong non-statistical sign distribution exists in the channel products of $\langle j,0,1\rangle \cdot \langle j,2,3\rangle$ and $\langle s,0,5\rangle \cdot \langle s,2,5\rangle$.

Table 4.2

Channel Reduced Widths and Amplitude Products (j-spin)

Res. No.	$\gamma^2_{j_1}$ (keV)	$\gamma^2_{j_3}$ (keV)	$\gamma^2_{j_5}$ (keV)	$\gamma_{j_1}\gamma_{j_3}$ (keV)	$\gamma_{j_3}\gamma_{j_5}$ (keV)	$\gamma_{j_1}\gamma_{j_5}$ (keV)
5	0.27	0.30	0.00	-0.28	0.00	-0.00
8	0.25	0.32	0.01	0.28	0.06	0.05
9	0.44	0.33	0.06	-0.38	0.14	-0.16
10	0.17	0.25	0.00	-0.21	-0.02	0.01
19	0.30	0.07	0.00	-0.15	0.02	-0.04
20	0.21	0.05	0.46	0.10	0.15	0.31
24	0.15	0.02	0.01	0.05	-0.01	-0.03
26	0.70	0.01	0.24	-0.07	-0.04	0.41
28	0.56	0.38	0.02	-0.46	0.09	-0.11
33	0.45	0.28	0.05	-0.36	-0.12	0.15
36	0.03	0.12	0.27	-0.05	-0.18	0.08
37	1.56	0.10	1.29	-0.39	-0.35	1.42
41	0.33	0.19	0.03	-0.25	0.08	-0.10
43	0.08	0.07	0.03	-0.07	0.05	-0.05
44	0.39	0.07	0.25	-0.16	-0.13	0.31
50	0.90	0.15	0.50	-0.37	-0.27	0.67
51	0.13	0.06	0.01	-0.09	0.03	-0.04
52	0.12	0.02	0.30	0.04	0.07	0.19
55	0.92	0.03	1.49	-0.16	-0.20	1.17

Table 4.2 (continued)

Res. No.	γ_{j1}^2 (keV)	γ_{j3}^2 (keV)	γ_{j5}^2 (keV)	$\gamma_{j1}\gamma_{j3}$ (keV)	$\gamma_{j3}\gamma_{j5}$ (keV)	$\gamma_{j1}\gamma_{j5}$ (keV)
56	0.72	0.51	0.02	-0.61	-0.10	0.12
59	0.24	0.25	0.00	-0.25	-0.00	0.00
63	0.14	0.39	0.02	-0.23	0.09	-0.05
65	0.53	0.38	0.13	-0.45	0.22	-0.26
69	0.02	0.06	0.00	-0.03	-0.00	0.00
71	0.13	0.13	0.00	-0.13	0.01	-0.01
72	0.21	0.20	0.09	-0.20	0.14	-0.14
75	0.55	0.03	0.46	-0.14	-0.12	0.50
76	0.23	0.16	0.02	-0.19	-0.05	0.06
78	0.48	0.26	0.32	-0.35	0.29	-0.39
82	0.36	0.33	0.24	-0.35	-0.28	0.30
83	0.77	0.79	0.00	-0.78	-0.02	0.02
84	0.10	0.01	0.30	0.04	0.06	0.17
85	0.44	0.05	0.98	-0.15	-0.22	0.66
89	0.69	0.46	0.06	-0.56	-0.17	0.21
93	0.06	0.08	0.02	-0.07	0.04	-0.03
94	0.12	0.18	0.13	-0.15	-0.16	0.13
95	0.16	0.15	0.06	-0.16	0.09	-0.09
101	0.12	0.46	0.03	-0.23	0.11	-0.05

Table 4.2 (continued)

Res. No.	γ_{j1}^2 (keV)	γ_{j3}^2 (keV)	γ_{j5}^2 (keV)	$\gamma_{j1}\gamma_{j3}$ (keV)	$\gamma_{j3}\gamma_{j5}$ (keV)	$\gamma_{j1}\gamma_{j5}$ (keV)
102	0.02	0.12	0.08	-0.04	0.10	-0.04
104	0.21	0.05	0.31	-0.10	-0.13	0.25
106	0.01	0.36	0.00	-0.06	0.03	-0.01
107	0.01	0.05	0.00	-0.02	0.02	-0.01
109	0.28	0.04	0.35	-0.11	-0.12	0.31
111	0.12	0.35	0.02	-0.20	-0.09	0.05
112	0.78	0.30	0.00	-0.48	0.01	-0.02

Table 4.3

Channel Reduced Widths and Amplitude Products (s-spin)

Res. No.	γ_{s1}^2 (keV)	γ_{s3}^2 (keV)	γ_{s5}^2 (keV)	$\gamma_{s1}\gamma_{s3}$ (keV)	$\gamma_{s3}\gamma_{s5}$ (keV)	$\gamma_{s1}\gamma_{s5}$ (keV)
5	0.27	0.11	0.19	-0.17	-0.14	0.22
8	0.25	0.18	0.15	0.21	-0.17	-0.19
9	0.44	0.29	0.09	-0.36	-0.17	0.20
10	0.17	0.08	0.18	-0.11	-0.12	0.18
19	0.30	0.05	0.03	-0.12	-0.04	0.10
20	0.21	0.46	0.05	0.31	0.15	0.10
24	0.15	0.00	0.02	0.01	-0.00	-0.06
26	0.70	0.12	0.13	0.29	0.13	0.30
28	0.56	0.23	0.17	-0.36	-0.20	0.31
33	0.45	0.02	0.31	-0.09	-0.08	0.37
36	0.03	0.04	0.34	0.03	0.12	0.09
37	1.55	0.52	0.87	0.90	0.67	1.16
41	0.33	0.16	0.06	-0.23	-0.10	0.14
43	0.08	0.09	0.01	-0.09	-0.03	0.03
44	0.39	0.06	0.26	0.15	0.12	0.32
50	0.90	0.11	0.54	0.32	0.24	0.69
51	0.13	0.05	0.02	-0.08	-0.03	0.05
52	0.12	0.26	0.05	0.18	0.12	0.08
55	0.92	0.77	0.74	0.84	0.76	0.83

Table 4.3 (continued)

Res. No.	γ_{s1}^2 (keV)	γ_{s3}^2 (keV)	γ_{s5}^2 (keV)	$\gamma_{s1}\gamma_{s3}$ (keV)	$\gamma_{s3}\gamma_{s5}$ (keV)	$\gamma_{s1}\gamma_{s5}$ (keV)
56	0.72	0.10	0.43	-0.27	-0.21	0.55
59	0.24	0.09	0.17	-0.15	-0.12	0.20
63	0.14	0.24	0.17	-0.18	-0.20	0.15
65	0.53	0.44	0.08	-0.48	-0.18	0.20
69	0.02	0.02	0.04	-0.02	-0.03	0.03
71	0.13	0.05	0.08	-0.08	-0.06	0.10
72	0.21	0.26	0.03	-0.24	-0.09	0.08
75	0.55	0.19	0.31	0.32	0.24	0.41
76	0.23	0.02	0.16	-0.06	-0.05	0.19
78	0.48	0.57	0.00	-0.52	-0.05	0.05
82	0.36	0.00	0.57	0.03	0.04	0.45
83	0.77	0.27	0.52	-0.46	-0.38	0.64
84	0.10	0.26	0.05	0.16	0.12	0.07
85	0.44	0.43	0.59	0.44	0.51	0.51
89	0.68	0.04	0.49	-0.17	-0.14	0.58
93	0.06	0.07	0.02	-0.07	-0.04	0.04
94	0.12	0.00	0.31	0.01	0.02	0.20
95	0.16	0.18	0.03	-0.17	-0.07	0.07
101	0.12	0.29	0.20	-0.18	-0.24	0.15

Table 4.3 (continued)

Res. No.	γ_{s1}^2 (keV)	γ_{s3}^2 (keV)	γ_{s5}^2 (keV)	$\gamma_{s1}\gamma_{s3}$ (keV)	$\gamma_{s3}\gamma_{s5}$ (keV)	$\gamma_{s1}\gamma_{s5}$ (keV)
102	0.02	0.19	0.01	-0.05	-0.05	0.01
104	0.21	0.10	0.26	0.14	0.16	0.23
106	0.01	0.16	0.20	-0.04	-0.18	0.05
107	0.01	0.04	0.02	-0.02	-0.03	0.01
109	0.28	0.12	0.27	0.18	0.18	0.27
111	0.12	0.06	0.32	-0.08	-0.13	0.19
112	0.78	0.12	0.18	-0.31	-0.15	0.37

Figure 4.6 Elastic and Three Inelastic Channel Widths and Sum of Reduced Widths versus Energy. The three inelastic channel reduced widths are in the angular momentum representation. The bracket <a,b,c> represents <j-spin,l',2j'>.

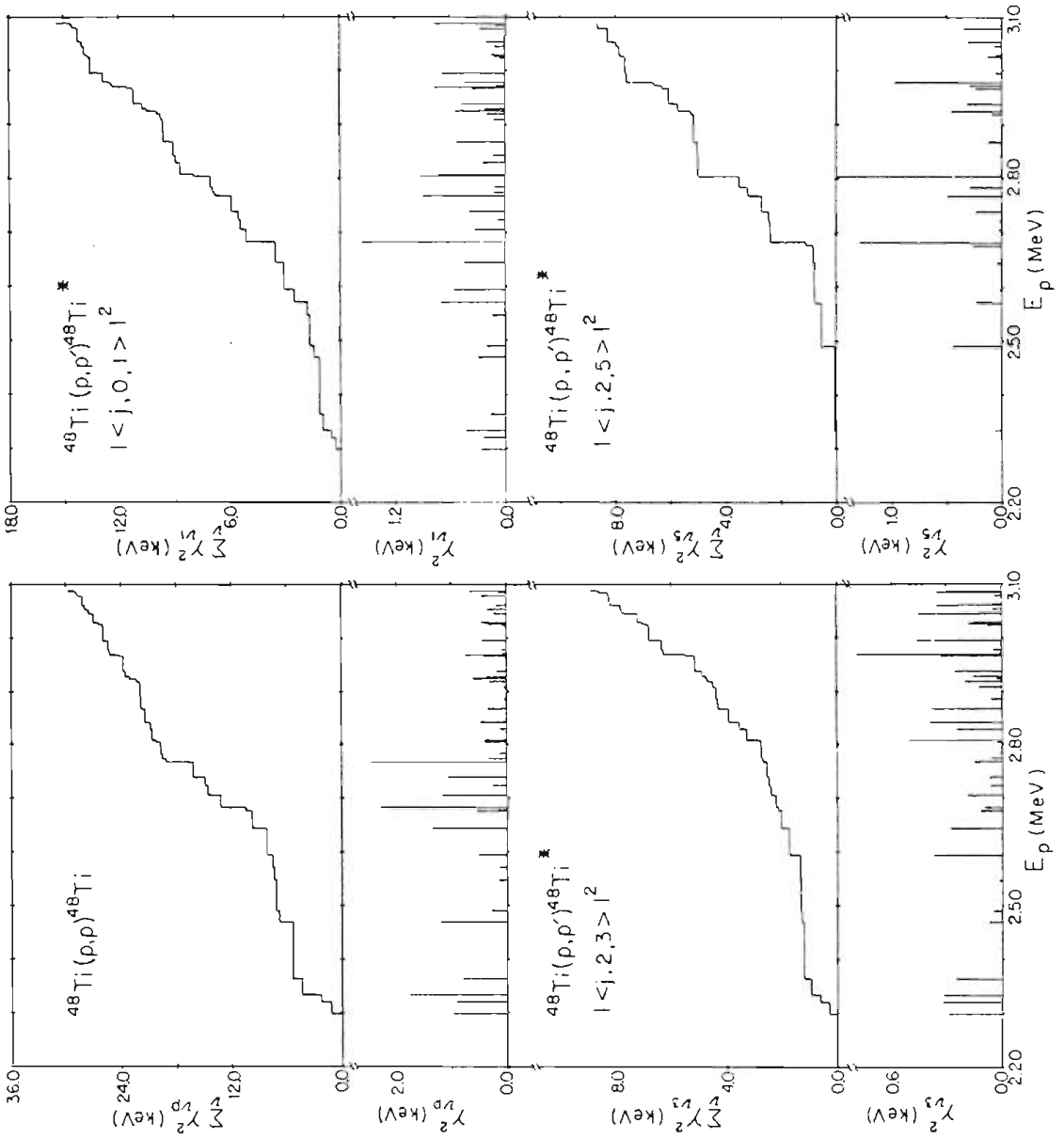
$^{48}Ti(p,p)^{48}Ti$
$^{48}Ti(p,p')^{48}Ti^*$ $1<j,0,1>1^2$
$^{48}Ti(p,p')^{48}Ti^*$ $1<j,2,3>1^2$
$^{48}Ti(p,p')^{48}Ti^*$ $1<j,2,5>1^2$
$\sum_\nu \chi^2_{\nu_p}$ (keV)
$\chi^2_{\nu_p}$ (keV)
$\sum_\nu \chi^2_{\nu_1}$ (keV)
$\chi^2_{\nu_1}$ (keV)
$\sum_\nu \chi^2_{\nu_3}$ (keV)
$\chi^2_{\nu_3}$ (keV)
E_p (MeV)

Figure 4.7 Total Inelastic and Three Inelastic Channel Widths and Sum of Reduced Widths versus Energy. The three inelastic channel reduced widths are in the channel spin representation. The bracket <a,b,c> represents <s-spin,l',2s'>.

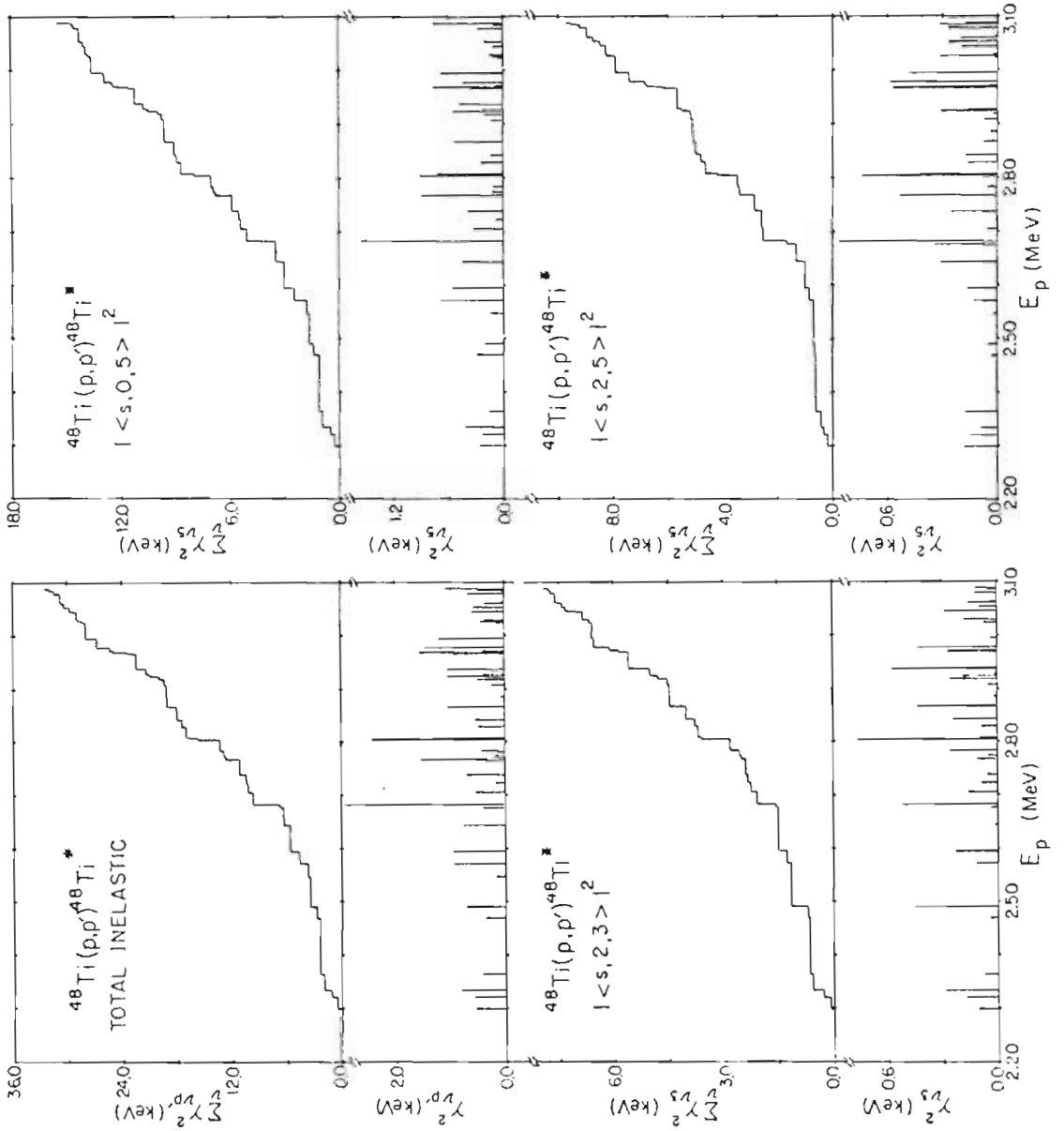
$^{48}Ti(p,p')^{48}Ti^*$
TOTAL INELASTIC
$^{48}Ti(p,p')^{48}Ti^*$
$|<s,2,3>|^2$
$^{48}Ti(p,p')^{48}Ti^*$
$|<s,2,5>|^2$
$^{48}Ti(p,p')^{48}Ti^*$
$|<s,0,5>|^2$
$\chi^2_{\nu_p}$ (keV)
$\chi^2_{\nu_s}$ (keV)
E_p (MeV)

Figure 4.8 Product of Channel Reduced Width Amplitudes and Sum of the Product versus Energy in the Angular Momentum Representation. The bracket <a,b,c> represents <j-spin,l',2j'>.

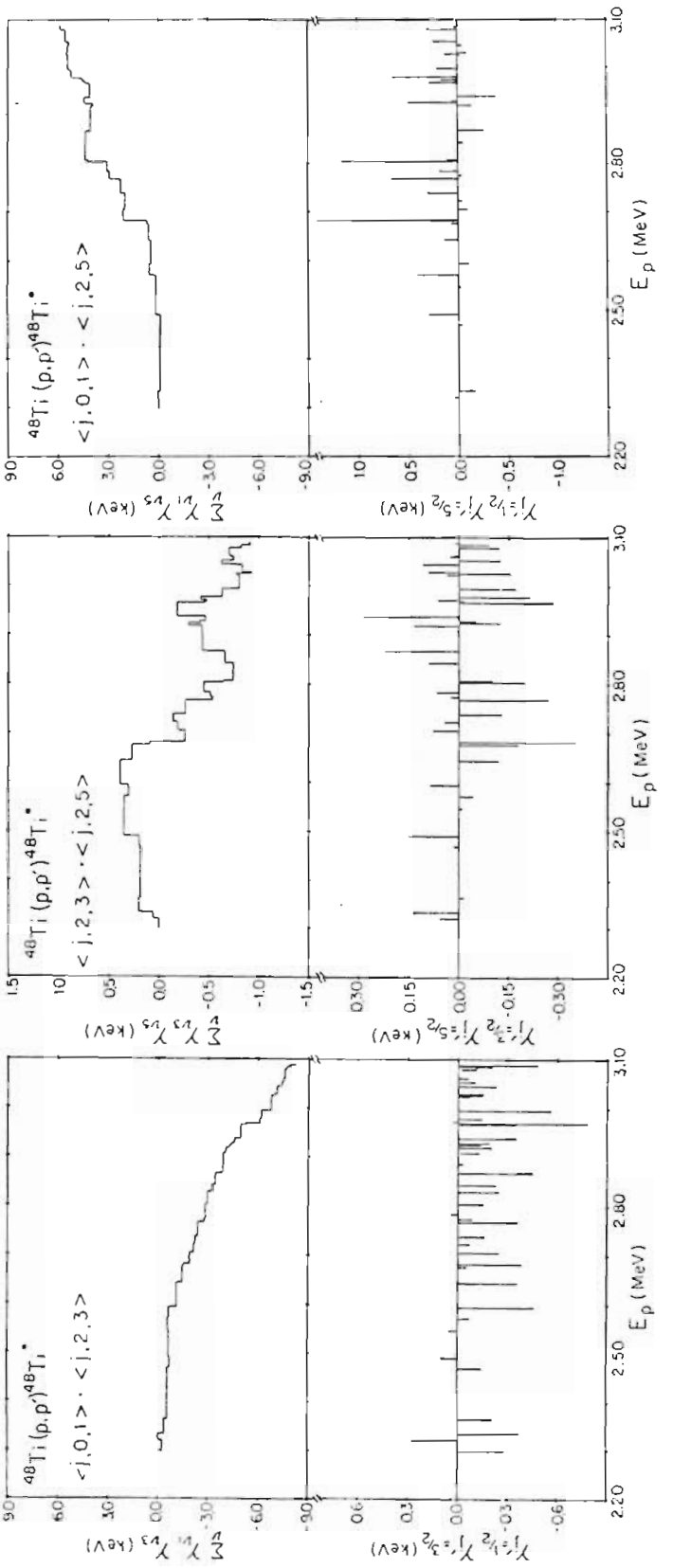
$^{48}Ti(p,p')^{48}Ti^*$
$<j,0,1> \cdot <j,2,3>$
$<j,2,3> \cdot <j,2,5>$
$<j,0,1> \cdot <j,2,5>$
$\sum_{\nu} \chi_{j_i} \chi_{\nu j_3}$ (keV)
$\chi_{j_i=1/2} \chi_{j_i=3/2}$ (keV)
$\chi_{j_i=3/2} \chi_{j_i=5/2}$ (keV)
$\chi_{j_i=1/2} \chi_{j_i=5/2}$ (keV)
E_p (MeV)

Figure 4.9 Product of Channel Reduced Width Amplitudes and Sum of the Product versus Energy in the Channel Spin Representation. The bracket <a,b,c> represents <s-spin,l',2s'>.

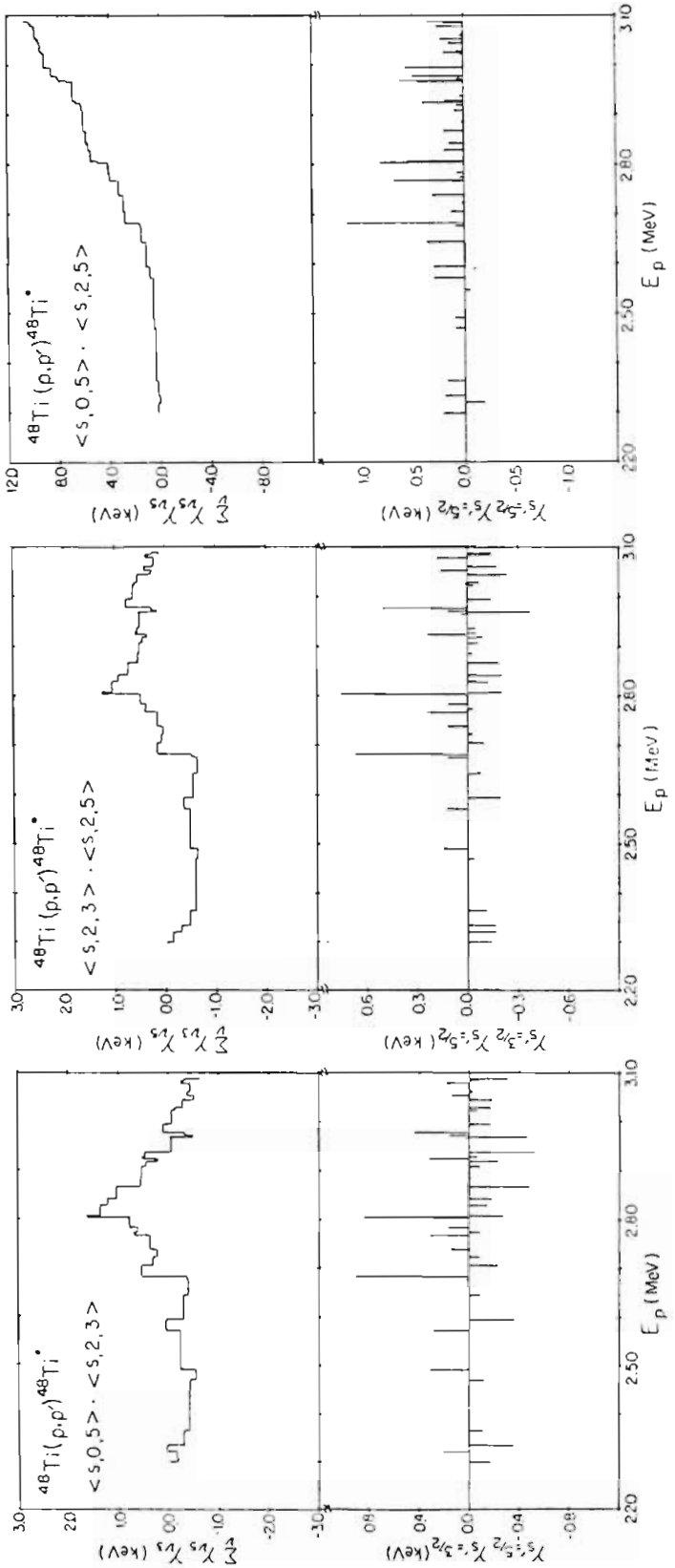
^{48}Ti(p,p')^{48}Ti*
<s,0,5> · <s,2,3>
$\sum_{\nu_3} \chi_{\nu_3}\chi_{\nu_3}$ (keV)
$\chi_{s_1=5/2}\chi_{s_1=3/2}$ (keV)
E_p (MeV)
^{48}Ti (p,p')^{48}Ti*
<s,2,3> · <s,2,5>
$\sum_{\nu_3} \chi_{\nu_3}\chi_{\nu_3}$ (keV)
$\chi_{s_1=3/2}\chi_{s_1=5/2}$ (keV)
E_p (MeV)
^{48}Ti (p,p')^{48}Ti*
<s,0,5> · <s,2,5>
$\sum_{\nu_3} \chi_{\nu_3}\chi_{\nu_3}$ (keV)
$\chi_{s_1=5/2}\chi_{s_1=5/2}$ (keV)
E_p (MeV)

Chapter 5

Statistical properties

A. Introduction

At the excitation energies involved in this experiment (about 10 MeV), there are too many levels to permit theoretical consideration of individual states. Therefore a statistical approach is adopted to describe spacing and width properties. The theoretical background is reviewed briefly, with emphasis placed on the properties of reduced widths and reduced width amplitudes. Explicit expressions are derived for the first time for the mixing ratio distribution when correlations are present.

5.A.1. Canonical Groups

In quantum physics a state is specified by the values of those quantities which are simultaneously measurable

(Morse and Feshbach, 1953). The corresponding operators leave the state unchanged. For example, according to the Schrodinger equation $H\Psi = E\Psi$, the possible energy levels E_i of a quantum system are eigenvalues of the Hamiltonian operator H.

Consider a similarity transformation $\bar{H}=UHU^{-1}$, where two operators $\bar{H}$ and H are linked by an arbitrary unitary matrix U via $\bar{\Psi} = U\Psi$. The invariance properties of eigenvalues E under such a transformation can be easily derived:

$$\begin{aligned} \bar{H}\bar{\Psi} &= UHU^{-1}\bar{\Psi} \\ &= UHU^{-1}U\Psi \\ &= UH\Psi = UE\Psi \\ &= EU\Psi = E\bar{\Psi} \end{aligned} \qquad (5.1)$$

The above transformation, which includes a similarity transformation of the operators and a simultaneous replacement of the function $U\Psi$ by $\bar{\Psi}$, is called a canonical transformation.

By specifying appropriate canonical transformation groups to preserve the invariance properties of the Hamiltonian under a similarity transformation, Dyson (1962) classified a quantal system into three cases in his so-called "three-fold way" theory. These three cases correspond to the symmetry properties (rotational and time reversal symmetry) of the system Hamiltonian H.

1) If the system Hamiltonian H is invariant under time reversal and rotations, or invariant under time reversal and not invariant under rotations but having integral spin, then H can be made real and symmetric ($H = H^* = \widetilde{H}$), and its corresponding canonical transformation group is orthogonal.

2) If the system Hamiltonian H is invariant under time-reversal and is not invariant under rotations, but has odd half integral spin, then the Hamiltonian is quaternion real ($H=H + \sum_{k}^{3} H_k \zeta_k$, $H_0=H_0^* =\widetilde{H}_0$, $H_k=H_k^*=-H_k$, $k=1,2,3$) and its corresponding canonical transformation group is symplectic.

3) If the system Hamiltonian H is not invariant under time reversal (regardless of its rotational invariance), then the Hamiltonian is complex ($H=H_0+iH_1$, $H_0=H_0^*=\widehat{H}_0$, $H_1=H_1^*=-\widetilde{H}_1$) and the corresponding canonical transformation group is unitary.

5.A.2. The Random Matrix Hypothesis and The Joint Probability for the Hamiltonian Matrix Elements

Since the orthogonal transformation group is an appropriate choice for describing the statistical behavior of compound states, in the following discussion only a real and symmetric Hamiltonian is considered.

To simplify the Hamiltonian matrix, Wigner (1932) proposed choosing eigenfunctions Ψ as functions of certain conserved quantities such as spin and parity. The goal was to reduce the Hamiltonian matrix into diagonal blocks (Mehta (1967)), as illustrated in Fig. 5.1. The eigenvalues of each block represent the local statistical behavior of a simple level sequence which has the same conserved quantities. The interaction between levels inside the same block is so strong that no further diagonalization is considered. Levels corresponding to two different blocks are statistically uncorrelated. Analysis is therefore greatly simplified by focussing attention on only one of the diagonal blocks: an $N \times N$ Hermitian matrix whose elements are assumed to be random variables with the maximum statistical independence allowed under the symmetry requirements. N is a large fixed positive integer.

Now, consider H as an $N \times N$ real symmetric matrix with

Figure 5.1 Hamiltonian Matrix Diagonalized into Blocks With Specific Spin and Parity.

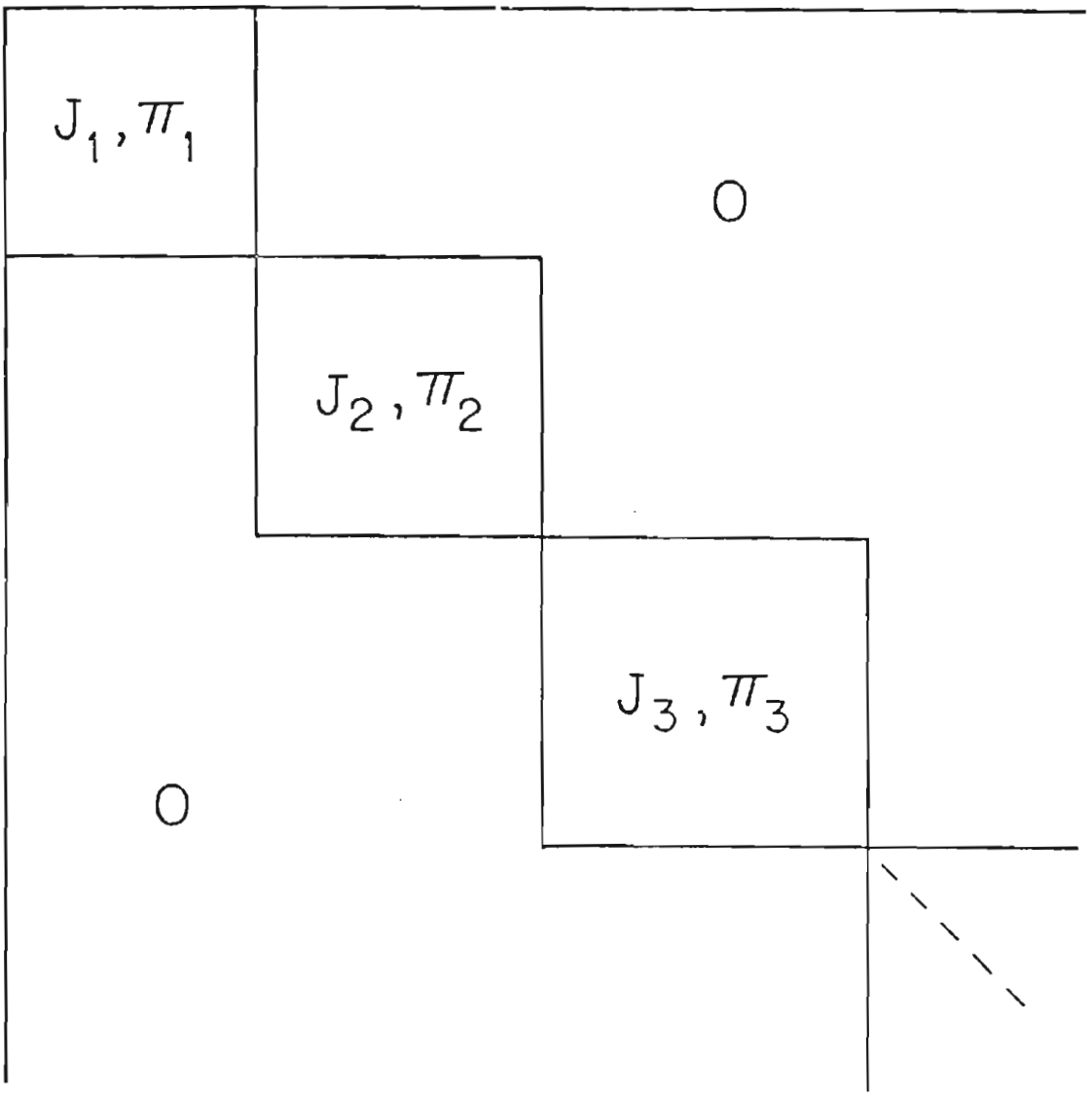
J_1, π_1
0
J_2, π_2
J_3, π_3
0

$N(N+1)/2$ real parameters. If the associated probability distribution function of H is denoted as

$$P(H) = P(H_{11}, H_{22} \cdots\cdots H_{NN}, H_{12} \cdots\cdots H_{N-1,N}) \qquad (5.2)$$

where H_{ij} are the matrix elements of H, then the joint differential probability that H_{11} is in the interval dH_{11} at H_{11}, and H_{12} is in the interval dH_{12} at H_{12}, etc., is

$$P(H_{11}, H_{12} \cdots\cdots H_{NN})\, dH_{11}\, dH_{12} \cdots\cdots dH_{NN} \qquad (5.3)$$

5.A.3. Spacing Distributions

Suppose the Hamiltonian matrix H is diagonalized by an orthogonal matrix O into a diagonal matrix H_D whose elements are eigenvalues of H, and the matrix O is formed by the corresponding eigenvectors. The element representation for this similarity transformation $H = O H_D O^{-1} = O H O$ can then be denoted as

$$H_{\mu\nu} = \sum_{\xi,\eta} O_{\mu\xi}\, E_\xi\, \delta_{\xi\eta}\, O_{\nu\eta}$$

$$= \sum_{\xi=1}^{N} E_\xi\, O_{\mu\xi}\, O_{\nu\xi} \qquad (5.4)$$

where E_ξ is the component of an N parameter function

$f(E_1, E_2 \ldots\ldots E_N)$ and $O_{\mu\nu}$ is the component of an $N \times N$ orthogonal matrix which contains $N(N-1)/2$ independent parameters (since there are $N(N-1)/2$ orthogonality and N normalization constraints) labelled by: $\alpha_1, \alpha_2, \ldots\ldots\ldots \alpha_{N(N-1)/2}$.

Since the $H_{\mu\nu}$ are functions of E's and α's, the energy spacing probability function $P(E_1, E_2 \ldots\ldots, E_N)$ can be obtained from $P(H_{11}, H_{12} \ldots\ldots H_{NN})$ with the related Jacobian determinant, i. e.,

$$P(E_1, E_2 \ldots\ldots E_N) = J_N \; P(H_{11}, H_{12} \ldots\ldots H_{NN}) \tag{5.5}$$

where

$$J_N = \begin{vmatrix} \frac{\partial H_{11}}{\partial E_1} & \frac{\partial H_{11}}{\partial E_2} & \cdots & \frac{\partial H_{11}}{\partial E_N} & \frac{\partial H_{11}}{\partial \alpha_1} & \frac{\partial H_{11}}{\partial \alpha_2} & \cdots & \frac{\partial H_{11}}{\partial \alpha_{N(N-1)/2}} \\ \cdots & \cdots & \cdots & \cdots & \cdots & \cdots & \cdots & \cdots \\ \cdots & \cdots & \cdots & \cdots & \cdots & \cdots & \cdots & \cdots \\ \frac{\partial H_{NN}}{\partial E_1} & \frac{\partial H_{NN}}{\partial E_2} & \cdots & \frac{\partial H_{NN}}{\partial E_N} & \frac{\partial H_{NN}}{\partial \alpha_1} & \frac{\partial H_{NN}}{\partial \alpha_2} & \cdots & \frac{\partial H_{NN}}{\partial \alpha_{N(N-1)/2}} \end{vmatrix} \tag{5.6}$$

Since according to Eqn. 5.4, $H_{\mu\nu}$ is a linear function of the energy eigenvalues E_λ, the elements of the first N columns in J_N will be independent of E_λ. However the remaining $N(N-1)/2$ columns have elements which are linear functions of the E_λ's. This implies that the Jacobian J_N

is a polynomial of degree $N(N-1)/2$ in energy eigenvalues. If one pair of the eigenvalues is equal, then the inverse transformation of Eqn. 5.5 is singular (because the eigenvectors are not unique); this implies that J_N vanishes when $E_i = E_j$, $i \neq j$. Therefore

$$J_N(E_1, E_2 \cdots E_N, \alpha_1, \cdots \alpha_{N(N-1)/2}) = \left(\prod_{\lambda < \mu}^{N} |E_\lambda - E_\mu| \right) h(\alpha_1, \alpha_2 \cdots \alpha_{N(N-1)/2}) \tag{5.7}$$

Substituting J_N into Eqn. 5.5, we obtain

$$P(E_1, E_2 \cdots\cdots E_N) \sim \prod_{\lambda < \mu}^{N} |E_\lambda - E_\mu| \cdot P(H_{11}, H_{12} \cdots H_{NN})$$

By making two assumptions, Porter and Rosenzweig (1960) derived the analytic form of $P(H_{11}, H_{12} \cdots H_{NN})$, the so-called Wishart distribution as

$$P(H_{11}, H_{12} \cdots H_{NN}) \sim \exp\{-A \cdot \mathrm{Tr}H^2 - B \cdot \mathrm{Tr}H\} \tag{5.8}$$

where Tr means trace. These two assumptions are:

1) P is invariant under a system coordinate rotation,

$$P(H)=P(H') \quad \text{or} \quad \frac{dP}{d\alpha}=0.$$

2) The distribution of each matrix element of H is independent of the others,

$$P(H)=f_{11}(H_{11})\,f_{22}(H_{22})\cdots f_{NN}(H_{NN})\,f_{12}(H_{12})\cdots f_{N-1,N}(H_{N-1,N})$$

The most stringent experimental tests on spacing distributions were performed by Liou et al. (1972) with neutron resonances. Wilson et al. (1975) made similar tests with proton resonances. The present status is reviewed by Brody et al. (1978). In addition to the spacing distribution, these two hypotheses have also been employed to derive distributions for other statistical properties. In next section the application to the reduced width distribution will be examined.

5.A.4. The Reduced Width Distribution

According to the R-matrix theory (reviewed by Lane and Thomas (1958)), the reduced width amplitude $\gamma_{\lambda c}$ associated with level λ and channel c is defined as:

$$\gamma_{\lambda c} = \left(\frac{\hbar^2}{2M_c a_c}\right)^{1/2} \int_{a_c} \varphi_c^* X_\lambda \, ds \qquad (5.9)$$

with M_c the channel mass, a_c the channel radius, ds the channel surface, φ_c the channel function and X_λ the characteristic wave function corresponding to level λ of the compound system.

The joint distribution function for $\gamma_{\lambda c}$ to be in the interval $d\gamma_{\lambda c}$ at $\gamma_{\lambda c}$ when $\gamma_{\mu c'}$ is in the interval $d\gamma_{\mu c'}$ at $\gamma_{\mu c'}$, etc., is denoted as:

$$P(\{\gamma_{\lambda c}\}) = P(\gamma_{1c}, \gamma_{1c'} \cdots \gamma_{2c}, \gamma_{2c'} \cdots\cdots) \qquad (5.10)$$

The invariance hypothesis implies that P is independent of the basis (the state vector X_λ), i. e., X_λ is invariant under an orthogonal transformation. With the relation between $\gamma_{\lambda c}$ and X_λ given by Eqn. 5.9, an orthogonal transformation of X_λ is equivalent to a transformation of $\gamma_{\lambda c}$. Therefore the invariance property

indicates

$$P(\{\gamma_{\lambda c}\}) = P(\{\gamma_{\lambda c'}\}) \tag{5.11}$$

where $\gamma_{\lambda c}$ and $\gamma_{\lambda c'}$ are related by

$$\gamma_{\lambda c} = O\,\gamma_{\lambda c'} \tag{5.12}$$

Furthermore, following the independence hypothesis, $P(\{\gamma_{\lambda c}\})$ can be written as

$$P(\{\gamma_{\lambda c}\}) = \prod_{\lambda} f_{\lambda}(\{\gamma_{\lambda c}\}) = f_1(\gamma_{1c})\, f_2(\gamma_{2c}) \cdots\cdots\cdots \tag{5.13}$$

To illustrate the procedure, we begin by deriving the width distribution $P(\{\gamma_{\lambda c}\})$ for the case of a single channel and two levels. Following Eqn. 5.13, $P(\{\gamma_{\lambda c}\})$ is equivalent to:

$$P(\{\gamma_{\lambda c}\}) = f_1(\gamma_{1c})\, f_2(\gamma_{2c}) \tag{5.14}$$

Define the Matrix O as

$$O = \begin{pmatrix} \cos\alpha & \sin\alpha \\ -\sin\alpha & \cos\alpha \end{pmatrix} \tag{5.15}$$

Eqn. 5.12 therefore yields the following relations

$$\gamma_{1c} = \gamma_{1c'}\cos\alpha + \gamma_{2c'}\sin\alpha$$
$$\gamma_{2c} = -\gamma_{1c'}\sin\alpha + \gamma_{2c'}\cos\alpha \qquad (5.16)$$

Taking the partial derivative with respect to α, the above equations yield

$$\frac{\partial \gamma_{1c}}{\partial \alpha} = \gamma_{2c} \qquad \text{and} \qquad \frac{\partial \gamma_{2c}}{\partial \alpha} = -\gamma_{1c} \qquad (5.17)$$

Applying the invariance condition in the form $\frac{d \ln P_c}{d \alpha} = 0$ to Eqn. 5.14, and substituting relations obtained in Eqn. 5.17, we obtain

$$\frac{f_1'(\gamma_{1c})}{f_1(\gamma_{1c})}\gamma_{2c} - \frac{f_2'(\gamma_{2c})}{f_2(\gamma_{2c})}\gamma_{1c} = 0 \qquad (5.18)$$

This equation indicates that $\frac{f_\lambda'(\gamma_{\lambda c})}{f_\lambda(\gamma_{\lambda c})}$ is a linear function of $\gamma_{\lambda c}$, say $\frac{f_\lambda'(\gamma_{\lambda c})}{f_\lambda(\gamma_{\lambda c})} = -a\gamma_{\lambda c}$, where a is an arbitrary constant. Therefore

$$f_\lambda(\gamma_{\lambda c}) = b \cdot \exp(-a\gamma_{\lambda c}) \qquad (5.19)$$

where b is the integration constant. Imposing the normalization condition $\int_{-\infty}^{\infty} f_\lambda(\gamma_\lambda)\, d\gamma_\lambda = 1$, the relation

between a and b is obtained

$$a=2\pi b^2 \tag{5.20}$$

Define the average reduced width $\overline{\gamma_{\lambda c}^2}$ as

$$\overline{\gamma_c^2}=\overline{\gamma_{\lambda c}^2}=\int_{-\infty}^{\infty}\gamma_{\lambda c}^2 f(\gamma_{\lambda c})\,d\gamma_{\lambda c} \tag{5.21}$$

Replacing $f(\gamma_{\lambda c})$ by Eqn. 5.19, $\overline{\gamma_{\lambda c}^2}$ is equivalent to

$$\overline{\gamma_{\lambda c}^2}=(b/a)\sqrt{(2\pi/a)} \tag{5.22}$$

With Eqn. 5.20 and Eqn. 5.22, values of a and b are obtained in terms of $\overline{\gamma_c^2}$

$$a=\frac{1}{\overline{\gamma_c^2}} \quad , \quad b=\frac{1}{(2\pi\ \overline{\gamma_c^2})^{1/2}}$$

Replacing these values of a and b in Eqn. 5.19 yields

$$f_\lambda(\gamma_{\lambda c})=(2\pi\ \overline{\gamma_c^2})^{-1/2}\exp(-\gamma_{\lambda c}^2/2\ \overline{\gamma_c^2}) \tag{5.23}$$

Substituting Eqn. 5.23 in Eqn. 5.13, the joint distribution for a single channel c is

$$P(\gamma_{1c},\gamma_{2c}\ldots.)=C\cdot\exp(-(\gamma_{1c}^2+\gamma_{2c}^2+\ldots)/2\ \overline{\gamma_c^2}) \tag{5.24}$$

where $C=(2\pi\ \overline{\gamma_c^2})^{-(1/2)N}$, and N is the total number of levels.

Generalizing with similar arguments to two levels and

two channels (T. J. Krieger and C. E. Porter(1963)) or (Porter (1960)) one obtains

$$f_\lambda(\gamma_{\lambda c}, \gamma_{\lambda c'}) = \frac{|M|^{1/2}}{2\pi} \exp\left(-\frac{1}{2}(\gamma_\lambda, M\gamma_\lambda)\right) \qquad (5.25)$$

where M is a two by two (for two channels) real symmetric positive definite matrix defined by

$$M = \overline{(\gamma_\lambda \times \gamma_\lambda)}^{-1} \qquad (5.26)$$

and $|M|$ is the determinant of matrix M. Therefore, for the two-channel, multi-level case,

$$P_{cc'} = \prod_\lambda \frac{|M|^{1/2}}{2\pi} \exp\left(-\frac{1}{2}(\gamma_\lambda, M\gamma_\lambda)\right) \qquad (5.27)$$

The significant difference between Eqn. 5.27 and Eqn. 5.24 is the occurrence of off-diagonal elements in the matrix M when more than one channel is present. This implies the possible existence of correlations between reduced width amplitudes corresponding to different channels. Generalizing Eqn. 5.27 to m channels, one obtains

$$P_{cc'c''\ldots} = \prod_{\lambda} \frac{|M|^{1/2}}{(2\pi)^{m/2}} \cdot \exp\left(-\frac{1}{2}(\gamma_\lambda, M\gamma_\lambda)\right) \qquad (5.28)$$

5.A.5. The Covariance Matrix and the Channel Width Correlation Coefficient

To obtain simple relations between reduced widths and the elements of the matrix M, a covariance matrix $\bar{\Sigma}$ is introduced for calculational convenience,

$$\bar{\Sigma} = M^{-1} = \overline{\gamma_\lambda \times \gamma_\lambda}$$

The diagonal elements $\overline{\gamma_{\lambda c}^2}$ of matrix $\bar{\Sigma}$ are equivalent to :

$$\overline{\gamma_c^2} = \bar{\Sigma}_{cc} = \frac{\mathrm{Adj}(M_{cc})}{|M|} \qquad (5.29)$$

where $\mathrm{Adj}(M_{cc})$ means the adjoint matrix of element M_{cc} in matrix M.

Since $|M| = M_{cc} \cdot \mathrm{Adj}(M_{cc}) + \sum_{c' \neq c} (-1)^{c+c'} M_{cc'} \cdot \mathrm{Adj}(M_{cc'})$,

the derivative of $|M|$ with respect to M_{cc} is

$$\frac{\partial |M|}{\partial M_{cc}} = Adj(M_{cc}) \tag{5.30}$$

Combining Eqn. 5.29 and Eqn. 5.30, a relation between the diagonal elements of matrix Σ and matrix M is obtained

$$\overline{\gamma_{\lambda c}^2} = \overline{\gamma_c^2} = \frac{1}{|M|} \frac{\partial |M|}{\partial M_{cc}} \tag{5.31}$$

Since $\overline{\gamma_{\lambda c}^2}$ averages over all levels, there is no λ dependence. In a similar manner, the relation between the off-diagonal elements $\overline{\gamma_{\lambda c} \gamma_{\lambda c'}}$ of the Σ and M matrices is

$$\overline{\gamma_{\lambda c} \gamma_{\lambda c'}} = \frac{1}{2|M|} \frac{\partial |M|}{\partial M_{cc'}} \tag{5.32}$$

where the factor two is a result of the symmetry property of matrix M. For completeness, we may rewrite Eqn. 5.32 as

$$\overline{\gamma_{\lambda c} \gamma_{\mu c'}} = \delta_{\lambda \mu} \frac{1}{2|M|} \frac{\partial |M|}{\partial M_{cc'}} \tag{5.33}$$

where $\delta_{\lambda \mu}$ is the Kronecker delta. For two channels c and c', Eqn. 5.31 and Eqn. 5.33 reduce to

$$\overline{\gamma_c^2} = \frac{M_{cc'}}{M_{cc} M_{c'c'} - M_{cc'}^2} \tag{5.34}$$

$$\overline{\gamma_{\lambda c}\,\gamma_{\lambda c'}} = \frac{-M_{c'c'}}{M_{cc}M_{c'c'}-M_{cc}^2} \tag{5.35}$$

Therefore, the channel correlation coefficient $C(\gamma_c, \gamma_{c'})$ of the reduced width amplitudes is

$$C(\gamma_c, \gamma_{c'}) = \frac{\overline{\gamma_{\lambda c}\,\gamma_{\lambda c'}}}{(\overline{\gamma_c^2}\;\overline{\gamma_{c'}^2})^{1/2}} = -\frac{M_{c'c'}}{(M_{cc}M_{c'c'})^{1/2}} \tag{5.36}$$

where the random phase approximation ($\overline{\gamma_{\lambda c}}=0$) is assumed. The reduced width correlation coefficient $C(\gamma_c^2, \gamma_{c'}^2)$ is

$$C(\gamma_c^2, \gamma_{c'}^2) = \frac{\overline{\gamma_{\lambda c}^2\,\gamma_{\lambda c'}^2} - \overline{\gamma_{\lambda c}^2}\;\overline{\gamma_{\lambda c'}^2}}{\{(\overline{\gamma_{\lambda c}^4} - (\overline{\gamma_{\lambda c}^2})^2)(\overline{\gamma_{\lambda c'}^4} - (\overline{\gamma_{\lambda c'}^2})^2)\}^{1/2}} = (C(\gamma_{\lambda c}, \gamma_{\lambda c'}))^2$$

(5.37)

This relation implies that only a positive width correlation is possible. However, a negative width correlation is observed between channels s-3/2 and s-5/2 in the present data.

5.A.6. The Probability Distribution for Mixing Ratios

In our data analysis the ratio of two reduced width amplitudes (mixing ratios) is determined. Consequently, it is convenient to transform Eqn. 5.28 into a function of mixing ratios. In this section the properties of these mixing ratio probability functions are examined for some special cases (two and three channels).

By convention the mixing ratio ζ is defined as $\zeta = \gamma_> / \gamma_<$, where $\gamma_>, \gamma_<$ correspond to the channel amplitude with higher spin and lower spin, respectively. Since the sign of ζ represents the relative sign between these two amplitudes, one of these amplitudes may be chosen positive, say $\gamma_< \geq 0$. For convenience a new variable ϕ is defined as $\phi = \tan^{-1}\zeta$, in order to map the infinitely ranged variable ζ ($-\infty \leq \zeta \leq \infty$) into the finitely ranged variable ϕ ($-90^\circ \leq \phi \leq 90^\circ$). The geometric representation of ϕ is shown in Fig. 5.2.a (Wells (1978)).

Figure 5.2 (a) Geometric Relation Between Amplitude Reduced Width and Mixing Ratio Parameters for Two Channels.

(b) Geometric Relation Between Reduced Width Amplitudes ($\gamma_1, \gamma_2, \gamma_3$) and Mixing Ratio Parameters (ϕ_1, ϕ_2) for Three Channels.

(c) Geometric Relation Between Three-Channel Reduced Width Amplitudes ($\gamma_1, \gamma_2, \gamma_3$) and the Spherical Coordinates (r, θ, ϕ).

a)

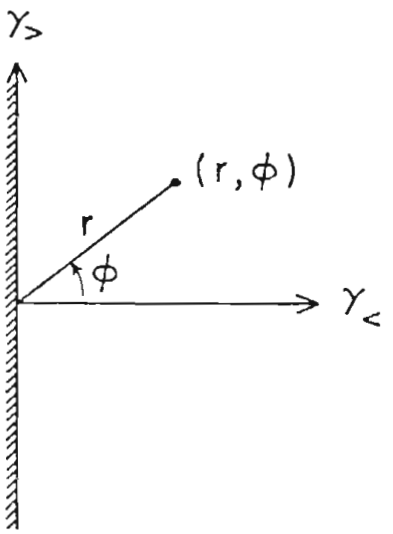
$\gamma_>$
(r, ϕ)
r
ϕ
$\gamma_<$

b)

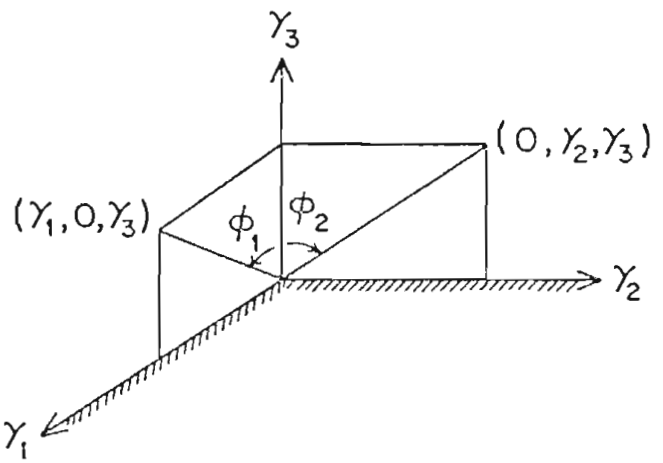
γ_3
$(0, \gamma_2, \gamma_3)$
$(\gamma_1, 0, \gamma_3)$
ϕ_1
ϕ_2
γ_2
γ_1

c)

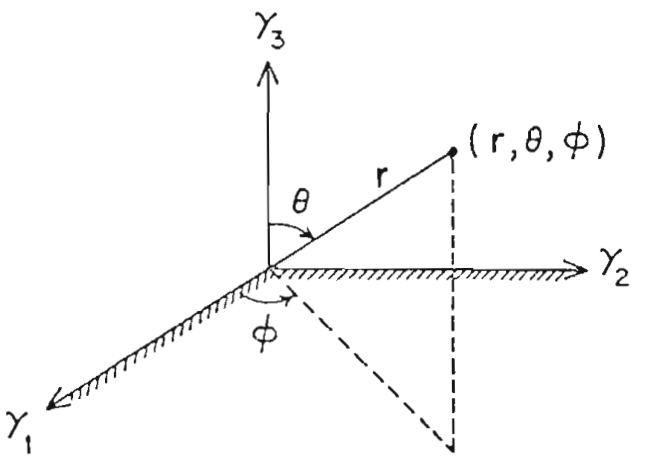
γ_3
(r, θ, ϕ)
r
θ
γ_2
ϕ
γ_1

I. The Two-Channel Mixing Ratio Probability Density Function

According to Eqn. 5.27, the probability density function of reduced widths for two channels is equivalent to:

$$P(\gamma_1,\gamma_2)=\frac{|M|^{1/2}}{\pi}\exp\left(-\frac{1}{2}M_{11}\gamma_1^2-\frac{1}{2}M_{22}\gamma_2^2-M_{12}\gamma_1\gamma_2\right) \tag{5.38}$$

where a factor of two arises from the restriction $\gamma_1 \geq 0$. Since the probability functions are invariant under coordinate system rotations, one obtains the relation

$$P(\gamma_1,\gamma_2)\,d\gamma_1\,d\gamma_2=P(r,\phi)\,dr\,d\phi \tag{5.39}$$

where $\gamma_1=r\cos\phi$ and $\gamma_2=r\sin\phi$ (Fig. 5.2.a). Therefore $P(r,\phi)$ and $P(\gamma_1,\gamma_2)$ are related by the Jacobian determinant $J(r,\phi)$

$$P(r,\phi)=J(r,\phi)\;P(\gamma_1(r,\phi),\gamma_2(r,\phi)) \tag{5.40}$$

and

$$J(r,\phi) = \begin{vmatrix} \cos\phi & -r\sin\phi \\ \sin\phi & r\cos\phi \end{vmatrix} = r$$

Thus

$$P(r,\phi) = \frac{|M|^{1/2}}{\pi} r \exp\{(-\frac{1}{2} r^2)(M_{11}\cos^2\phi + M_{22}\sin^2\phi + M_{12}\sin 2\phi)\} \tag{5.41}$$

where r ($r^2 = \gamma_1^2 + \gamma_2^2$) is the square root of the total inelastic reduced width and ϕ is related to the relative strength in different channels. If only the relative strength is of interest, one can integrate over the variable r (discarding information about the total strength) and obtain the marginal probability density function of ϕ as

$$P(\phi) = \int_{-\infty}^{\infty} P(r,\phi)\, dr$$

$$= \frac{|M|^{1/2}}{\pi (M_{11}\cos^2\phi + M_{22}\sin^2\phi + M_{12}\sin 2\phi)} \tag{5.42}$$

The marginal probability density function of δ is therefore

$$P(\delta) = \frac{\partial \phi}{\partial \delta} \; P(\phi(\delta))$$

$$= \frac{|M|^{1/2}}{\pi (M_{11} + M_{22}\,\delta^2 + 2M_{12}\,\delta)} \qquad (5.43)$$

where

$$|M| = \frac{1}{(\overline{\gamma_1^2}\;\overline{\gamma_2^2} - (\overline{\gamma_1\gamma_2})^2)}\;, \quad M_{11} = \overline{\gamma_2^2} \cdot |M|$$

$$M_{22} = \overline{\gamma_1^2} \cdot |M| \;, \quad M_{12} = -\overline{\gamma_1\gamma_2} \cdot |M|$$

If the average reduced widths in two channels are equal ($\overline{\gamma_1^2} = \overline{\gamma_2^2}$), then Eqn. 5.42 and Eqn. 5.43 reduces to

$$P(\phi) = \frac{C}{1 + M' \sin 2\phi} \qquad (5.44)$$

$$P(\delta) = \frac{C}{1 + \delta^2 + 2M'\delta} \qquad (5.45)$$

where

$$M' = \frac{M_{12}}{M_{11}} = -\frac{\overline{\gamma_1\gamma_2}}{(\overline{\gamma_1^2}\;\overline{\gamma_2^2})^{1/2}}$$

$$C = \frac{|M|^{1/2}}{\pi M_{11}} = \frac{(\overline{\gamma_1^2}\;\overline{\gamma_2^2} - (\overline{\gamma_1\gamma_2})^2)^{1/2}}{\pi\,(\overline{\gamma_1^2}\;\overline{\gamma_2^2})^{1/2}}$$

Furthermore, if there is no channel correlation ($M'=0$), then $P(\phi)$ reduces to a uniform distribution and $P(\delta)$ reduces to a Cauchy distribution.

II. The Three-Channel Mixing Ratio Probability Density Function

According to Eqn. 5.28 the probability density function for reduced width amplitudes in three channels $\gamma_1, \gamma_2, \gamma_3$ is

$$P(\gamma_1,\gamma_2,\gamma_3) = \frac{2\cdot|M|^{1/2}}{(2\pi)^{3/2}} \cdot$$

$$\exp\left(-\frac{1}{2}\left(M_{11}\gamma_1^2+M_{22}\gamma_2^2+M_{33}\gamma_3^2\right)-\left(M_{12}\gamma_1\gamma_2+M_{23}\gamma_2\gamma_3+M_{13}\gamma_1\gamma_3\right)\right) \tag{5.46}$$

where a factor of two arises from the restriction that γ_3 is always positive. Six different mixing ratios can be generated by combinations of $\gamma_1, \gamma_2, \gamma_3$, but only two are independent. We thus define these two mixing ratios δ_1, δ_2 as $\delta_1 = \gamma_1/\gamma_3$, $\delta_2 = \gamma_2/\gamma_3$. Since γ_3 is defined as always positive, two new variables ϕ_1, ϕ_2 can be defined as $\phi_1 = \tan^{-1}\delta_1$ $(-90° \le \phi_1 \le 90°)$ $\phi_2 = \tan^{-1}\delta_2$ $(-90° \le \phi \le 90°)$. The geometric representation is shown in Fig. 5.2.b.

In order to obtain the marginal probability density function for (δ_1, δ_2) and (ϕ_1, ϕ_2), we transform from the cartesian coordinate system $(\gamma_1, \gamma_2, \gamma_3)$ into the spherical

coordinate system (r,θ,ϕ). From Fig. 5.2.c, the relations between these two coordinate systems are

$$\gamma_1 = r\cdot\sin\theta\cdot\cos\phi$$

$$\gamma_2 = r\cdot\sin\theta\cdot\sin\phi$$

$$\gamma_3 = r\cdot\cos\theta \quad (0\le\theta\le\pi/2) \tag{5.47}$$

Therefore

$$P(r,\theta,\phi) = J(r,\theta,\phi)\,P(\gamma_1(r,\theta,\phi),\gamma_2(r,\theta,\phi),\gamma_3(r,\theta,\phi))$$

$$= r^2\sin\theta\cdot 2\cdot\frac{|M|^{1/2}}{(2\pi)^{3/2}}\cdot\exp\left(-\frac{r^2}{2}(M_{11}\sin^2\theta\cos^2\phi\right.$$

$$+M_{22}\sin^2\theta\sin^2\phi+M_{33}\cos^2\theta+2M_{12}\sin^2\theta\cos\phi\sin\phi$$

$$\left.+2M_{23}\sin\theta\cos\theta\sin\phi+2M_{13}\sin\theta\cos\theta\cos\phi)\right) \tag{5.48}$$

From Eqn. 5.47, one obtains

$$\delta_1 = \gamma_1/\gamma_3 = \tan\theta\cdot\cos\phi$$

$$\delta_2 = \gamma_2/\gamma_3 = \tan\theta\cdot\sin\phi \tag{5.49}$$

or

$$\phi = \tan^{-1}(\delta_2/\delta_1)$$

$$\theta = \tan^{-1}(\delta_1^2+\delta_2^2)^{1/2} \tag{5.50}$$

Therefore

$$P(r,\delta_1,\delta_2)=J(r,\delta_1,\delta_2)\,P(r,\theta(\delta_1,\delta_2),\phi(\delta_1,\delta_2))$$

$$=\frac{2\,r^2}{(1+\delta_1^2+\delta_2^2)^{3/2}}\;\frac{|M|^{1/2}}{(2\pi)^{3/2}}\exp\left(-\frac{r^2}{2}\left(M_{11}\frac{\delta_1^2}{(1+\delta_1^2+\delta_2^2)}-\right.\right.$$

$$+M_{22}\cdot\frac{\delta_2^2}{1+\delta_1^2+\delta_2^2}+M_{33}\cdot\frac{1}{1+\delta_1^2+\delta_2^2}+2M_{12}\cdot\frac{\delta_1\delta_2}{1+\delta_1^2+\delta_2^2}$$

$$\left.\left.+2M_{23}\cdot\frac{\delta_2}{1+\delta_1^2+\delta_2^2}+2M_{13}\cdot\frac{\delta_1}{1+\delta_1^2+\delta_2^2}\right)\right) \tag{5.51}$$

where

$$|M|=(\overline{\gamma_1^2}\;\overline{\gamma_2^2}\;\overline{\gamma_3^2}+2\,\overline{\gamma_1\gamma_2}\;\overline{\gamma_2\gamma_3}\;\overline{\gamma_1\gamma_3}-\overline{\gamma_2^2}\,(\overline{\gamma_1\gamma_3})^2-\overline{\gamma_3^2}\,(\overline{\gamma_1\gamma_2})^2-\overline{\gamma_1^2}\,(\overline{\gamma_2\gamma_3})^2)^{-1}$$

$$M_{11}=(\overline{\gamma_2^2}\;\overline{\gamma_3^2}-(\overline{\gamma_2\gamma_3})^2)\cdot|M|$$

$$M_{22}=(\overline{\gamma_1^2}\;\overline{\gamma_3^2}-(\overline{\gamma_1\gamma_3})^2)\cdot|M|$$

$$M_{33}=(\overline{\gamma_1^2}\;\overline{\gamma_2^2}-(\overline{\gamma_1\gamma_2})^2)\cdot|M|$$

$$M_{12}=(\overline{\gamma_1\gamma_3}\;\overline{\gamma_2\gamma_3}-\overline{\gamma_1\gamma_2}\;\overline{\gamma_3^2})\cdot|M|$$

$$M_{23}=(\overline{\gamma_1\gamma_2}\;\overline{\gamma_1\gamma_3}-\overline{\gamma_2\gamma_3}\;\overline{\gamma_1^2})\cdot|M|$$

$$M_{13}=(\overline{\gamma_1\gamma_2}\;\overline{\gamma_2\gamma_3}-\overline{\gamma_1\gamma_3}\;\overline{\gamma_2^2})\cdot|M| \tag{5.52}$$

From Eqn. 5.47, $r^2=\gamma_1^2+\gamma_2^2+\gamma_3^2$, where r represents the total inelastic reduced width strength. As mentioned before, if only the relative strength between different channels is of interest, the marginal probability density function for δ_1, δ_2 can be obtained by integrating out the total strength r, i. e.,

$$P(\delta_1, \delta_2) = \int_0^\infty P(r, \delta_1, \delta_2)\, dr$$

$$= \frac{|M|^{1/2}}{2\pi} \frac{1}{(M_{11}\delta_1^2 + M_{22}\delta_2^2 + M_{33} + 2M_{12}\delta_1\delta_2 + 2M_{23}\delta_2 + 2M_{13}\delta_1)^{3/2}} \tag{5.53}$$

Thus

$$P(\phi_1, \phi_2) = J(\phi_1, \phi_2)\, P(\delta_1(\phi_1, \phi_2), \delta_2(\phi_1, \phi_2))$$

$$= \frac{|M|^{1/2}}{2\pi} \sec^2\phi_1 \sec^2\phi_2 \cdot$$

$$\frac{1}{(M_{11}\tan^2\phi_1 + M_{22}\tan^2\phi_2 + M_{33} + 2M_{12}\tan\phi_1\tan\phi_2 + 2M_{23}\tan\phi_2 + 2M_{13}\tan\phi_1)^{3/2}} \tag{5.54}$$

Thus $P(\delta_1, \delta_2)$ and $P(\phi_1, \phi_2)$ are the probability density functions for the two mixing ratios. The distribution functions for either of these mixing ratios can be obtained by integrating out the other:

$$P(\phi_1) = \int_{-\pi/2}^{\pi/2} P(\phi_1, \phi_2)\, d\phi_2 \tag{5.55}$$

$$P(\delta_2) = \int_{-\infty}^{\infty} P(\delta_1, \delta_2)\, d\delta_1 \tag{5.56}$$

With a little manipulation, $P(\phi_1)$ and $P(\delta_2)$ reduce to the two channel distribution functions Eqn. 5.42 and Eqn. 5.43, respectively. The comparison between the data

histogram and the theoretical prediction from Eqn. 5.42 (two channels) for j-spin and s-spin are shown in Fig. 5.3 and Fig. 5.4, respectively. The theoretical values are normalized to the data by multiplying a factor equal to (Total No. of Pes.) $\cdot \pi$ /Ibin in the histogram, where Ibin is the number of bins. Of course there is little to compare for the weakly correlated channels. However, for the highly correlated channels $j\text{-}\emptyset_{3/}$ and $s\text{-}\emptyset_{5/}$, the agreement seems excellent. This implies that the mixing ratio distributions follow the random matrix hypothesis with the independence and invariance assumptions. To our knowledge, this is the first experimental test on the reduced width amplitude probability density functions (Eqn. 5.39).

For the special case where the averaged reduced widths in each channel are the same, i.e., $\overline{\gamma_1^2} = \overline{\gamma_2^2} = \overline{\gamma_3^2}$ and also if there is no channel correlation ($M_{12} = M_{23} = M_{13} = 0$), then Eqn. 5.53 and Eqn. 5.54 reduce to

$$P(\xi_1, \xi_2) = \frac{|M|^{1/2}}{2\pi} \quad \frac{(M_{11})^{-3/2}}{(1+\xi_1^2+\xi_2^2)^{3/2}} \tag{5.57}$$

$$P(\emptyset_1, \emptyset_2) = \frac{|M|^{1/2}}{2\pi} \quad \frac{\sec^2\emptyset_1 \sec^2\emptyset_2 (M_{11})^{-3/2}}{(1+\tan^2\emptyset_1+\tan^2\emptyset_2)^{3/2}} \tag{5.58}$$

Figure 5.3 Distribution of Ø for Inelastic Decay from 5/2+ Resonances in ^{49}V in the Angular Momentum Representation. The smooth curve is the two-channel mixing ratio distribution predicted by making the independence and invariance assumptions.

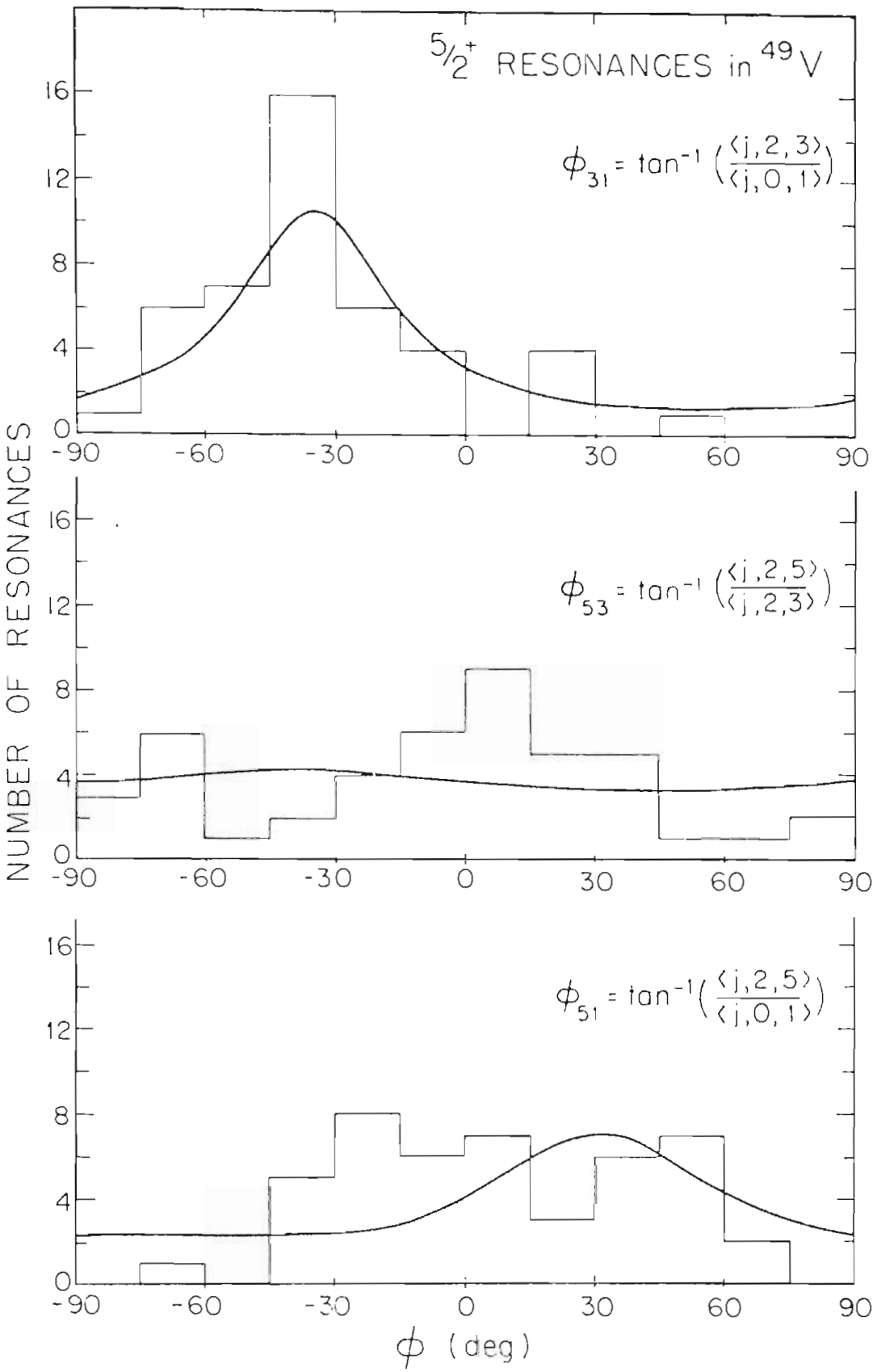
5/2+ RESONANCES in 49V
$\phi_{31} = \tan^{-1}\left(\frac{\langle j,2,3\rangle}{\langle j,0,1\rangle}\right)$
$\phi_{53} = \tan^{-1}\left(\frac{\langle j,2,5\rangle}{\langle j,2,3\rangle}\right)$
$\phi_{51} = \tan^{-1}\left(\frac{\langle j,2,5\rangle}{\langle j,0,1\rangle}\right)$
NUMBER OF RESONANCES
0
4
8
12
16
-90
-60
-30
0
30
60
90
ϕ (deg)

Figure 5.4 Distribution of ϕ for Inelastic Decay from $5/2^+$ Resonances in ^{49}V in the Channel Spin Representation. The smooth curve is the two-channel mixing ratio distribution predicted by making the independence and invariance assumptions.

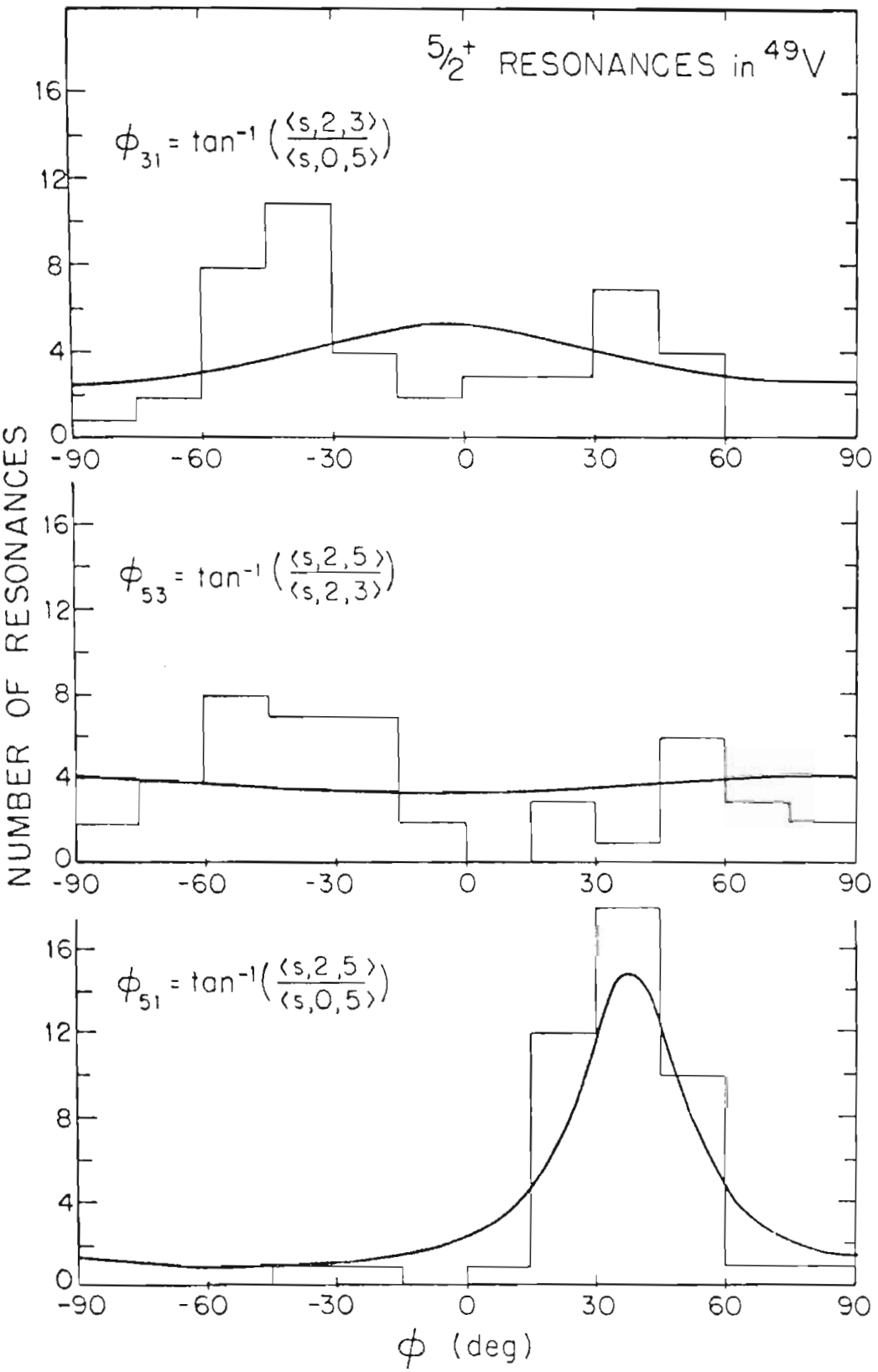
5/2+ RESONANCES in 49V
φ31 = tan-1 (⟨s,2,3⟩/⟨s,0,5⟩)
φ53 = tan-1 (⟨s,2,5⟩/⟨s,2,3⟩)
φ51 = tan-1 (⟨s,2,5⟩/⟨s,0,5⟩)
NUMBER OF RESONANCES
φ (deg)
0
4
8
12
16
-90
-60
-30
0
30
60
90

B. Data Analysis

5.B.1. Non-Statistical Effects

As mentioned earlier, we analyzed in all 80 resonances, of which 45 are 5/2+ states and 35 are 3/2+ states. The data histograms of normalized mixing ratios (equal channel averaged reduced width) for 5/2+ resonances are shown in Fig. 5.5 and Fig 5.6 for j-spin and s-spin, respectively. The dashed lines are uniform distributions corresponding to the extreme statistical case: a distribution with no channel correlations and with equal channel averaged reduced width. Clearly a strong non-statistical effect exists in j-$\emptyset_{3/}$, where only 5 out of 45 resonances have positive signs and in s-$\emptyset_{5/}$, where only 2 out of 45 resonances have negative signs. In both cases, the mixing ratios of most of the resonances are centered in one region.

Wells(1979) used a Monte-Carlo technique to specify the degree of significance of a similar non-statistical effect. In this technique, a statistic (call it Z^2) is defined by comparing the data histogram with the extreme

Figure 5.5 The Normalized Distribution of γ for Inelastic Decay from $5/2^+$ Resonances in ^{49}V in the Angular Momentum Representation. The dashed line is the uniform distribution predicted with no channel correlations.

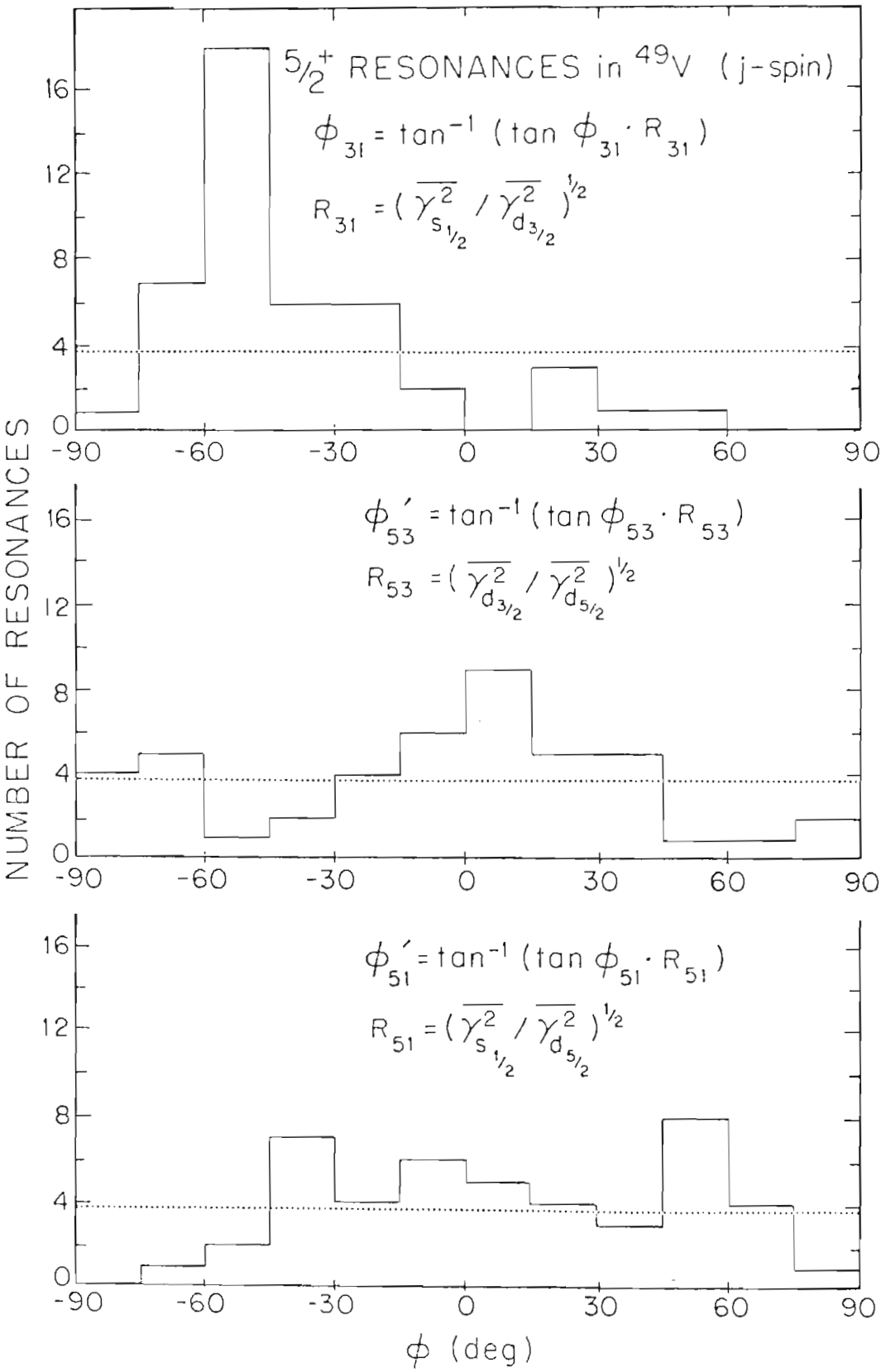
$5/2^+$ RESONANCES in ^{49}V (j-spin)
$\phi_{31} = \tan^{-1}(\tan\phi_{31} \cdot R_{31})$
$R_{31} = (\overline{\gamma^2_{s_{1/2}}} / \overline{\gamma^2_{d_{3/2}}})^{1/2}$
$\phi'_{53} = \tan^{-1}(\tan\phi_{53} \cdot R_{53})$
$R_{53} = (\overline{\gamma^2_{d_{3/2}}} / \overline{\gamma^2_{d_{5/2}}})^{1/2}$
$\phi'_{51} = \tan^{-1}(\tan\phi_{51} \cdot R_{51})$
$R_{51} = (\overline{\gamma^2_{s_{1/2}}} / \overline{\gamma^2_{d_{5/2}}})^{1/2}$
NUMBER OF RESONANCES
0
4
8
12
16
-90
-60
-30
0
30
60
90
ϕ (deg)

Figure 5.6 The Normalized Distribution of Ø for Inelastic Decay from $5/2^+$ Resonances in ^{49}V in the Channel Spin Representation. The dashed line is the uniform distribution predicted with no channel correlations.

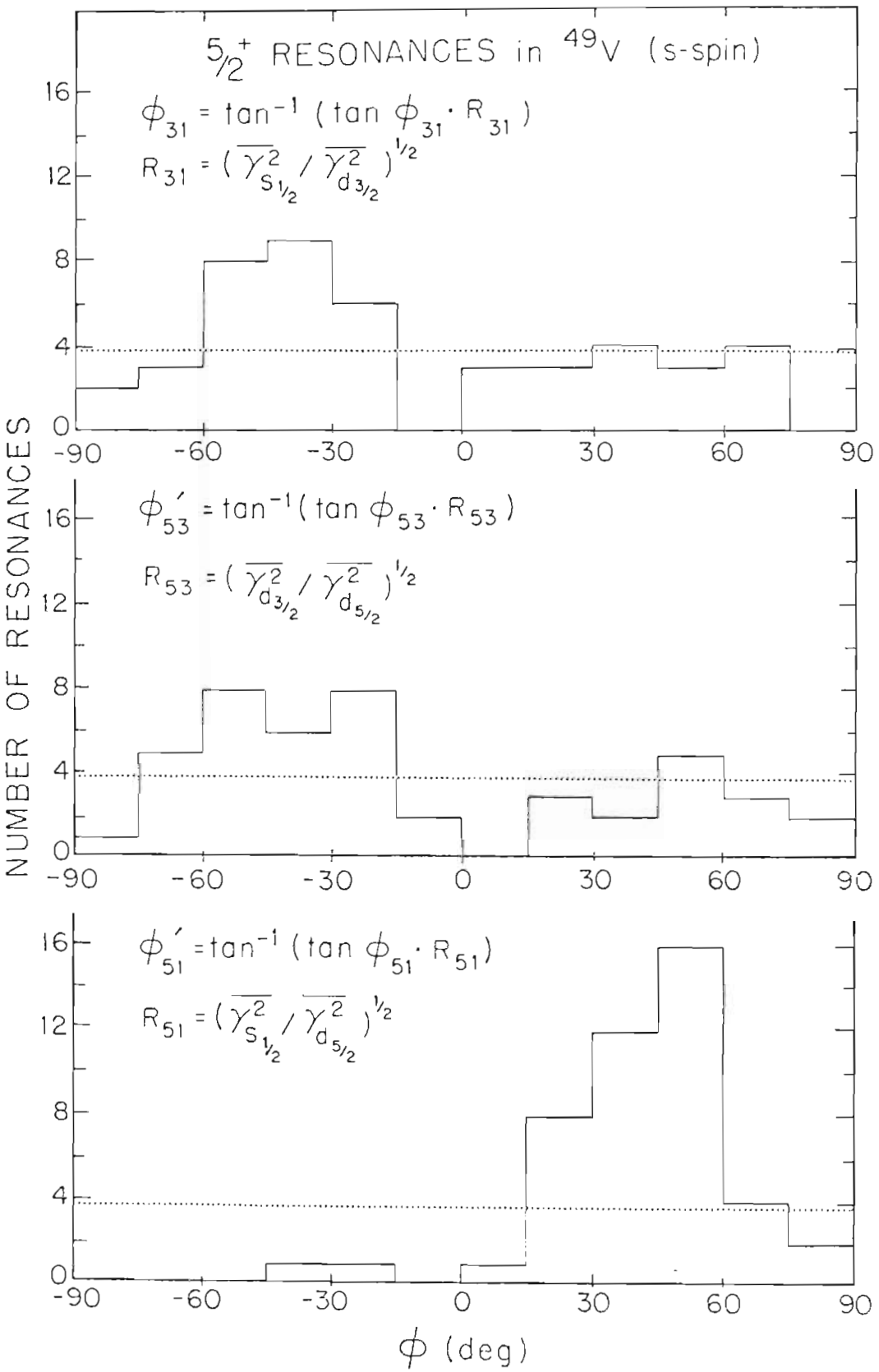
$5/2^+$ RESONANCES in ^{49}V (s-spin)
$\phi_{31} = \tan^{-1}(\tan\phi_{31} \cdot R_{31})$
$R_{31} = (\overline{\gamma^2_{s_{1/2}}} / \overline{\gamma^2_{d_{3/2}}})^{1/2}$
$\phi'_{53} = \tan^{-1}(\tan\phi_{53} \cdot R_{53})$
$R_{53} = (\overline{\gamma^2_{d_{3/2}}} / \overline{\gamma^2_{d_{5/2}}})^{1/2}$
$\phi'_{51} = \tan^{-1}(\tan\phi_{51} \cdot R_{51})$
$R_{51} = (\overline{\gamma^2_{s_{1/2}}} / \overline{\gamma^2_{d_{5/2}}})^{1/2}$
NUMBER OF RESONANCES
0
4
8
12
16
-90
-60
-30
0
30
60
90
ϕ (deg)

statistical distribution.

$$Z^2 = \sum_{i=1}^{N} (N_i - \frac{N_R}{N_B})^2$$

where N_i is the number of resonances which have value Ø in the ith bin (bins are of equal width), N_R is the total number of resonances, and N_B is the number of bins.

The probability distribution of Z for 45 resonances and 100,000 samples shown in Fig. 5.7 was generated by the following procedure:

1) Use a random number generator to generate 45 random numbers ranging from -90° to 90° in the Ø space, and then sort these Ø values into bins (bin size equal to 15°).

2) Calculate the corresponding value of Z^2 as one sample.

3) Repeat procedures 1 and 2 100,000 times, and then sort these various Z^2 values into bins of Z (bin size equal to 0.5).

The calculated Z values for the observed 45 5/2+ resonances with 12 bins are:

Figure 5.7 Distribution of the Z Statistic for 100,000 Cases. There are 45 resonances distributed in 12 ϕ bins for each case.

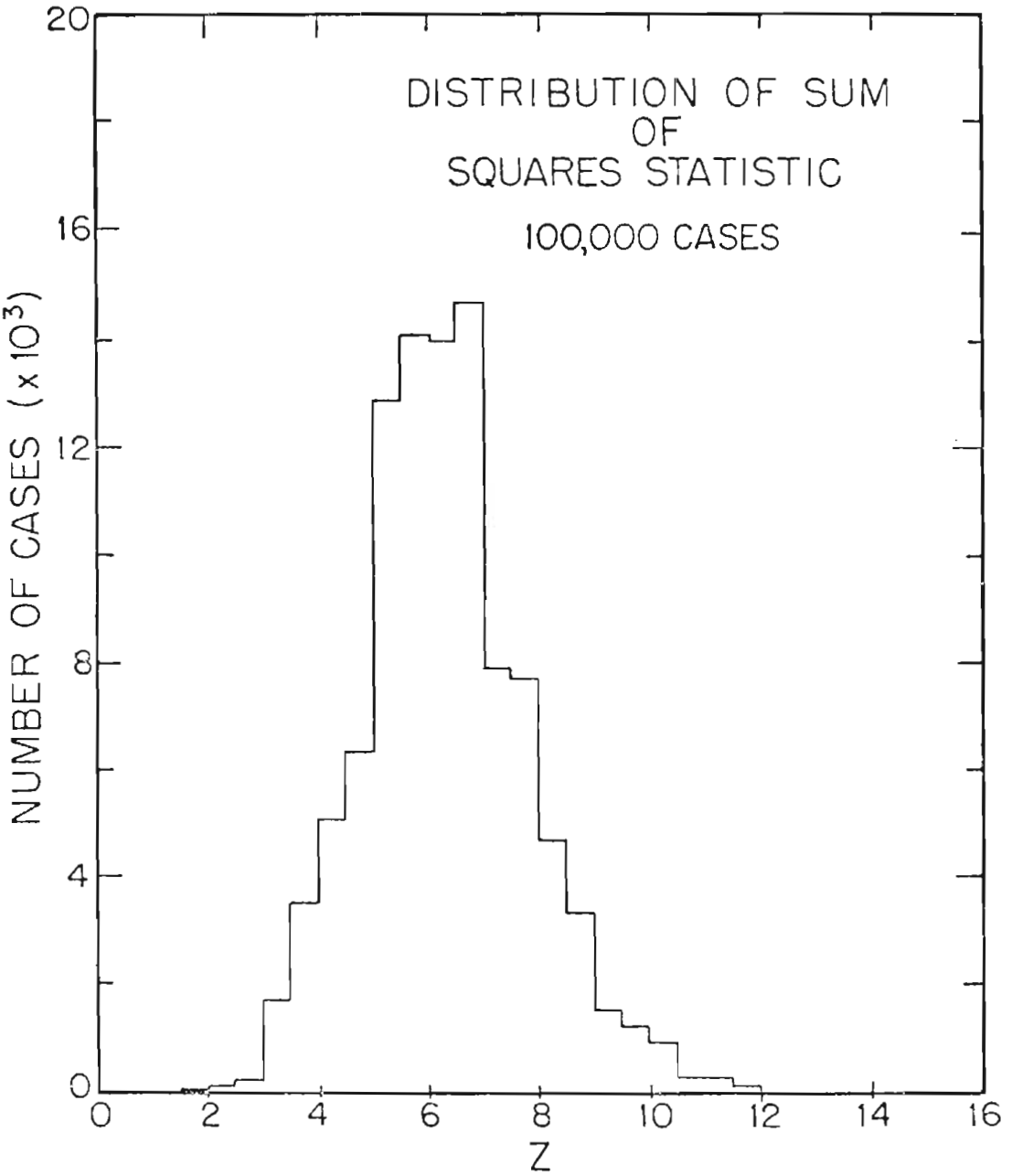
DISTRIBUTION OF SUM
OF
SQUARES STATISTIC
100,000 CASES
NUMBER OF CASES (x 10³)
20
16
12
8
4
0
0
2
4
6
8
10
12
14
16
Z

	ϕ_{31}	ϕ_{53}	ϕ_{51}
Z(j-spin)	17.10	8.14	8.26
Z(s-spin)	9.17	8.73	17.84

Comparing the above values with the distribution shown in Fig. 5.7, there is no case in 100,000 samples with Z>12, 4101 cases with Z>9, 12124 cases with Z>8. Therefore, the probability for the observed data to be sampled from a uniform distribution is less than 10^{-5} in the case of j-ϕ_{31} and s-ϕ_{51}, and around 10^{-1} to 10^{-2} for the remaining mixing ratios.

5.3.2 Proton Strength Functions and The Statistical Fluctuations of Reduced Widths

The proton strength function S, defined by $S = \overline{\gamma^2}/D$, is shown for both 3/2+ and 5/2+ resonances in Table 5.1, where $\overline{\gamma^2}$ is the average reduced width in channel c, and D is the observed average level spacing. The reduced widths were calculated using the relation

$$\gamma_{\lambda c}^2 = \frac{\Gamma_{\lambda c}}{2P}$$

where $\Gamma_{\lambda c}$ is the partial width of resonance λ in channel

Table 5.1

D-Wave Strength Functions of Compound Nucleus ^{97}

J	5/2+
No. of Res.	45
D(keV)	17.952
$\overline{\gamma_p^2}$(keV)	0.552
S	0.031
$\overline{\gamma_{p'}^2}$(keV)	0.735
S	0.041
$\overline{\gamma_{d_1}^2}$(keV)	0.343
S	0.019
$\overline{\gamma_{d_3}^2}$(keV)	0.199
S	0.011
$\overline{\gamma_{d_5}^2}$(keV)	0.193
S	0.011
$\overline{\gamma_{s_1}^2}$(keV)	0.343
S	0.019
$\overline{\gamma_{s_3}^2}$(keV)	0.176
S	0.010
$\overline{\gamma_{s_5}^2}$(keV)	0.216
S	0.012

c, and P_c is the Coulomb penetrability for channel c.

Since there is no analog state in the energy range studied, the reduced width distribution is expected to follow the Porter-Thomas distribution:

$$P(x) = \frac{1}{\sqrt{2\pi x}} \exp\left(-\frac{x}{2}\right), \text{ where } x = \frac{\gamma^2}{\overline{\gamma^2}} \qquad (5.59)$$

The amplitude reduced width distribution P(y), where $y^2 = x$ is therefore equivalent to:

$$P(y) = J(x)P(x(y))$$

$$= \frac{\partial x}{\partial y} P(x(y))$$

$$= \frac{1}{\sqrt{2\pi}} \exp\left(-\frac{y^2}{2}\right) \qquad (5.60)$$

This is a Gaussian distribution with zero mean.

Comparisons between experimental reduced width histograms and the theoretical prediction of the Porter-Thomas distribution are shown in Fig. 5.8 for elastic and total inelastic channels, Fig. 5.9 for inelastic channels in j-spin, and Fig. 5.10 for inelastic channels in s-spin. A log-log scale was used to accentuate the effect of missing small levels. Most channels have a lower cutoff at Y=0.001 and agree very well with the Porter-Thomas distribution.

Figure 5.8 The Distribution of Elastic and Total Inelastic Partial Reduced Widths. The smooth curve is the Porter-Thomas distribution.

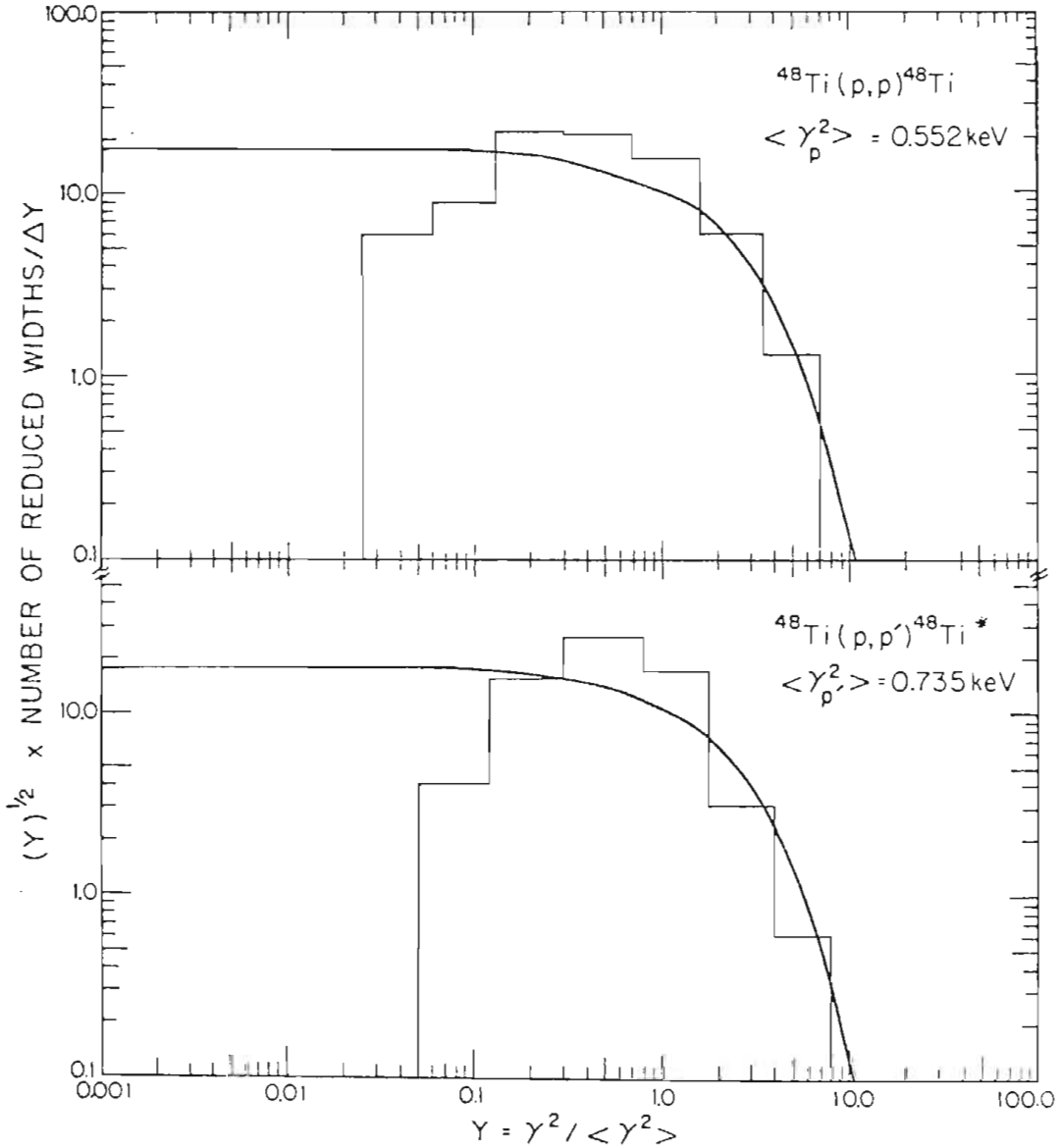
$^{48}Ti(p,p)^{48}Ti$
$<\gamma_p^2>$ = 0.552 keV
$^{48}Ti(p,p')^{48}Ti^*$
$<\gamma_{p'}^2>$ = 0.735 keV
$(Y)^{1/2}$ x NUMBER OF REDUCED WIDTHS/ΔY
$Y = \gamma^2 / <\gamma^2>$
100.0
10.0
1.0
0.1
0.001
0.01
0.1
1.0
10.0
100.0

Figure 5.9 The Distribution of Inelastic Reduced Widths in Channels <j,0,1>, <j,2,3>, and <j,2,5>. The smooth curve is the Porter-Thomas distribution.

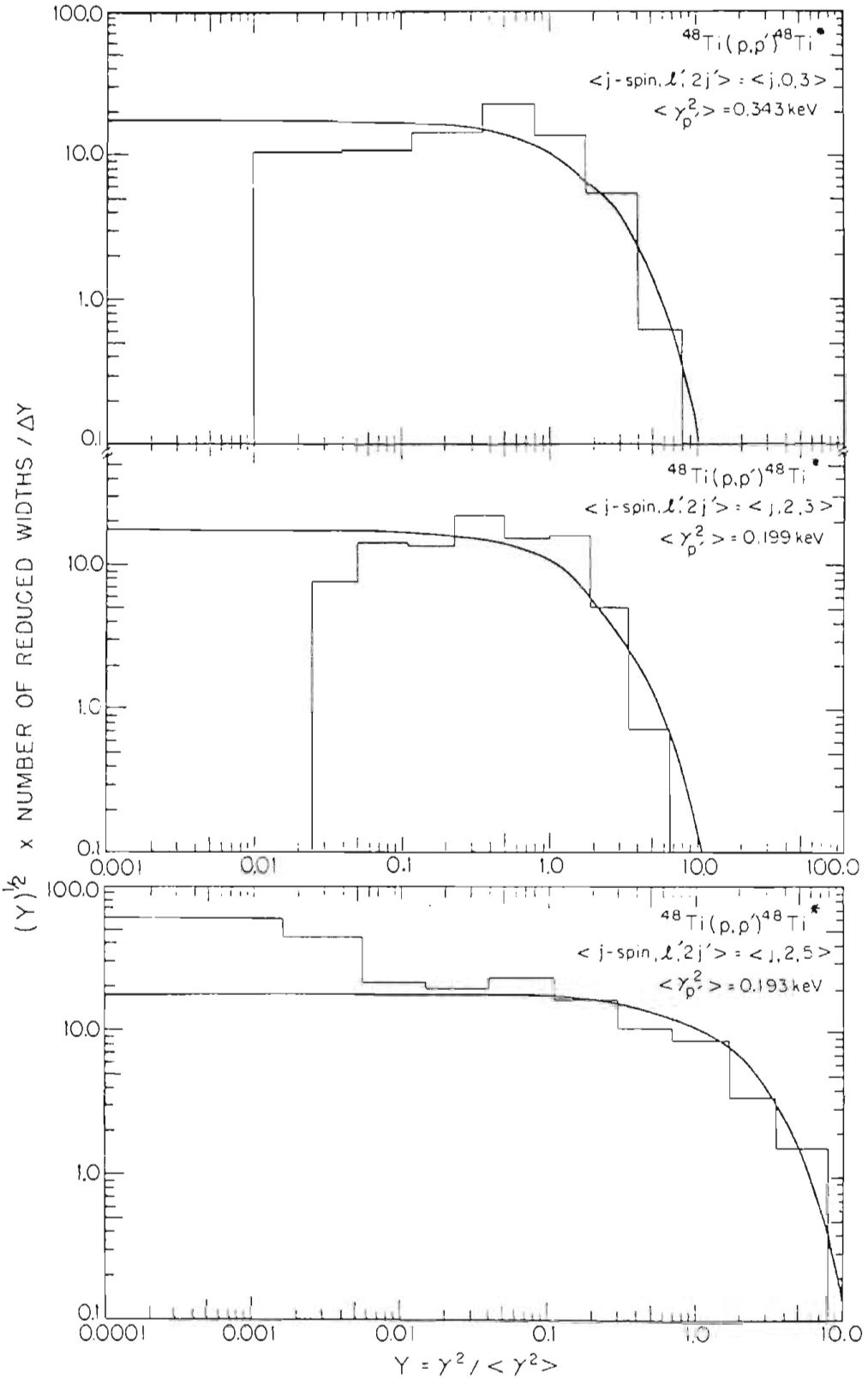
$^{48}Ti(p,p')^{48}Ti^*$
$<j\text{-spin}, \ell' 2j'> = <j, 0, 3>$
$<\gamma_p^2> = 0.343$ keV
$^{48}Ti(p,p')^{48}Ti^*$
$<j\text{-spin}, \ell' 2j'> = <j, 2, 3>$
$<\gamma_p^2> = 0.199$ keV
$^{48}Ti(p,p')^{48}Ti^*$
$<j\text{-spin}, \ell' 2j'> = <j, 2, 5>$
$<\gamma_p^2> = 0.193$ keV
$(Y)^{1/2}$ x NUMBER OF REDUCED WIDTHS / ΔY
$Y = \gamma^2 / <\gamma^2>$
100.0
10.0
1.0
0.1
0.0001
0.001
0.01
0.1
1.0
10.0
100.0

Figure 5.10 The Distribution of Inelastic Reduced Widths in Channels <s,0,5>, <s,2,3>, and <s,2,5>. The smooth curve is the Porter-Thomas distribution.

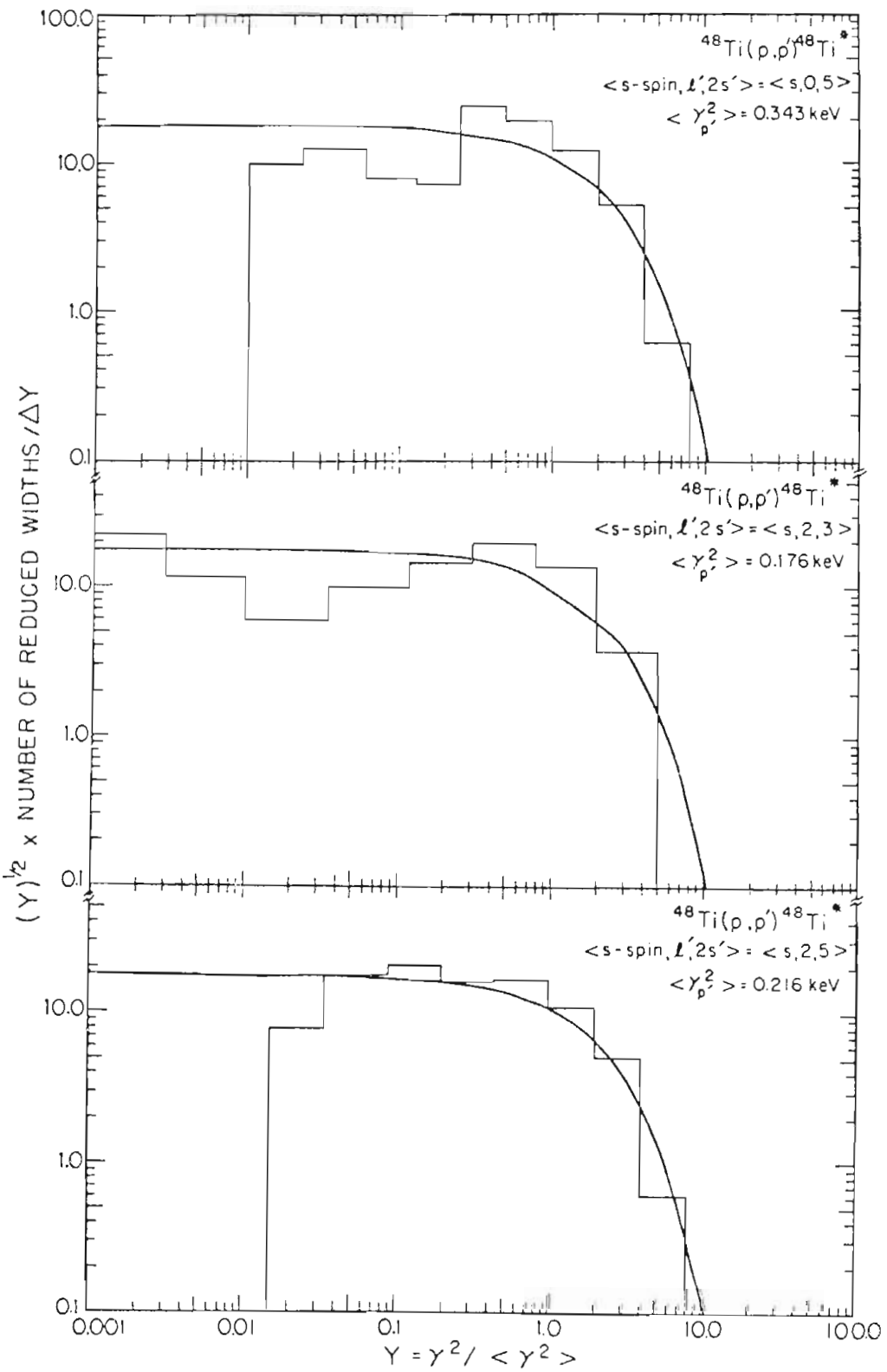
$^{48}Ti(p,p')^{48}Ti^*$
<s-spin, ℓ', 2s'> = <s, 0, 5>
$\langle \gamma_{p'}^2 \rangle$ = 0.343 keV
$^{48}Ti(p,p')^{48}Ti^*$
<s-spin, ℓ', 2s'> = <s, 2, 3>
$\langle \gamma_{p'}^2 \rangle$ = 0.176 keV
$^{48}Ti(p,p')^{48}Ti^*$
<s-spin, ℓ', 2s'> = <s, 2, 5>
$\langle \gamma_{p'}^2 \rangle$ = 0.216 keV
100.0
10.0
1.0
0.1
0.001
0.01
0.1
1.0
10.0
100.0
$(Y)^{1/2}$ x NUMBER OF REDUCED WIDTHS / ΔY
$Y = \gamma^2 / \langle \gamma^2 \rangle$

5.B.7. Linear Correlation Coefficients

The linear correlation coefficient r for two sets of variables x_i and y_i is defined as:

$$r(x,y) = \frac{\sum_{i=1}^{N} ((x_i - \overline{x_i})(y_i - \overline{y_i}))}{\left(\sum_{i=1}^{N} (x_i - \overline{x_i})^2 \sum_{i=1}^{N} (y_i - \overline{y_i})^2 \right)^{1/2}} \qquad (5.61)$$

If r is equal to +1 or -1, then x and y are completely correlated ($y = a+bx$). If r is equal to zero, then x and y are independent. The value of the correlation coefficient r does not directly indicate the significance of the correlation. A distribution free test on the significance of correlation which the coefficient r actually represents was introduced by Baudinet-Robinet (1974), where a permutation distribution of r(x,y) was calculated for independent random variables (x,y) generated from arbitrary continuous distributions. This permutation distribution closely agrees with a bivariate normal distribution with the correlation coefficient equal to zero, where

$$t_o = \left(\frac{(N-2)\,r^2}{1-r^2} \right)^{1/2}$$

reduces to a Student's t-variable with $\nu = N-2$ degrees of freedom. Therefore the independence of x and y will be rejected, on a significance level α, where

$$P\,(|t| > t_o) = \alpha$$

Moreover, the corresponding confidence interval for the coefficient r can be obtained as:

$$P \approx 1-2\alpha$$

Calculated values of linear correlation coefficients for different channels are listed as the superdiagonal terms on Table 5.2 and 5.3 for j-spin and s-spin representations, respectively. The corresponding confidence values are listed as the subdiagonal terms.

The significant correlations between different channels again indicate the occurrence of non-statistical effects. These correlations may arise from the existence of a doorway state common to these two channels (Feshbach, 1962) or from direct reactions (Hufner, 1967).

According to Lane (1971), if there is a linear relation between two amplitudes, say $\gamma' = a\gamma + b$, where b is random, then the exact correlation relation $\rho(\gamma'^2, \gamma^2) = (\rho(\gamma', \gamma))^2$ can be obtained with the following assumptions:

Table 5.2

Linear Correlation Coefficients Between Channels (j-spin)

	γ_p^2	$\gamma_{p'}^2$	γ_{j1}^2	γ_{j3}^2	γ_{j5}^2	γ_{j1}	γ_{j3}	γ_{j5}
γ_p^2	1.	.492	.592	.110	.245	---	---	---
$\gamma_{p'}^2$	>99.9%	1.	.935	.191	.774	---	---	---
γ_{j1}^2	>99.9%	>99.9%	1.	.199	.591	---	---	---
γ_{j3}^2	<90.0%	<90.0%	<95.0%	1.	-.375	---	---	---
γ_{j5}^2	<95.0%	>99.9%	>99.9%	>99.0%	1.	---	---	---
γ_{j1}	---	---	---	---	---	1.	-.763	.512
γ_{j3}	---	---	---	---	---	>99.9%	1.	-.102
γ_{j5}	---	---	---	---	---	>99.9%	<75.0%	1.

Table 5.3

Linear Correlation Coefficients between Channels (s-spin)

	γ_p^2	$\gamma_{p'}^2$	γ_{s1}^2	γ_{s3}^2	γ_{s5}^2	γ_{s1}	γ_{s3}	γ_{s5}
γ_p^2	1.	.492	.592	.077	.405	---	---	---
$\gamma_{p'}^2$	>99.9%	1.	.935	.644	.831	---	---	---
γ_{s1}^2	>99.9%	>99.9%	1.	.456	.707	---	---	---
γ_{s3}^2	<75.0%	>99.9%	>99.9%	1.	.281	---	---	---
γ_{s5}^2	>99.5%	>99.9%	>99.9%	<97.5%	1.	---	---	---
γ_{s1}	---	---	---	---	---	1.	-.058	.876
γ_{s3}	---	---	---	---	---	<75.0%	1.	.013
γ_{s5}	---	---	---	---	---	>99.9%	<60.0%	1.

1. $\overline{\gamma} = 0$, $\overline{b} = 0$

2. $\overline{\gamma b} = \overline{\gamma^3 b} = \overline{\gamma b^3} = 0$

3. $\overline{\gamma^2 b^2} = \overline{\gamma^2}\ \overline{b^2}$

4. $\overline{\gamma^4} = 3(\overline{\gamma^2})^2$, $\overline{b^4} = 3(\overline{b^2})^2$ (5.62)

Expanding the relation $\rho(\gamma'^2, \gamma^2) = (\rho(\gamma', \gamma))^2$ in terms of γ and γ', one obtains:

$$\overline{\gamma^2 \gamma'^2} - \overline{\gamma^2}\ \overline{\gamma'^2} = 2\,(\overline{\gamma\gamma'})^2 \qquad (5.63)$$

The values of $\overline{\gamma^2\gamma'^2} - \overline{\gamma^2}\,\overline{\gamma'^2}$ and $2\,(\overline{\gamma\gamma'})^2$ for 45 $5/2^+$ resonances are listed in Table 5.4. The data do not agree with Eqn. 5.63.

Table 5.4

Values of $\overline{\gamma_1^2\gamma_2^2} - \overline{\gamma_1^2}\,\overline{\gamma_2^2}$ and $2(\overline{\gamma_1\gamma_2})^2$

γ_1	γ_2	$\overline{\gamma_1^2\gamma_2^2} - \overline{\gamma_1^2}\,\overline{\gamma_2^2}$	$2(\overline{\gamma_1\gamma_2})^2$
γ_{j1}	γ_{j3}	0.010	0.079
γ_{j3}	γ_{j5}	-0.020	0.001
γ_{j1}	γ_{j5}	0.059	0.035
γ_{s1}	γ_{s3}	0.024	0.000
γ_{s3}	γ_{s5}	0.010	0.000
γ_{s1}	γ_{s5}	0.046	0.114

Summary

The method for determining the magnitude and relative signs of inelastic decay amplitudes has been extended to l=2 resonances. With the restriction that the exit orbital angular momentum l'≤2, there are three decay amplitudes: $s_{1/2}$, $d_{3/2}$, and $d_{5/2}$. There are three magnitudes and two relative signs which can be determined; these can be more succinctly expressed as two mixing ratios. This method was applied to a case where purely statistical behavior was expected.

Angular distributions of inelastically scattered protons and de-excitation gamma rays were measured for eighty d-wave resonances in the $^{48}Ti(p,p'\gamma)$ reaction. Forty five resonances were assigned as 5/2+ states and thirty five resonances were assigned as 3/2+ states. Mixing ratios for the three inelastic decay amplitudes were uniquely determined for 5/2+ resonances, while for 3/2+ states two solutions were found for each resonance.

General angular distribution theory was briefly discussed. The specific angular distribution equations for d-wave resonances were obtained in two representations, and transformations between these two representations for the l'=2 channel were presented. The physically allowed regions for Legendre polynomial

coefficients were derived and various limiting cases discussed.

The general statistical theory of fluctuations was briefly reviewed, and the random matrix hypothesis as applied to reduced width distributions was discussed. Distributions for the mixing ratios including channel-channel correlations were derived.

The reduced widths show no anomalous energy dependence, and agree very well with the Porter-Thomas distribution. However, there are strong correlations between the amplitudes in different channels, thus disagreeing with the extreme statistical model. The mixing ratio distributions do agree with the statistical theory including correlations: the success of this more stringent test thus leads additional evidence for the general framework of the statistical theory. The physical origin of these correlations has not yet been explained.

BIBLIOGRAPHY

Baudinet-Robinet, Y., Nucl. Phys. A222 (1974) 525.

Bevington, P. R., " Data Reduction and Error Analysis for the Physical Sciences" (McGraw-Hill Book Company, Inc., New York, 1969). p. 223.

Brody, T. A., Flores, J., Mello, P. A., French, J. B. and Wong, S.S.M. "Notas de fisica-the Statistical Theory of Spectra in Nuclear Physics" Vol. 1 nº3 (1978).

Coester, F. and Jauch, J. M., Helv. Phys. Acta, 26 (1953) 3.

Dittrich, T. P., unpublished Ph. D. dissertation, N. C. State Univ. (1976)

Dyson, F. J., J. Math. Phys. 3 (1962) 1199.

Fano, U., Phys. Rev., Vol. 90 (1952) 577.

Feshbach, H., Kerman, A. K., and Lemmer, R. H., Ann. of Phys. 23 (1963) 47.

Ferguson, A. J., "Angular Correlation Methods in Gamma-Ray Spectroscopy" (North-Holland Publishing Company, Amsterdam, 1965). p. 22, p. 195.

Goldfarb, L. J. B., "Angular Correlation and Polization" from P. M. Endt and M. Demeur, Nuclear Reaction. (North-Holland Publishing Company, Amsterdam, 1959), Vol. I, Chap. IV.

Gove, H. E., "Nuclear Reaction", Vol. 1, edited by Endt, P. M. and Demeur, M., North-Holland, Amsterdam (1959) 259.

Krieger, T. J. and Porter, C. E., J. Math. Phys. 4 (1963) 1272.

Heisenberg, W., Z. Phys. 120, 513, (1943) 673.

Hüfner, J., Nabaux, C. and Weidenmüller, H. A., Nucl. Phys. A105 (1967) 489.

Lane, A. M., Ann. Phys. 63 (1971) 171.

Lane, A. M. and Thomas, R. G., Rev. Mod. Phys. 30 (1958) 257.

Liou, H. I., Camarda, H. S., Wynchank, S., Slagowitz, M.,

Hacken, G., Rahn, F., and Rainwater, J., Phys. Rev. C5 (1972) 674.

Marion, J. B., Owens, H. C. and Arnette, T. I., Ork Ridge, "Tables for the Transformation between the Laboratory and Center-of-Mass Coordinate Systems and for the Calculation of the Energies of Reaction Products" (1959) p. 3.

Metha, M. L., "Random Matrices" (Academic Press Inc., New York, 1967) p. 14.

Morse , P. M. and Feshbach, H. "Methods of Theoretical Physics" (McGraw-Hill Book Company, Inc., New York, 1953).

Parks, P. P., Newson, H. W. and Williamson, R. M., Rev. Sci. Instr. 29 (1958) 834.

Porter, C. E., ed. "Statistical Theories of Spectra: Fluctuations" (Academic Press Inc., New York (1965)) 3.

Porter, C. E. and Rosenzweig, N., Ann. Acad. Sci. Fennicae AVI 44 (1960) 5.

Prochnow, N. H., Unpublished Ph. D. Dissertation, Duke Univ. (1971).

Satchler, G. R., Thesis, Oxford Univ. (1955).

Sellin, D. L., Unpublished Ph. D. Dissertation, Duke Univ. (1969).

Wells, W. K., Unpublished Ph. D. Dissertation, Duke Univ. (1978).

Wigner, E. P. and Eisenbud L., Phys. Rev. 72 (1947) 29.

Wilson, W. M., Bilpuch, E. G., and Mitchell, G. E., Nucl. Phys. A245 (1975) 285.